SYNTHESIS AND CHARACTERIZATION OF 2,6-DIISOPROPYLPHENOXY TETRAPYRAZINOPORPHYRAZINES AS POTENTIAL MOLECULAR QUBITS

A Thesis Presented for the
Master of Science
Degree
The University of Tennessee, Knoxville

Benjamin Marx
December 2022

Copyright © 2022 by Benjamin Marx
All rights reserved.

ACKNOWLEDGEMENTS

First, I'd like to thank Dr. Nemykin, our resident phthalocyanine expert, for his continued support and patience this last year and a half. Some didn't think we'd get to this point but here we are! I also thank Dr. Nemykin for his assistance with the computational analysis of the compounds presented. I also need to thank my committee, Dr. Ziling (Ben) Xue and Dr. Ampofo Darko, for their valuable feedback on this thesis and during the defense process.

A huge, huge thank you to everyone in our group for motivating me to keep working to run reactions or learn a new instrument, no matter how many times it took. A very special thanks to Laurel Harrison for keeping me sane while we started this thing from scratch, for being an all-around awesome person, and the best lab BFF a guy could ask for! The rest of the ever-evolving Nemykin group, Briana Schrage, Dustin Nevonen, Tanner Blesener, AJ Thayer, and Morris Oyelowo, thank y'all for all the love and patience as well. All the deep instrument room conversations, struggles building desks, and entertaining lab dinners have been some of my best memories during my time at UTK.

I'd also like to thank the Baccile lab for their guidance, unwavering emotional support and generally being friendly neighbors while I found my grad school sea legs and set up our lab my first year. Much appreciation for sharing Dr. Frank Rossi's wealth of organic chem knowledge to bounce ideas off and I always really enjoyed his stories from many years of teaching!

I also greatly appreciate the efforts and time of Vernon Stafford, a grad student in the Jenkins group, for providing mass spectrometry data for all compounds presented.

Thank you to the chem department staff for being reliable resources while I set up the lab my first year: Bo in the glassblowing shop, Carlos our NMR manager, Heather, Landon, and Josh in Chemstores, and Tim in the machine shop, as well as our administrative staff, Linda, Pam, and Rhonda. Y'all really keep the department together!

Finally, I need to shout out my family for helping me finish grad school strong; thank you for listening while I vented on hour long phone calls and sending pictures of our pets when I needed a mood boost.

ABSTRACT

This thesis reports the synthesis of metal-free and metal-containing phthalocyanine derivatives using methods typical for that class of functional dyes. A mixture of the target compounds prepared here, one paramagnetic and one diamagnetic tetrapyrazinoporphyrazine, will be tested for their potential use in spintronics – the application of spin-active species in molecular electronics. Phthalocyanines and their derivatives are well-known for their ease of preparation and tunability; they have been utilized as sensitizers for photodynamic therapy of cancer and solar cells, as well as in catalysis and chemical sensing. Tetrapyrazinoporphyrazine complexes are compared with the parent phthalocyanine as their chemistry is similar but electronically are distinct. All compounds synthesized were investigated spectroscopically (UV-Vis, magnetic circular dichroism), electrochemically, and computationally; all methods showed the expected results typical of tetrapyrazinoporphyrazines. The paramagnetic vanadyl complex was confirmed by EPR spectroscopy and elucidated by single crystal X-ray diffraction. The green-colored macrocycles are substituted on their periphery by 2,6-diisopropylphenoxy groups; this creates a large nanoporous crystal stabilized by hydrophobic interactions that is useful for spintronic investigations. Under certain solvent conditions, a red linear trimeric product was isolated, and its optical properties and partial characterization is reported as well.

TABLE OF CONTENTS

CHAPTER ONE INTRODUCTION 1
What are phthalocyanines? 1
Molecular Qubits 4
Tetrapyrazinoporphyrazines and this work 7
CHAPTER TWO MATERIALS AND METHODS 9
Instrumentation 9
UV-Vis spectroscopy 9
Magnetic Circular Dichroism 9
Electrochemistry 12
Spectroelectrochemistry 14
Fluorescence spectroscopy 16
Computational analysis 17
X-ray crystallography 17
Experimental procedures 18
Preparation of 5,6-Bis(2,6-diisopropylphenoxy)pyrazine-2,3-dicarbonitrile (1) 18
Preparation of vanadyl tetrapyrazinoporphyrazine (2) 18
Preparation of trimeric linear product (3) 18
Preparation of titanyl tetrapyrazinoporphyrazine (4) 19
Preparation of magnesium tetrapyrazinoporphyrazine (5) 19
Preparation of metal free tetrapyrazinoporphyrazine (6) 19
CHAPTER THREE RESULTS AND DISCUSSION 21
Synthetic strategy 21
Spectroscopy and mass spectrometry 23
Single-crystal X-ray crystallography 32
Redox properties 37
DFT and TDDFT calculations 37
CHAPTER FOUR CONCLUSIONS 55
REFERENCES 56
APPENDIX 62
VITA 89

LIST OF FIGURES

Figure 1.1. Structures of the porphyrinoids plus the derivative presented in this work (PyzPz) 2
Figure 1.2. Cyclotetramerization mechanism for the formation of phthalocyanines. 3
Figure 1.3. UV-Vis absorption spectrum of a zinc tetra-tert-butyl phthalocyanine in dichloromethane 5
Figure 2.1. Graphical representation of the three types of MCD signals and their origins in electronic structure 11
Figure 2.2. Simplified illustration of the electrochemical cell used for CV and DPV experiments 13
Figure 2.3. Simplified illustration of the spectroelectrochemical cuvette used in this thesis. 15
Scheme 3.1. Synthetic route for the preparation of target compounds **2-6** 22
Figure 3.1. Experimental UV-Vis (solid), MCD, and fluorescence (dashed) spectra of the target compounds along with their TDDFT-predicted absorption spectra. 24
Figure 3.2. MALDI HR-MS comparison of theoretical versus experimental for **2** 25
Figure 3.3. MALDI HR-MS comparison of theoretical versus experimental for trimer **3**. 25
Figure 3.4. MALDI HR-MS comparison of theoretical versus experimental for **4** 26
Figure 3.5. MALDI HR-MS comparison of theoretical versus experimental for **5** 26
Figure 3.6. MALDI HR-MS comparison of theoretical versus experimental for **6** 27
Figure 3.7. ^{1}H NMR (500 MHz) of trimer **3** in $CDCl_3$ 28
Figure 3.8. ^{13}C NMR{^{1}H} NMR (125 MHz) of trimer **3** $CDCl_3$ 28
Figure 3.9. ^{1}H NMR (500 MHz) of **4** in $CDCl_3$ 29
Figure 3.10. ^{13}C{^{1}H} NMR (125 MHz) of **4** in $CDCl_3$ 29
Figure 3.11. ^{1}H NMR (500 MHz) of **5** in $CDCl_3$ 30
Figure 3.12. ^{13}C{^{1}H} NMR (125 MHz) of **5** in $CDCl_3$ 30
Figure 3.13. ^{1}H NMR (500 MHz) of **6** in $CDCl_3$ 31
Figure 3.14. ^{13}C{^{1}H} NMR (125 MHz) of **6** in $CDCl_3$ 31

Figure 3.15. EPR spectrum of vanadyl complex **2** in frozen solution (DCM:THF 50/50 v/v) at 153 K.....33
Figure 3.16. IR spectrum of vanadyl complex **2**.....34
Figure 3.17. IR spectrum of titanyl complex **4**.....34
Figure 3.18. IR spectrum of magnesium complex **5**.....35
Figure 3.19. IR spectrum of metal-free complex **6**.....35
Figure 3.20. X-ray crystal structure of vanadyl complex **2** (a-c) and trimer **3** (d); (a): top view of **2**: (b): side view of **2**; (c): packing diagram for **2**.....36
Figure 3.21. Plots of CV (black) and DPV (red) referenced to the ferrocene/ferrocenium couple for all macrocycles.....38
Figure 3.22. Chemical oxidation and SEC spectral transformations for vanadyl complex **2**.....40
Figure 3.23. Chemical oxidation and SEC spectral transformations for titanyl complex **4**.....41
Figure 3.24. Chemical oxidation and SEC spectral transformations for magnesium complex **5**.....42
Figure 3.25. Chemical oxidation and SEC spectral transformations for metal free complex **6**.....43
Figure 3.26. DFT-predicted (M06 functional) energy diagram for the target compounds.....44
Figure 3.27. DFT-predicted (M06 functional) selected frontier MOs for vanadyl complex **2**. (a): α set; (b): β set.....45
Figure 3.28. DFT predicted (M06 functional) selected frontier MOs for linear trimer **3**..46
Figure 3.29. DFT-predicted (M06 functional) selected frontier MOs for titanyl complex **4**.....47
Figure 3.30. DFT-predicted (M06 functional) selected frontier MOs for magnesium complex **5**.....48
Figure 3.31. DFT-predicted (M06 functional) selected frontier MOs for metal free complex **6**.....49

CHAPTER ONE
INTRODUCTION

What are phthalocyanines?

Phthalocyanines (Pcs) are a beautiful synthetic class of dye structurally related to porphyrins (Figure 1.1) that are found naturally as heme in that they share an 18π aromatic core macrocycle. However, Pcs themselves are not found anywhere in nature. These compounds have become so ubiquitous since their accidental discovery in the early 20th century that you are likely wearing some of these compounds as Pcs are the second most significant class of colorant and are widely used for blue and green dyes for paints, cyan printing inks, as blue or cyan dyes for textiles like blue jeans, and have even seen use as energy absorbing agents in optical data recording.[1,2,3,4] The global market for these intense coloring agents is expected to surpass $2 billion in 2026.[5] The compound stumbled upon by Braun and Tcherniac was the metal free variety but phthalocyaninato complexes with all common transition metals are now well reported, with first row transition metals attracting the most attention because their ionic radii allow them to fit nicely inside the Pc macrocycle. For example, iron phthalocyanine (FePc) was the first metallophthalocyanine (MPc) intentionally synthesized and characterized by Sir Reginald Patrick Linstead in 1934, who also elucidated the core Pc structure that year.[6, 7, 8, 9, 10]

Phthalocyanines can be viewed as four isoindoline units connected by nitrogen bridges that form as a result of cyclotetramerization either unassisted (creating the free base ligand) or with a metal ion template. This process is represented by the general mechanism shown in Figure 1.2 with a phthalonitrile (PN) as the starting material. However, Pcs can be synthesized two other ways with similar mechanisms. The Wyler method uses phthalic anhydrides, phthalimides, and phthalic acid as precursors; this is preferred for industrial scale syntheses due to the high cost of PNs. Second, the 1,3-diiminoisoindoline (DII) method is more reactive and can directly undergo self-condensation as DII already resembles a Pc subunit.[11] Synthetic procedures for organic soluble phthalocyanines typically entail mixing one of these precursors with a metal salt (for MPcs) in refluxing anhydrous solvent; certain high boiling solvents such as medium-chain alcohols or N,N-dimethylaminoethanol (DMAE) can create basic conditions in which the alkoxy moiety of the

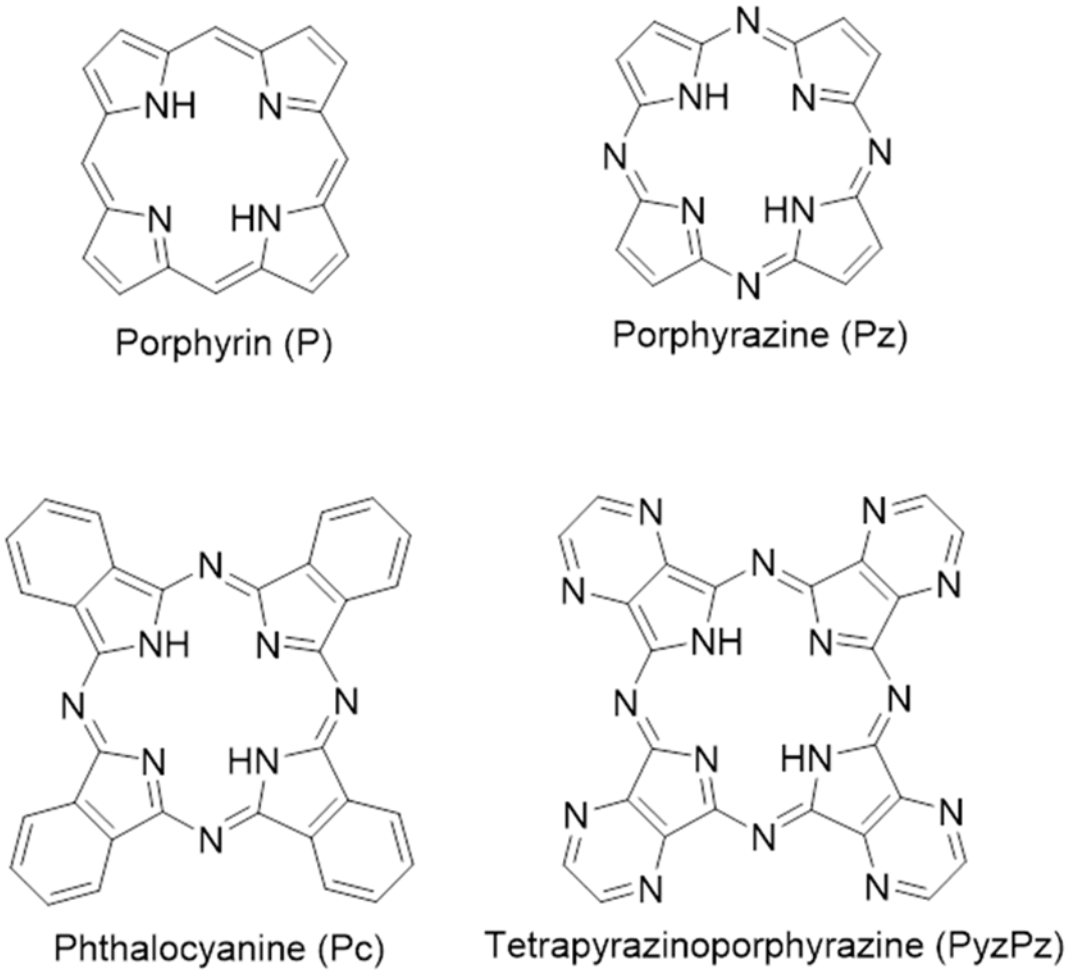

Figure 1.1. Structures of the porphyrinoids plus the derivative presented in this work (PyzPz).

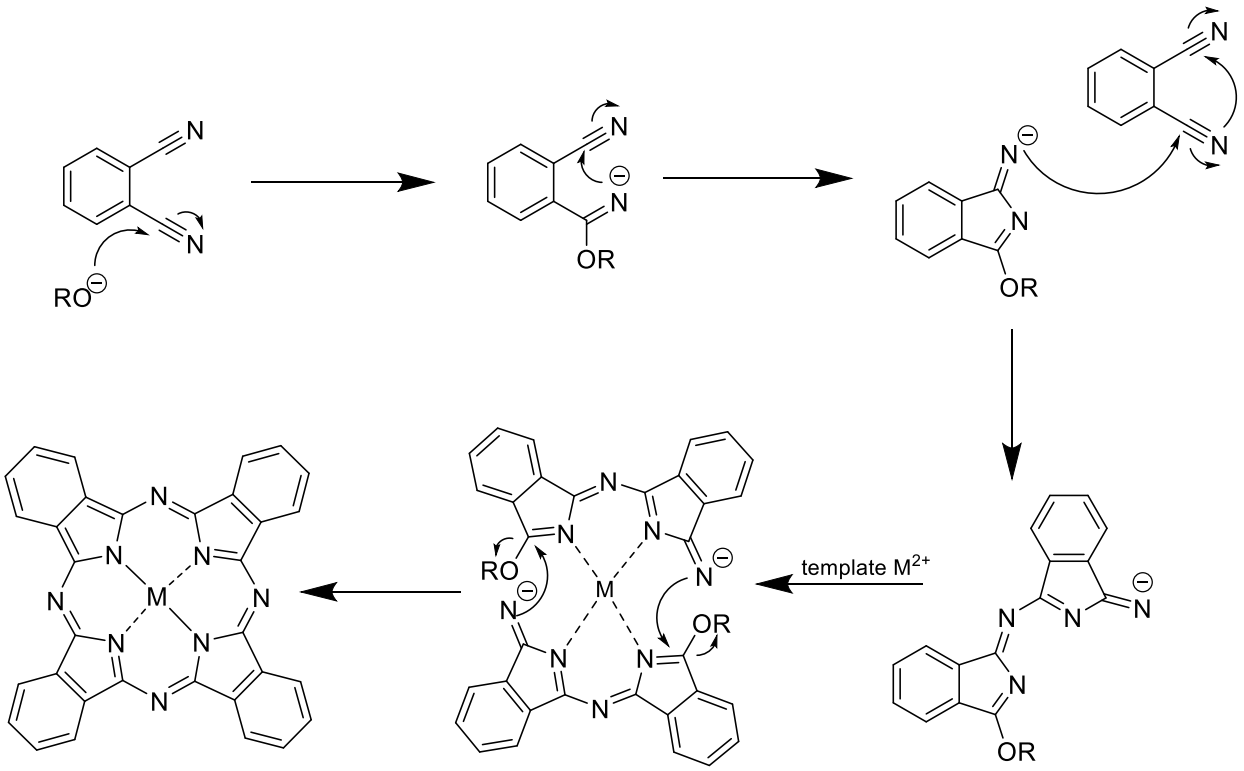

Figure 1.2. Cyclotetramerization mechanism for the formation of phthalocyanines. Adapted from reference 11.

solvent acts as a nucleophile to initiate the cyclotetramerization – if no such solvent is used, then nucleophilic additives like urea are often employed in the reaction mixture.

The parent Pc macrocycle possesses a closed conjugated aromatic system of 18π electrons whose most common metalated species enjoy D_{4h} symmetry while the metal-free variety drops to the D_{2h} point group. These conditions give phthalocyanines easily tunable optical properties and the typical Pc compound gives a very characteristic UV-Vis spectrum in the visible range (example shown in Figure 1.3) that makes these chromophores ripe for use in numerous applications (vide supra). The spectrum is immediately recognized by a higher energy Soret (or B) band usually found in the 300-400 nm range and a lower energy Q-band in the 600-700 nm region. Phthalocyanine's optical and electronic properties, thus its absorption spectrum, can be altered either by addition of axial ligands bound to the metal center or by substitution of the macrocycle's periphery, which is accomplished by reacting appropriately substituted precursors with the desired metal salt.

One particularly exciting recent use for phthalocyanines that takes advantage of their characteristic intense absorption as well as their easily tunable optical properties is theranostic photosensitizing agents in photodynamic therapy of cancer (PDT).[12, 13] As previously mentioned, the phthalocyanine Q-band is typically found between 600-700 nm which is within the so-called optical window of human tissue (600-1300 nm), outside of which light cannot penetrate deep enough in the body to allow treatment to be feasible.[14] The photosensitizer (dye) is injected into the bloodstream and naturally localizes in the cancerous tissue; the area is then irradiated with laser light corresponding to the wavelength of maximum absorbance for the given dye compound which transfers that energy into conversion of triplet state oxygen into cytotoxic singlet oxygen, killing all cells nearby. The procedure is minimally invasive and Pc's high photostability makes it a reliable photosensitizing compound – work is ongoing using Pcs as well as some porphyrins to further improve the outlook for relatively superficial cancers like melanoma using this technique.

Molecular Qubits

*L*ight *a*mplification by *s*timulated *e*mission of *r*adiation (laser) technology has revolutionized the technological world since its invention in 1960, seeing uses in everything from minimally invasive surgeries to harmless cat toys.[15] However, the quantum mechanics behind their

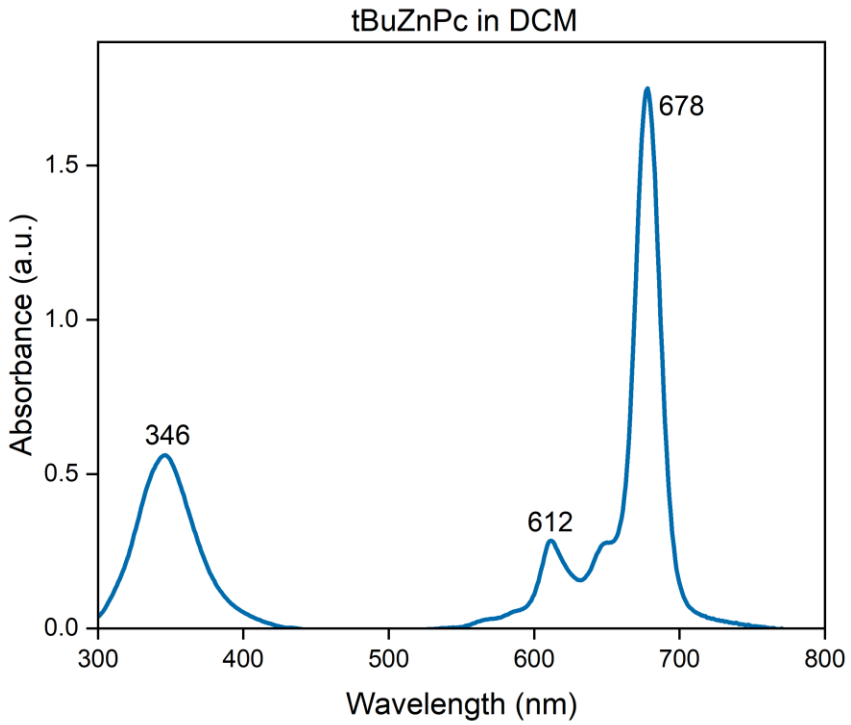

Figure 1.3. UV-visible absorption spectrum of a zinc tetra-tert-butyl phthalocyanine in dichloromethane.

operation is now being used for a more complex application: quantum computing. The physical concept referred to here is coherence, when the electromagnetic waves emitted by a light source are temporally in-phase with each other, allowing the light to be considerably more focused and intense. A quantum computer is a system defined as a machine that can harness the intricacies of a many-particle quantum wavefunction to work out some computational problem.[16] Thus, the key to efficient quantum computing is to control the degree of coherence of different electromagnetic waves to confer information storage to a given system, which is not a trivial task.

This is accomplished by constructing quantum bits, or qubits, that are a quantum system with two states typically created by the Zeeman effect, the splitting of degenerate energy levels by an external magnetic field. As with any quantum system, spins in that environment can exist in a superposition between the two states, creating a quantum oscillator. That oscillator defines a qubit and is analogous to a traditional computing system with binary bits in the form of 1s and 0s. It is the interactions between these individual spin oscillators in a larger system that research in the field of quantum computing is concerned with. Legitimate qubits must also meet the criteria DiVincenzo laid out in 2000, the most significant being a long coherence time, referred to as the timescale T_2.[17] T_2 is the time it takes for the oscillators to lose coherence due to loss or gain of energy from the molecular or external environments. One challenge of any computing system is its ability to function efficiently at ambient temperatures, but quantum computer designers are concerned with temperature dependence for a different reason: spin-lattice relaxation times decline exponentially with increasing temperature according to the Boltzmann distribution, detrimentally affecting coherence as well. Research in this field has been driven toward using coordination complexes as qubits because of the ability to create a wide range of ligand fields and tune their electronic properties, allowing researchers to target a desired level of coherence in these systems. Key factors for longer coherence times at ambient temperatures in coordination complex qubits include more covalent character of the metal-ligand bonds, low spin-orbital coupling constants, and a lower ground-state orbital angular momentum.[16, 18] Metal phthalocyanines have been investigated for this purpose due to their well-known electronic structure and wide availability.[19, 20, 21, 22] In particular, Hadt and coworkers have shown titanyl phthalocyanine doped with vanadyl phthalocyanine and zinc phthalocyanine doped with copper phthalocyanine to be feasible quantum bit systems.[23, 24] Paramagnetic complexes (VO^{2+} and Cu^{2+}) make excellent qubits because their

unpaired electrons are free to oscillate but phthalocyanines are notorious for their propensity to aggregate due to strong π-π stacking interactions. As a result, intermolecular metal-metal distances are on the order of just a few angstroms and the Pcs' individual magnetic moments can interfere, thus degrading coherence times. The dilution (or doping) of the paramagnetic centers by isostructural diamagnetic analogs improves spin coherence to make these systems potential qubits; however, doing so also reduces spin densities per unit of volume. Balancing these two properties will enable the paired phthalocyanine systems to best meet the criteria for potential qubits.

Tetrapyrazinoporphyrazines and this work

Phthalocyanines have numerous analogs and derivatives that are prepared using similar methods but whose physical properties differ significantly; one example are the tetrapyrazinoporphyrazines (PyzPz) also known as AzaPcs, shown compared to the parent phthalocyanine macrocycle in Figure 1. The benzo moiety in Pc is substituted by a pyrazine ring that stabilizes the PyzPz's frontier MOs - the HOMO more so than the LUMO – resulting in a hypsochromic shift in the absorption spectrum by 40-50 nm and a change in visible color from deep blue to more cyan and green hues.[25] As emission is always lower in energy than absorption due to the Franck-Condon principle, these compounds are able to show strong red fluorescence while Pcs' fluorescence maxima are in the NIR region.[26] These compounds have been investigated for uses like their Pc cousins that include PDT, nonlinear optics, catalysis, sensing, and now quantum computing.[25] Investigations by McKeown and coworkers help solve the problem of decreased spin densities caused by the dilution procedure; his group synthesized phthalocyanines and tetrapyrazinoporphyrazines substituted by bulky 2,6-diisopropylphenoxy groups on the periphery of the macrocycle that are oriented perpendicular to the plane of the macrocyclic core.[27, 28] This arrangement prevents aggregation of any form, keeping metal centers and their magnetic moments far enough apart that coherence is not detrimentally affected but not too far apart that the paramagnetic centers can't couple and prohibit coherence. According to McKeown, these molecules also crystallize into a large cubic framework of Pc or TPyzPz dimers with massive voids held together by hydrophobic interactions of neighboring isopropyl groups that work to keep the metal centers spaced apart. The work presented in this thesis will combine these two precedents by preparing paramagnetic vanadyl and diamagnetic titanyl tetrapyrazinoporphyrazines with bulky 2,6-diisopropylphenoxy peripheral substituents that will be investigated by continuous wave and

pulsed EPR techniques as a mixture of the two compounds in various dilution ratios to determine their feasibility for spintronic applications.

CHAPTER TWO
MATERIALS AND METHODS

Instrumentation

UV-Vis spectroscopy

When highly conjugated molecules are irradiated by visible light, electrons are excited from occupied molecular orbitals (MOs) to unoccupied ones. These events occur only at certain wavelengths of light and are observed by way of a UV-visible absorption spectrum, a plot of absorbance intensity versus wavelength. UV-Vis is the predominant analytical technique to analyze phthalocyanines and their derivatives and as such will be presented often throughout this thesis. The internal components of the instrument are described here. The incident white light containing all visible wavelengths is generated by a xenon lamp which first encounters the entrance slit of the monochromator that concentrates the light into a focused beam. This beam then is reflected a rotatable diffraction grating which is what separates the white light into its respective wavelengths; both the slit and diffraction grating are components of the monochromator. The exit slit filters and focuses the multi-colored light into a narrow beam of a specified wavelength and directs it toward the sample, typically dissolved in solvent and held in a quartz cuvette. As the light beam passes through the sample solution, some is absorbed, some is transmitted, and both of these are recorded by the detector.

Magnetic Circular Dichroism

Magnetic circular dichroism (MCD) spectroscopy is another absorption technique that uses a strong magnetic field to split degenerate or closely spaced energy levels. This effect gives a spectrum that is considerably more detailed than the normal UV-Vis spectrum in which overlapping peaks and transitions can be difficult to discern. MCD is relatively esoteric when it comes to analytical techniques so MCD theory regarding phthalocyanines in discussed in some detail. The MCD measurement process starts with the light source, also a xenon lamp that generates white light containing all UV-Vis-NIR wavelengths. The light passes through a monochromator that filters and separates it into specific wavelengths or ranges of light. A 45° polarizer transforms the raw, unpolarized light into linearly polarized light that is further altered by the photoelastic modulator (PEM). Electric pulses are applied to the PEM at a frequency of

about 50 KHz which splits the linearly polarized light into equal amounts of left and right circularly polarized light that alternates with each voltage pulse. That light then travels through the sample, which is dissolved in solvent and held in a glass or quartz cuvette. There are two types of magnets that can be used to create the fields used in MCD measurement and induce Zeeman splitting in the analyte. Phthalocyanines and other macrocycles are MCD-active due to their aromatic ring current that permits interaction with an external field. Most commonly used is a permanent magnet with a field of 1.2-1.6 Tesla; in that arrangement the sample cuvette is placed in a chamber in the center of the magnet and there are openings on either side of the magnet that permit light to pass through. The second option is an electromagnet, whose advantage is the field can be varied but it requires cooling of the power supply which can disrupt efforts to run an experiment at higher fields if overheating occurs. As with the UV-Vis instrument, a detector measures the amounts of light transmitted and absorbed; these are typically red photomultiplier tubes are used for the normal scan range (250-850 nm); conversely, when MCD spectra at longer wavelengths than 850 nm are desired, an InGaAs detector is substituted.

The different forms of MCD signals also needs to be discussed; there are three types: Faraday A-, B-, and C-terms, shown in Figure 2.1. The overlapping signals that can be better resolved by MCD compared to a UV-Vis spectrum are the due to excited states that are degenerate or close in energy, that when placed in an external magnetic field (H in Figure 2.1) split apart, permitting a more resolved spectrum. Whereas UV-Vis can be described by the Beer-Lambert Law and a simple equation for intensity, the intensity of MCD signals for allowed electronic transitions and accounts for the Franck-Condon and Born-Oppenheimer approximations can be described by Equation 1.[29]

$$\frac{\Delta A_{l-r}}{E} = 152.5Bcl\left[A\left(-\frac{df}{dE}\right) + \left(B + \frac{C}{kT}\right)f\right] \quad (1)$$

$\Delta A_{l\text{-}r}$ represents the differential absorption of left (lcp) and right circularly polarized light (rcp), E is the energy coordinate (in cm^{-1}), B is the magnetic field strength, c is sample concentration, l is the path length (in cm), f is the normalized Gaussian band shape function, k is the Boltzmann constant, and T is temperature. A, B and C are variables that correspond to the Faraday terms

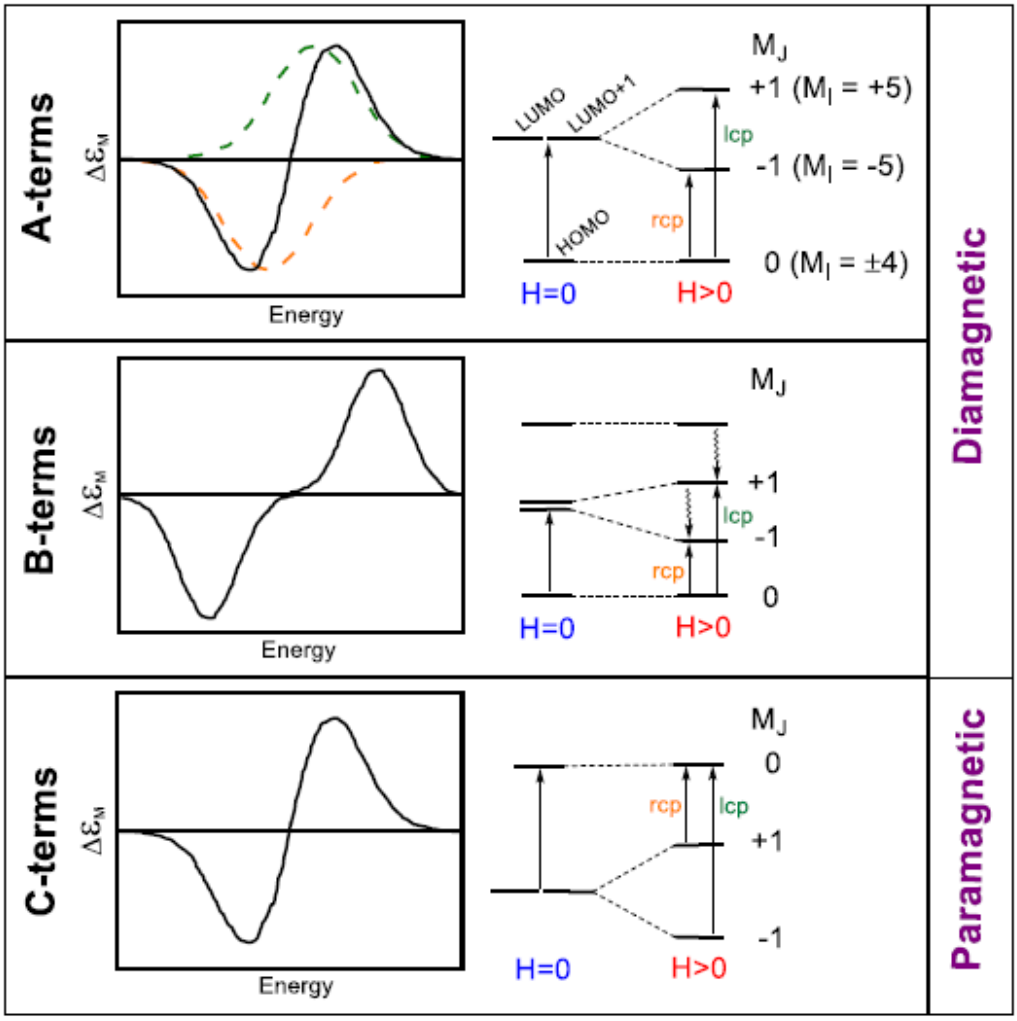

Figure 2.1. Graphical representation of the three types of MCD signals and their origins in electronic structure. Copied with permission from reference 30.

present in the MCD spectrum. Faraday A-terms arise from Zeeman splitting of an orbitally degenerate excited state and appear on the spectrum as a characteristic derivative shape due to the energetic separation of the lcp and rcp light-absorbing band centers. The Faraday B-term appears as a Gaussian shaped peak from second-order effects of magnetic field-induced mixing of zero-field states via magnetic transition dipole moments. If the sample is not three-fold or higher in symmetry, there will be no orbitally degenerate states that can be split apart by the Zeeman effect and B-terms would dominate the MCD spectrum; however, this does not apply to phthalocyanines as they are four-fold symmetric. In higher symmetry molecules, B-terms are still present but are significantly less intense than A- and C-terms. Finally, C-terms are strongly temperature dependent ($1/kT$) because of the Boltzmann population distribution for a degenerate ground state. Only the lowest energy split state contributes to the MCD spectrum, so a symmetric Gaussian C-term is observed at very low temperatures, but at higher temperatures the C-term is asymmetric due to band-center separation of the lcp and rcp absorbing transitions. Increasing temperature will transform this signal into a symmetric A-term like derivative-shaped signal.

Electrochemistry

An additional method to induce excitation of an electronic transition between a redox-active compound's MOs is by applying an electrical potential. Electrochemistry tells a chemist at what potentials reduction and oxidation events take place in the compound of interest and the typical experimental setup used for all work in this thesis is shown in Figure 2.2. The cylindrical cell is made of glass and has an approximate volume of 10 mL. The sample is dissolved in a dry solvent (DCM for this work) at a concentration of at least 1 mg/mL; the solution of electrolyte (tetrabutylammonium perchlorate, TBAP) in solvent and then the compound to be analyzed is stirred in. TBAP is the most common electrolyte for its low cost and high commercial availability; however, other large salts may be used if conditions dictate. The electrolyte concentration is 0.1 M. The cell is covered with a Teflon cap that has five total holes, three for the electrodes and two smaller ones for purging the internal atmosphere, for which a balloon of either nitrogen or argon gas is employed. All electrochemical experiments reported on here used a three-electrode setup. The working electrode is the surface at which the redox events occur – a glassy carbon working electrode was used in all experiments but a platinum one is common as well. An Ag/Ag^+ reference

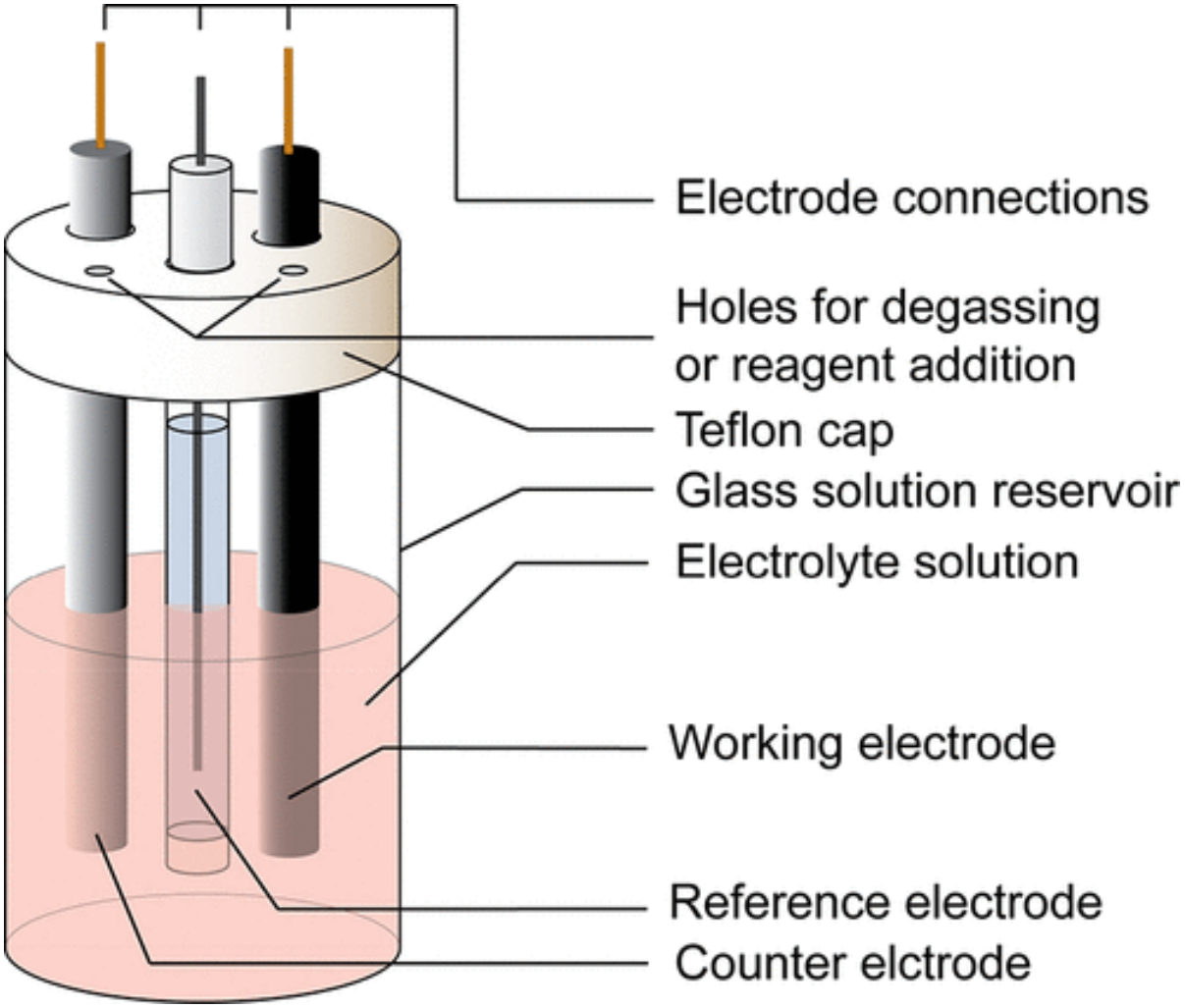

Figure 2.2. Simplified illustration of the electrochemical cell used for CV and DPV experiments.[31]

electrode was used, whose role is to provide a constant potential which the other electrodes are referenced to by the computer program. The final electrode used is a platinum wire auxiliary which is an electron sink or source that facilitates the transfer of electrons from the potentiostat to the sample solution. All three electrodes are attached by alligator clamps to wires that lead to the potentiostat that is controlled by an external computer.

Two distinct but complimentary electrochemical experiments were performed for this thesis: cyclic voltammetry (CV) and differential pulse voltammetry (DPV). CV is the most commonly electrochemical technique, and it entails a continuous scan of the potential as a function of time, first over a positive potential range then to a range of negative potentials. Oxidation events are found in the positive voltages while reductions are in the negative voltage region. DPV, on the other hand, uses a series of voltage pulses which sweeps across an entire range of potentials one direction at a time. Current is measured at each pulse and the current difference is plotted versus potential applied. DPV supplements CV by allowing resolution of overlapping redox peaks as the scan rate is considerably slower than that of CV.

Spectroelectrochemistry

Any redox active species can be observed by electrochemistry but if the analyte is a chromophore like the ones studied in this thesis, the electron transfer processes can also be probed by spectroelectrochemistry (SEC), the UV-Vis spectral measurement of the sample while a constant electrical potential is applied and observing the resultant changes in the UV-Vis spectrum. The experimental setup used in analyzing the compounds presented is illustrated in Figure 2.3. A custom-made quartz cuvette holds about 2 mL of sample and has a 1 mm path length that the light beam crosses; this solution is prepared in a similar way to the solution for electrochemical experiments, using the same electrolyte but at a concentration of 0.3 M. This concentration is higher because the electrical process at work is bulk electrolysis of the solution not smaller-scale redox events at the working electrode. The cuvette is held by a special holder that fits in the usual cuvette slot in the UV-Vis instrument. The cuvette itself is once again sealed with a Teflon cap that creates an inert environment once the solution is purged with nitrogen or argon gas. The SEC setup also utilizes a three-electrode apparatus in which the working electrode is a platinum mesh which permits the redox events to occur over the entire surface of the mesh while in solution. The reference and auxiliary electrodes are once again Ag/Ag^{+} and platinum wires and all three are

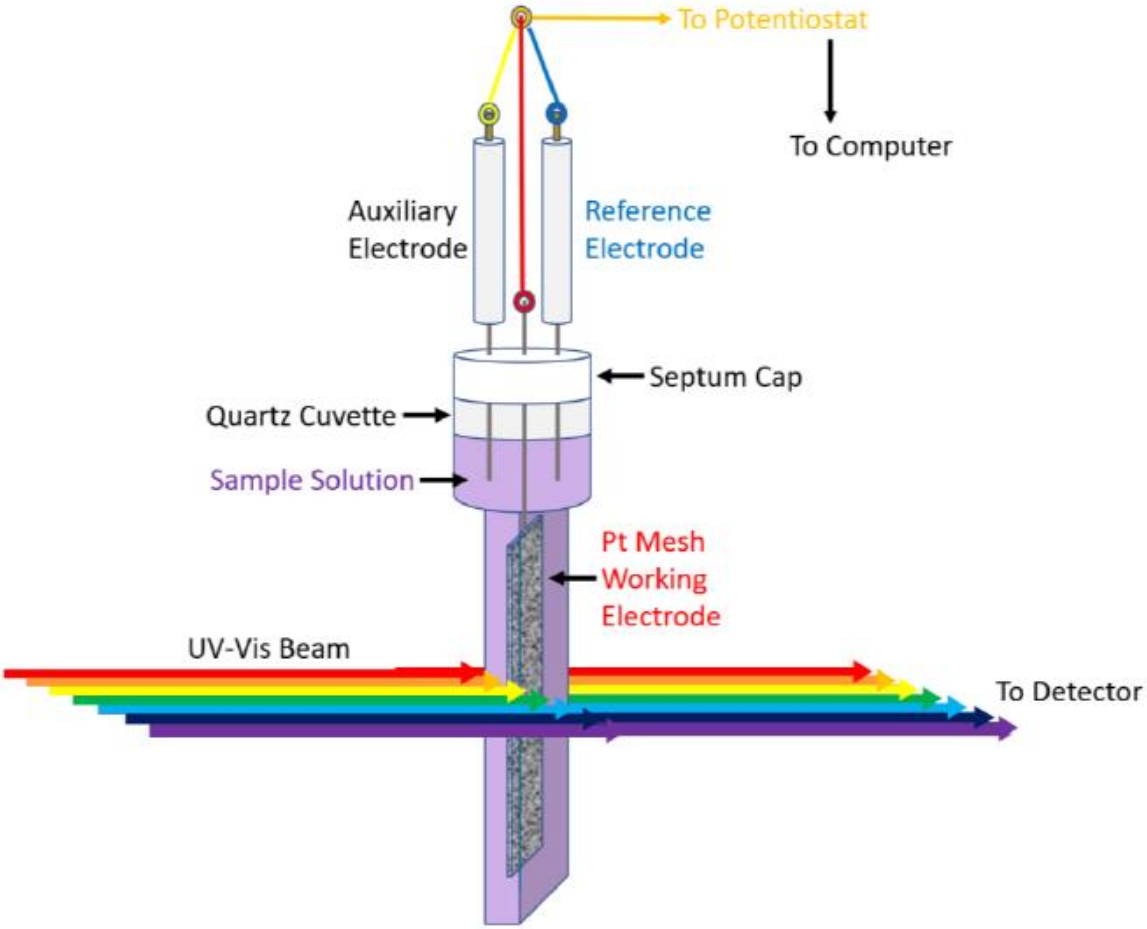

Figure 2.3. Simplified illustration of the spectroelectrochemical cuvette used in this thesis. Copied with permission from reference 30.

connected to a potentiostat in the same way. Lastly, as the potentiostat wires interfere with the UV-Vis measurement compartment closing, that chamber is covered with miscellaneous materials to ensure no external light is absorbed during spectral scans.

Data acquisition for SEC involves running the UV-Vis spectrum multiple times while applying a constant potential through the three electrodes. The spectra are superimposed and a pattern in spectral features is revealed. Important characteristics include isosbestic points, a given wavelength on the spectrum where all the individual traces cross, which represents an equilibrium between multiple species in solution: in this work, neutral and oxidized species. On either side of an isosbestic point, the spectrum will either increase or decrease in intensity, indicating a change in concentration (according to the Beer-Lambert Law) of that species. These changes can tell the scientist where on the analyte molecule the redox event is occurring when compared with molecular orbital analysis.

Fluorescence spectroscopy

All compounds presented with the exception of the vanadyl complex were also characterized by fluorescence (or emission) spectroscopy and this data used to calculate their quantum yields. The vanadyl ion (VO^{2+}) is a paramagnetic d^1 system and as such does not exhibit fluorescence due to the unpaired electron undergoing intersystem crossing. Emission is induced by exciting the sample dissolved in solvent held in a cuvette by laser light of a desired wavelength which must be within the absorption profile of the compound, typically near the λ_{max}, and the number of photons emitted by the sample is measured. The instrument is set up so that the incident light and detector are oriented 90° relative to each other in order to prevent the detector from being overwhelmed; therefore, the cuvette used must be completely clear on all sides as opposed to the cuvette used in UV-Vis measurements that is only clear on two sides to accommodate the linear path of the beam that instrument uses. Fluorescence spectra are predictably red-shifted and the mirror image of their corresponding UV-Vis spectra; this is a result of the Franck-Condon principle that states an excited particle relaxes in energy vibrationally, shedding the energy difference as heat, before relaxing completely to the electronic ground state with emission of a photon of light.

Quantum yield (Φ_f) is defined as the ratio of photons emitted via fluorescence over the number of photons absorbed and gives the researcher information about the efficiency of the processes leading to direct relaxation of the excited particle rather than competing processes such

as intersystem crossing or charge transfer. Quantum yield can be measured in two ways, the absolute method and the relative method – the latter was used for this work and is the more common method of the two.[32] The relative method compares the integrated fluorescence intensity of a well-known reference compound (Rhodamine 6G for the compounds in this thesis, $\Phi_f = 0.95$) versus the sample compound with an unknown Φ_f.[33] Both the sample and reference are analyzed in solution, thus the refractive index of the solution must be known and their absorbances are measured as well. The relative method is considered a reliable measure of quantum yield because the solutions of the sample and reference are assumed to absorb the same number of photons when they have identical absorbances at the excitation wavelength for the given compound, thus the calculation is simplified. The experiment is best run as multiple trials with measurements of the absorbance and fluorescence intensity at the excitation wavelength and then creating a calibration curve of the latter versus the former whose slope gives the quantum yield of the unknown as a fraction of the quantum yield of the reference. The equation used for this calculation is as follows:

$$Q_s = Q_r (m_s/m_r)(n_s/n_r) \quad (2)$$

Where Q is the fluorescence quantum yield, s is the unknown sample, r is the reference, m is the slope of the plot of integrated fluorescence intensity versus absorbance, and n is the refractive index of the solvent.

Computational analysis

All calculations were run using Gaussian 16. The TPSSh exchange-correlation functional[34, 35] with Wachter's full-electron basis set[36] for transition metals and the 6-311G(d) basis set[37] for the other atoms was used for all geometry optimizations. Vibrational frequencies were calculated to ensure all geometries were local minima. The M06 functional was used in single-point and TDDFT calculations with the same basis sets.[38] QMForge was used for the molecular orbital composition analyses.[39]

X-ray crystallography

X-ray data for complex **2** and open-chain trimer **3** were collected with a Cu microsource on a Bruker D8 Venture diffractometer at 100 K using an Oxford Cryostream low-temperature apparatus. Experimental data sets were reduced with Bruker SAINT. Absorption correction was done using SADABS. Structures were solved using Superflip (**2**)[40] or SHELXS (**3**)[41] and refined

using the Crystals for Windows program.[42] Disordered water and acetonitrile solvents observed in the pores of compounds **2** were eliminated with the PLATON SQUEEZE procedure.[43] Complete structural data on **2** can be accessed using CCDC reference number 2208789. It also available in the Supporting Information. The crystals for the open-chain compound **3** were too small and thus the best dataset only allowed to refine the structure using isotropic spheres (R ~32%). Thus, this structure was used only to establish the connectivity in the molecule and was not deposited to CCDC database although the CIF file is available from the author of this thesis on request.

Experimental procedures

Preparation of 5,6-Bis(2,6-diisopropylphenoxy)pyrazine-2,3-dicarbonitrile (1)

Compound **1** was prepared according to a previously published procedure by Novakova and coworkers.[44]

Preparation of vanadyl tetrapyrazinoporphyrazine (2)

1 (1.002 g, 2.076 mmol), vanadium trichloride (0.5 equiv), and urea (0.150 g) was dissolved in dry N,N-dimethylaminoethanol (2 mL) in argon atmosphere and boiled for 4 hr. Upon cooling, deionized water (100 mL) was added to the reaction mixture and the resulting precipitate was collected and washed thoroughly with more water. The solid was purified by means of a silica plug eluting with 3:1 DCM/acetone then further washed with 1:1 water/methanol and pure methanol to give a green solid in 59% yield (1.236 g). IR: 1032 cm^{-1} (ν_{VO}). UV-Vis (DCM): λ_{max} (ε) = 634 nm (91,880 M^{-1} cm^{-1}). HRMS (MALDI-TOF, positive mode) m/z: calcd for $C_{120}H_{137}N_{16}O_9V$ 1998.0226, found 1998.0215 $[M+H]^+$.

Preparation of trimeric linear product (3)

N,N-Dimethylaminoethanol (2 mL) purged with argon in a Schlenk flask, titanium tetrachloride (0.5 equiv) added via syringe and smoke allowed to completely evolve. **1** (414 mg, 0.858 mmol) added and mixture heated to ~ 100 °C for 3 hr. Upon cooling, purple solution poured into deionized water (100 mL) and filtered. Purified by column chromatography on silica gel eluting with DCM to give a small amount of a red solid. ^{1}H NMR (500 MHz, $CDCl_3$): δ = 7.71 (dd, 10H), 7.53 (dd, 11H), 7.06 (d, 12H), 6.90 (t, 6H), 4.78 (bs, 3H, N*H*), 4.22 (m, 23H), 3.16 (sept, 12H), 1.27 (d, 72H), 0.92 (m, 72H). $^{13}C\{^1H\}$ NMR (125 MHz, $CDCl_3$): δ = 167.91 (C=O),

150.09, 133.79, 132.63, 131.02, 128.96, 123.59, 120.77, 68.33, 38.91, 30.53, 29.09, 27.30, 23.92, 23.13, 22.89, 14.19, 11.11. UV-Vis (DCM): λ_{max} = 556 nm. HRMS (MALDI-TOF, positive mode) m/z calcd for $C_{90}H_{105}N_{11}O_8$ 1467.8148, found 1467.8110 $[M]^+$.

Preparation of titanyl tetrapyrazinoporphyrazine (4)

1 stirred in dry quinoline (3 mL) in argon atmosphere for ~ 10 mins then titanium tetrachloride (0.5 equiv) added and mixture heated to 150-160 °C for 1 hr. Upon cooling, the green solution was poured into 1:1 MeOH/deionized water and the precipitate filtered off, then further washed with the same ratio (200 mL) as well as 8:2 MeOH/water (400 mL). The product was dissolved in DCM and filtered through a membrane frit to remove the titanium dioxide byproduct and evaporated to give a green solid in 36% yield (0.416 g). ^{1}H NMR (500 MHz, $CDCl_3$): δ = 7.63 (t, 8H), 7.48 (d, 16H), 3.33 (m, 16H), 1.38 (d, 93H). $^{13}C\{^1H\}$ NMR (125 MHz, $CDCl_3$): δ = 152.95, 147.84, 147.79, 141.90, 141.15, 140.22, 127.02, 124.66, 28.42, 23.67. IR: 2964, 1249, 1010 cm^{-1}. UV-Vis (DCM): λ_{max} (ε) = 635 nm (120,693 M^{-1} cm^{-1}). HRMS (MALDI-TOF, positive mode) m/z: calcd for $C_{120}H_{137}N_{16}O_9Ti$ 1995.0271, found 1995.0270 $[M+H]^+$.

Preparation of magnesium tetrapyrazinoporphyrazine (5)

Magnesium ribbon (55 mg, 2.3 mmol) with a few crystals of iodine was boiled in dry N,N-dimethylaminoethanol (3 mL) for 1 hr in argon atmosphere. **1** (2.18 g, 4.6 mmol) was added and the mixture was boiled for 6 hrs. After cooling, the mixture was poured into 1:1 MeOH/deionized water (100 mL) and the resulting precipitate filtered. The solid was further washed with increasing amounts of MeOH to 9:1. The product was purified by silica gel column chromatography eluting with 4:1 DCM/acetone to give a cyan solid in 34% yield (1.49 g). ^{1}H NMR (500 MHz, $CDCl_3$): δ = 7.49 (t, 8H), 7.36 (d, 16H), 3.28 (m, 16H), 1.25 (d, 96H). $^{13}C\{^1H\}$ NMR (125 MHz, $CDCl_3$): δ = 151.67, 149.91, 148.09, 142.59, 141.23, 126.77, 124.53, 28.27, 23.62. IR: 2963, 1247 cm^{-1}. UV-Vis (DCM): λ_{max} (ε) = 630 nm (104,864 M^{-1} cm^{-1}). HRMS (MALDI-TOF, positive mode) m/z: calcd for $C_{120}H_{137}N_{16}O_8Mg$ 1955.0685, found 1955.0693 $[M]^+$.

Preparation of metal free tetrapyrazinoporphyrazine (6)

5 was dissolved in equal parts (5 mL) dry THF and acetic acid and heated at 75 °C for 2 hr. After cooling, the mixture was poured into deionized water (150 mL) and the precipitate filtered. The solid was thoroughly washed with water and methanol then purified by silica gel column chromatography eluting with DCM then 4:1 DCM/MeOH to give a cyan solid in 52%

yield (0.763 g). ^{1}H NMR (500 MHz, $CDCl_3$): δ = 7.59 (t, 8H), 7.45 (d, 16H), 3.32 (m, 16H), 1.32 (d, 96H), -2.09 (bs, 2H, N*H*). $^{13}C\{^{1}H\}$ NMR (125 MHz, $CDCl_3$): δ = 152.33, 147.98, 141.25, 141.19, 126.85, 124.59, 28.38, 23.66. IR: ~3300, 2963, 2870, 1246 cm^{-1}. UV-Vis (DCM): λ_{max} (ε) = 649 nm (94,058 M^{-1} cm^{-1}). HRMS (MALDI-TOF, positive mode) m/z: calcd for $C_{120}H_{139}N_{16}O_8$ 1933.0992, found 1933.0969 $[M+H]^+$.

CHAPTER THREE
RESULTS AND DISCUSSION

Synthetic strategy

Both titanyl (**4**) and vanadyl (**2**) tetrapyrazinoporphyrazines outlined in Scheme 3.1 were not reported previously. The direct reaction between pyrazinedicarbonitrile **1** and vanadium trichloride (VCl_3) in boiling N,N-dimethylaminoethanol (DMAE) results in the formation of a green-colored reaction mixture which after the standard purification steps (see experimental section for details) leads to the isolation of pure vanadyl tetrapyrazinoporphyrazine **2**. A similar reaction with titanium tetrachloride ($TiCl_4$) in neat DMAE led to a dark purple solution which, after purification, was identified as the trimeric linear hydrolysis product **3** using X-ray diffraction, MALDI-TOF, and NMR data. Use of titanium butoxide instead of $TiCl_4$ also does not lead to the desired macrocycle product. The reaction of the pyrazinedicarbonitrile **1** with titanium butoxide in bromonaphthalene also does not lead to the desired product **4**. However, the reaction between nitrile **1** and titanium tetrachloride in boiling quinoline showed initial formation of a green color that disappeared upon further refluxing. Optimization of the synthesis of desired complex **4** was obtained by varying reaction temperature and time. Under the optimized conditions, the product **4** was obtained in the reaction between pyrazinedicarbonitrile **1** with titanium tetrachloride in quinoline at ~150 °C for 1 hour. Alternatively, we thought that complex **4** could be formed by the interaction of the metal free tetrapyrazinoporphyrazine **6** with titanium tetrachloride or titanium butoxide. In turn, the metal free tetrapyrazinoporphyrazine **6** can be formed by demetalation of magnesium complex **5** with acetic acid. The acid-catalyzed mechanism for this process is described by Kolarova and coworkers.[45] Magnesium complex **5** can be prepared from the nitrile **1** and magnesium alkoxide in dry, boiling DMAE. Using this strategy, we have prepared magnesium complex **5** without any issues in reasonable yield. Using acetic acid, compound **5** was transformed into metal free species $\mathbf{[6H_n]^{n+}}$, protonated at the pyrazine nitrogens. Clean deprotonation of this compound was challenging and required the use of triethylamine or stronger bases. Once formed, metal free complex **6** was tested in the metalation reaction with titanium tetrachloride and titanium butoxide. Despite testing several different reaction conditions, formation of the desired titanyl complex **4** in reasonable yield was not observed. Thus, for this work, direct formation of the target

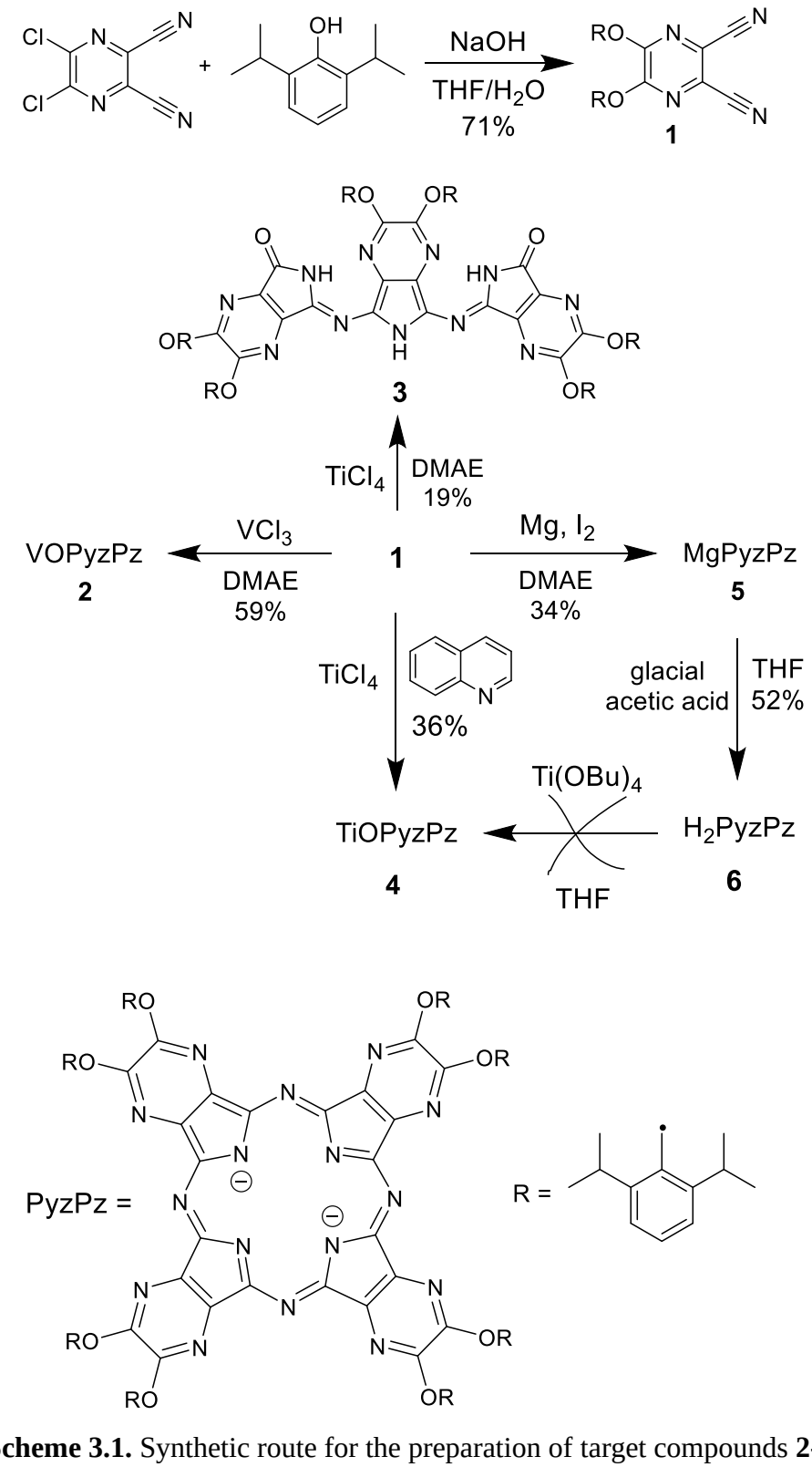

Scheme 3.1. Synthetic route for the preparation of target compounds **2-6**.

titanyl complex **4** in the reaction between nitrile **1** and titanium tetrachloride in dry, hot quinoline was found to be the optimal reaction condition.

Spectroscopy and mass spectrometry

The UV-Vis and MCD spectra of these new macrocycles along with the trimeric product are shown in Figure 3.1. UV-Vis spectroscopy was performed on a Jasco V-770 spectrophotometer and MCD spectra were collected using a Jasco J-1500 CD spectrometer and a 1.6 Tesla permanent magnet. As expected, the metal complexes have one characteristic Q-band, while the lowering of symmetry from D_{4h} to D_{2h} in the metal-free compound leads to splitting of the Q-band into Q_x and Q_y components.[46, 47] The Soret band in all four macrocycles can be found in the 350 nm region. In addition, in the titanyl, vanadyl, and the metal-free compounds, a prominent band is found in the 420 nm region, which has a significant charge-transfer character (see TDDFT calculations discussion below). This band is also present in the magnesium complex, although at significantly lower intensity. In the MCD spectra, the Q-band observed for the metal-containing macrocycles is associated with a very strong MCD *A*-term centered at an energy close to the energy of the observed Q-band. In the case of the metal-free compound, the Q-band region is associated with five observable *B*-terms located at 649, 628, 611, 591, and 559 nm. As expected, the Soret band is associated with the observed *A*-term centered in the 350 nm region. In addition, an *A*-term has been observed in the 400-450 nm region of the MCD spectrum. This term is associated with the absorption centered in this region. In general, the Q-band in compounds **2**, **4-6** is blue-shifted compared to the phthalocyanine analogs which is typical of tetrapyrazinoporphyrazino complexes. In the case of the red-colored open trimer **3**, the UV-Vis spectrum consists of strong absorption in the 450-560 nm region and has characteristic vibronic structure. No detectable MCD spectrum was observed for the trimer as it has no macrocycle structure. No fluorescence has been observed for the open-shell vanadyl complex, while the fluorescence of the titanyl, magnesium, and metal-free compounds are shown in Figure 3.1 along with the fluorescence spectrum of the open-chain trimer. These spectra, collected using a Horiba Scientific QM-8075-11-C spectrofluorometer, are typical for tetrapyrazinoporphyrazino compounds and other chromophores and are mirror images of the lowest energy absorption bands. High resolution mass spectra run at UT-Knoxville's Biological and Small Molecule Mass Spectrometry Core using a Waters MALDI-TOF SYNAPT G2-Si spectrometer of all compounds are in good agreement with their expected formulas (Figures 3.2-

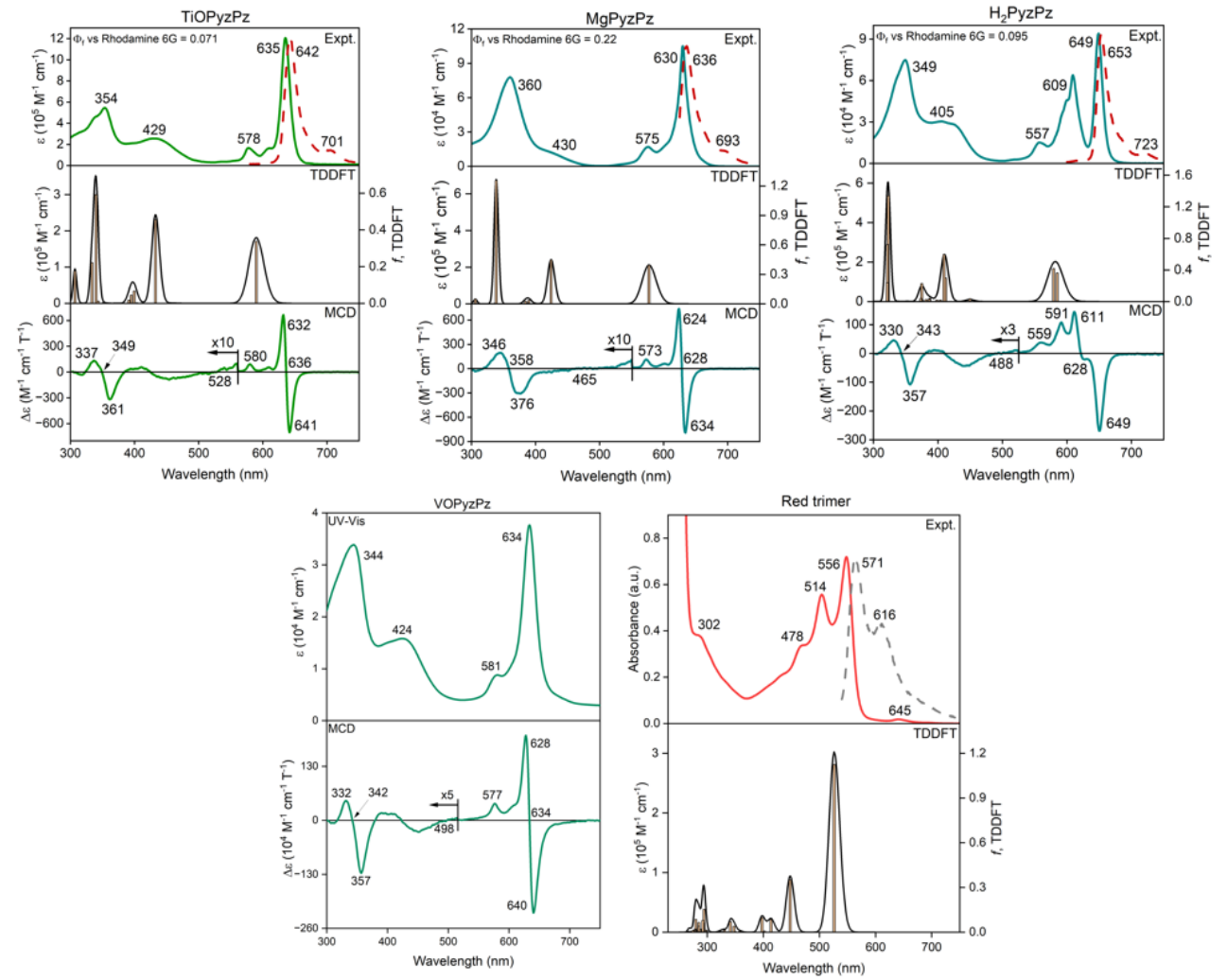

Figure 3.1. Experimental UV-Vis (solid), MCD, and fluorescence (dashed) spectra of the target compounds along with their TDDFT-predicted absorption spectra.

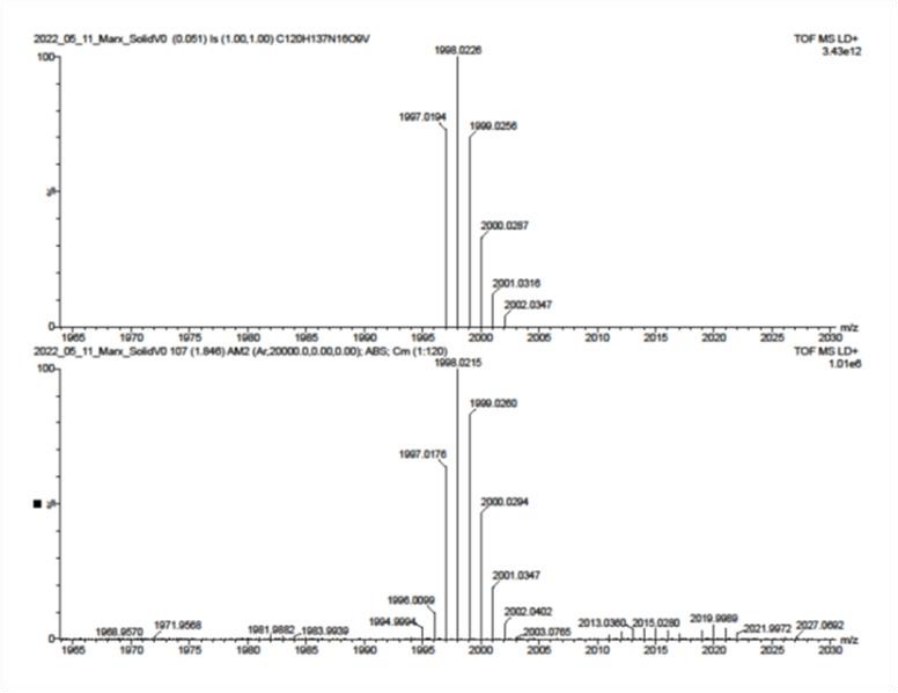

Figure 3.2. MALDI HR-MS comparison of theoretical versus experimental for **2**.

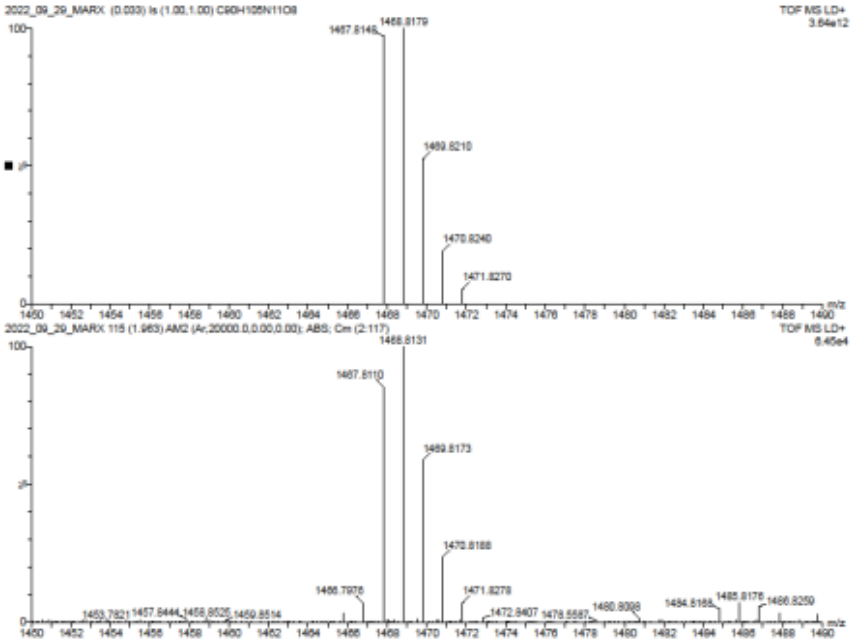

Figure 3.3. MALDI HR-MS comparison of theoretical versus experimental for trimer **3**.

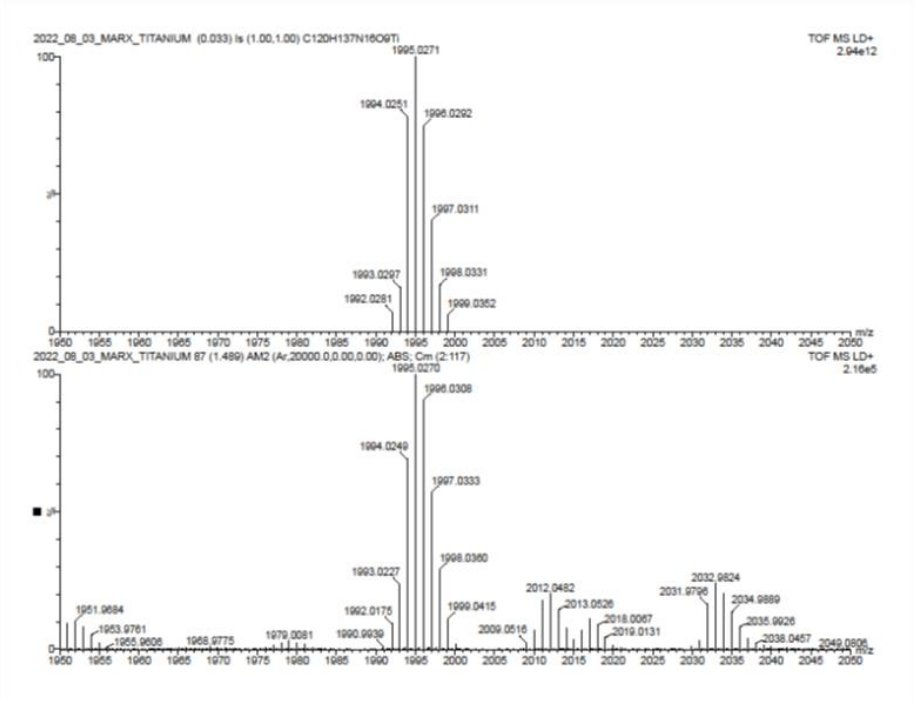

Figure 3.4. MALDI HR-MS comparison of theoretical versus experimental for **4**.

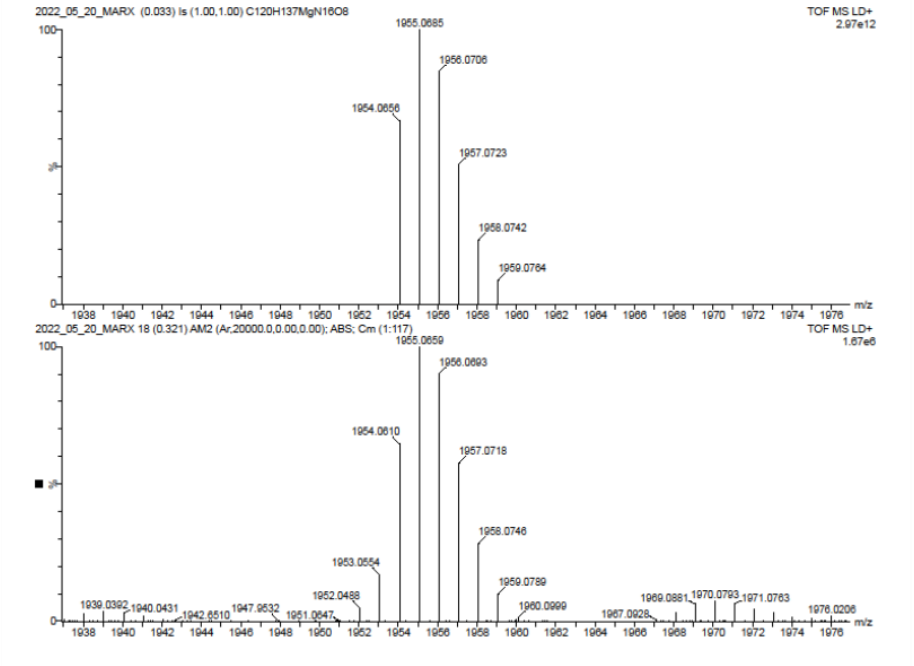

Figure 3.5. MALDI HR-MS comparison of theoretical versus experimental for **5**.

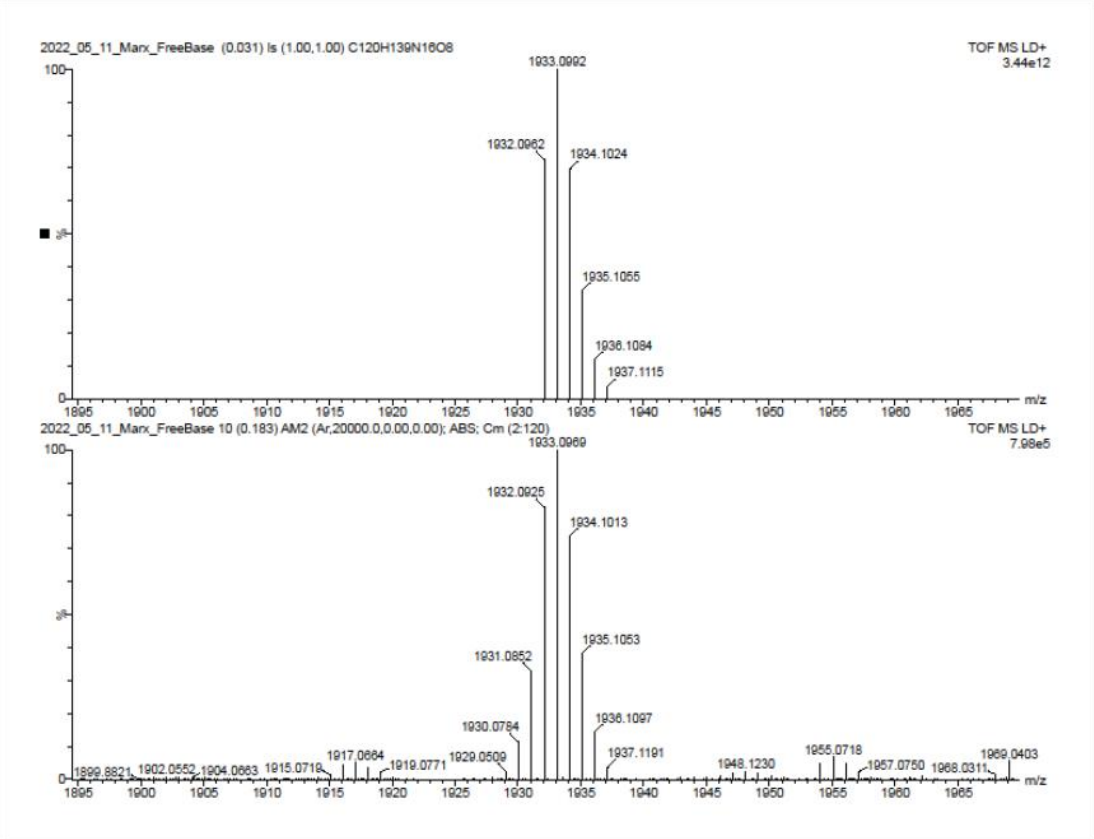

Figure 3.6. MALDI HR-MS comparison of theoretical versus experimental for **6**.

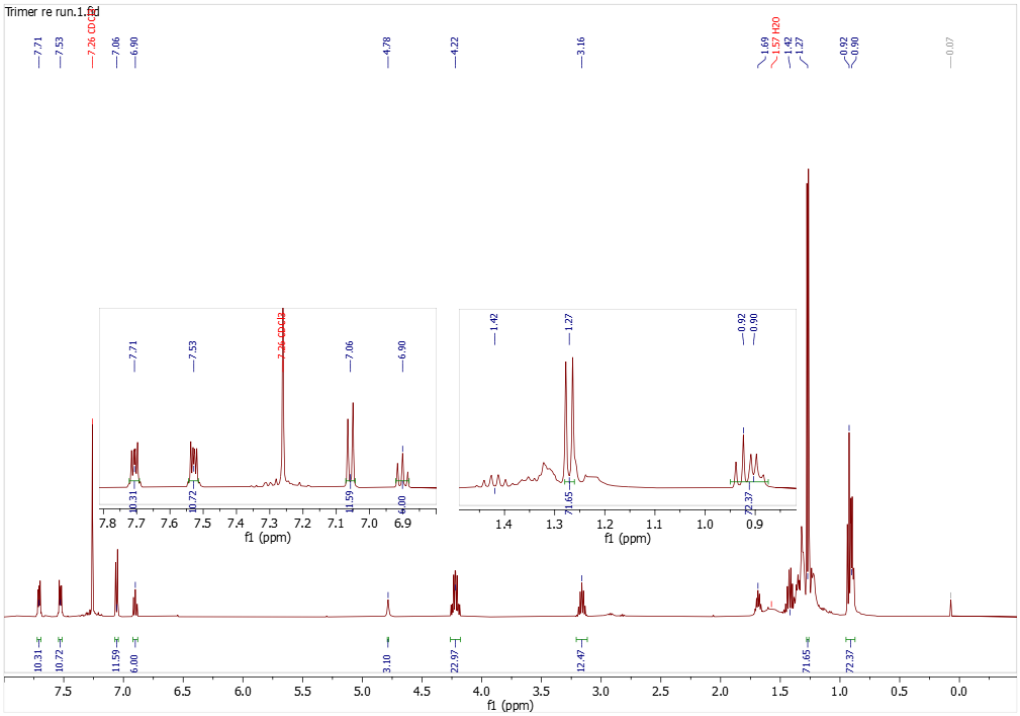

Figure 3.7. ^{1}H NMR (500 MHz) of trimer **3** in $CDCl_3$.

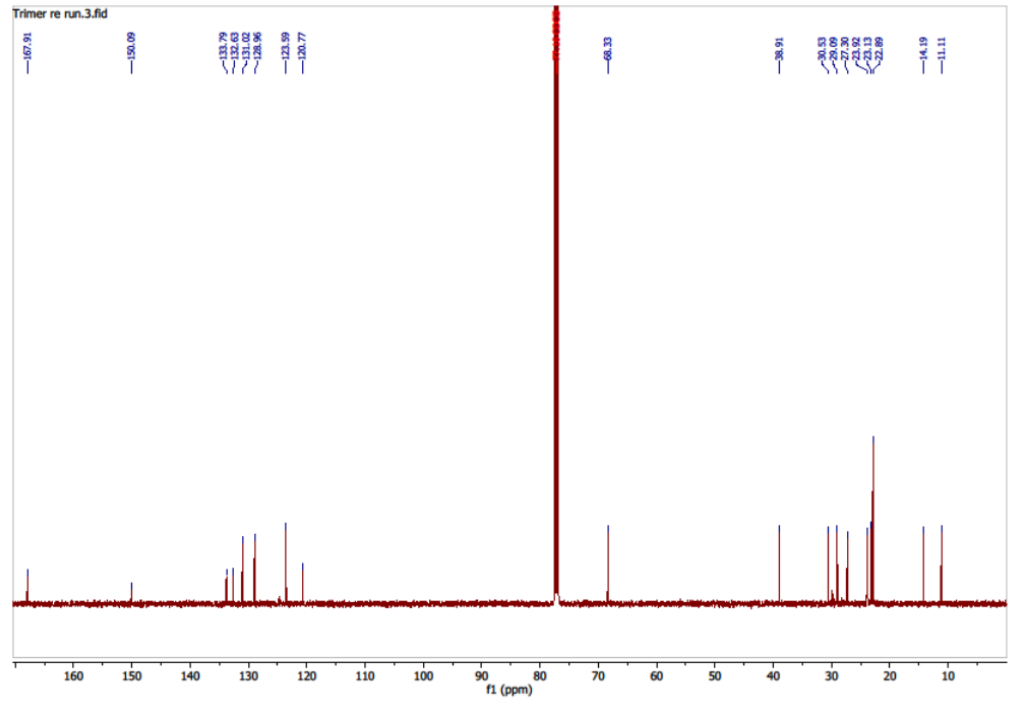

Figure 3.8. $^{13}C\{^{1}H\}$ NMR (125 MHz) of trimer **3** $CDCl_3$.

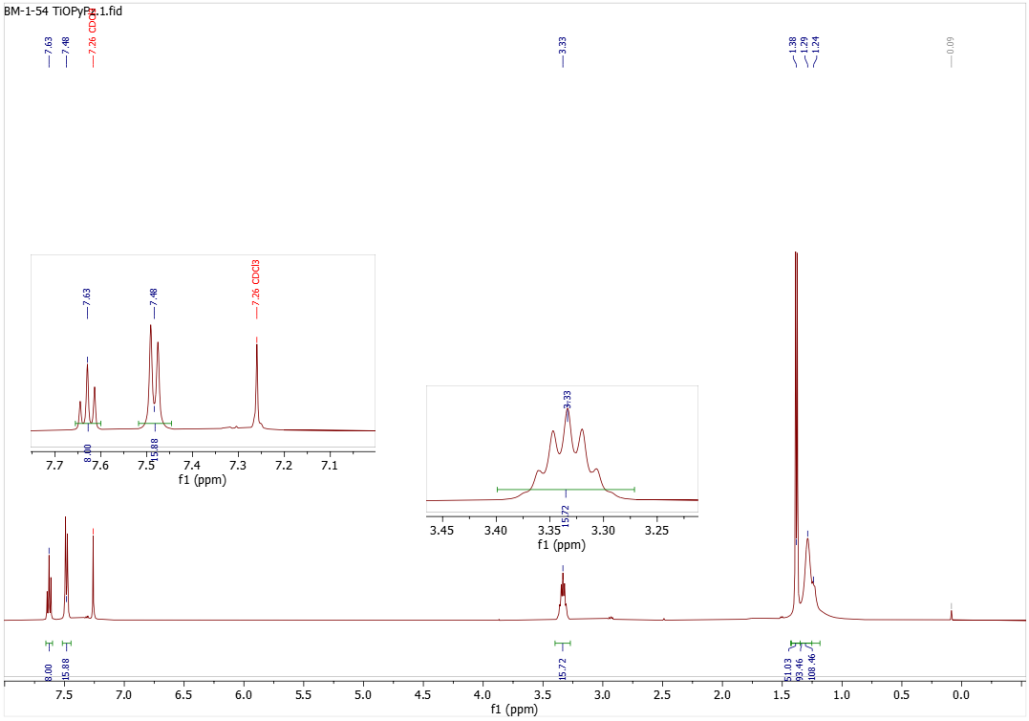

Figure 3.9. ^{1}H NMR (500 MHz) of **4** in $CDCl_3$.

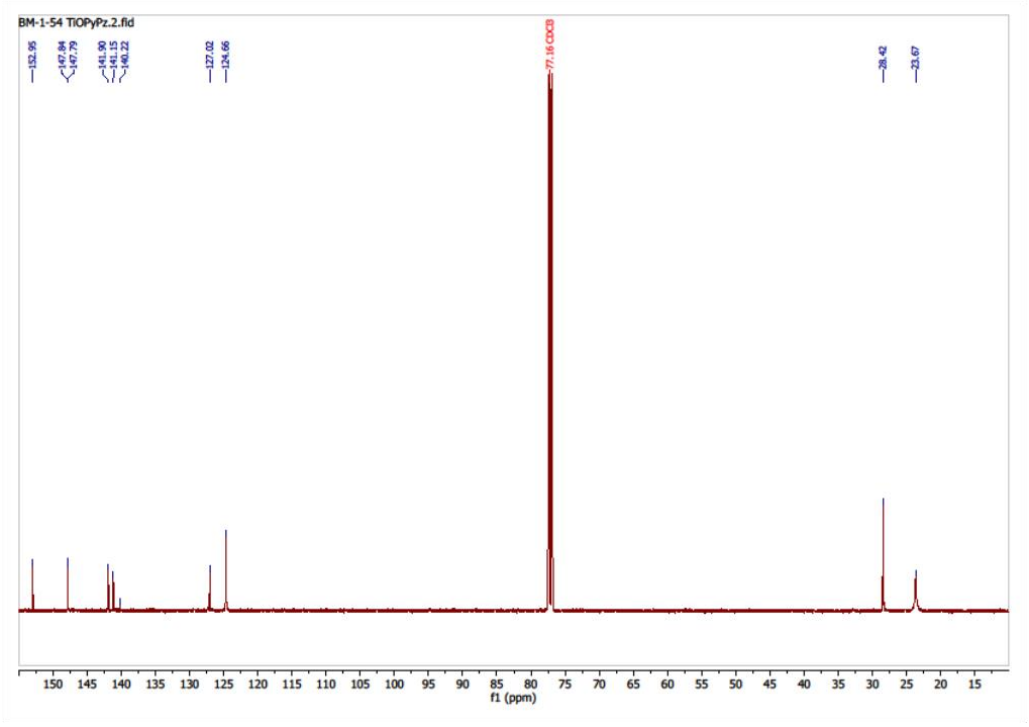

Figure 3.10. $^{13}C\{^{1}H\}$ NMR (125 MHz) of **4** in $CDCl_3$.

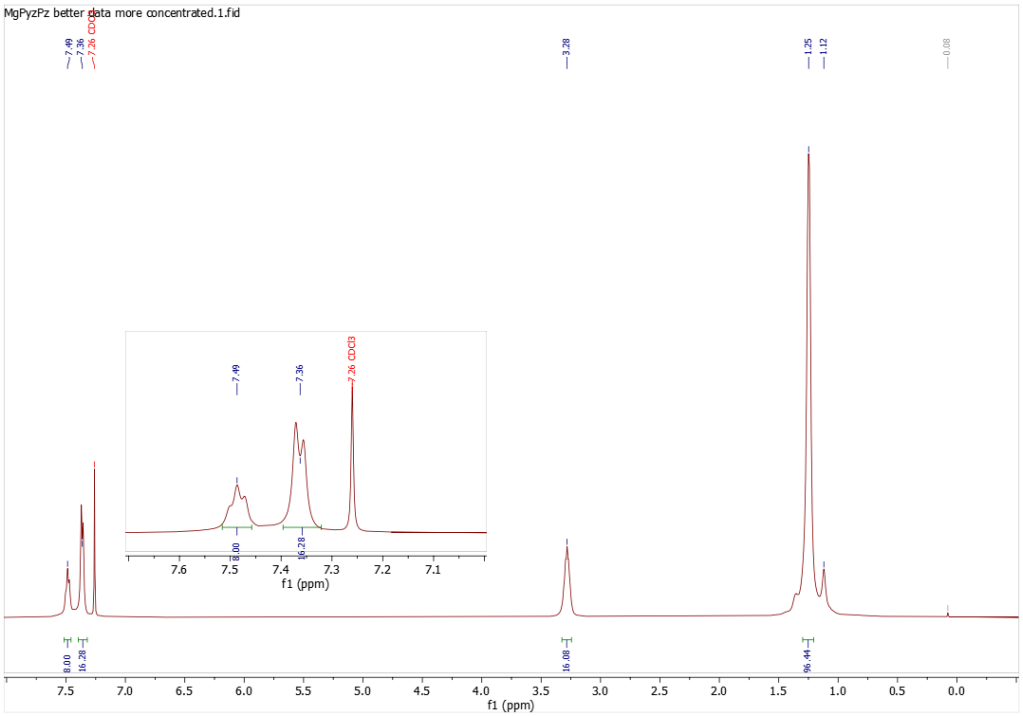

Figure 3.11. ^{1}H NMR (500 MHz) of **5** in $CDCl_3$.

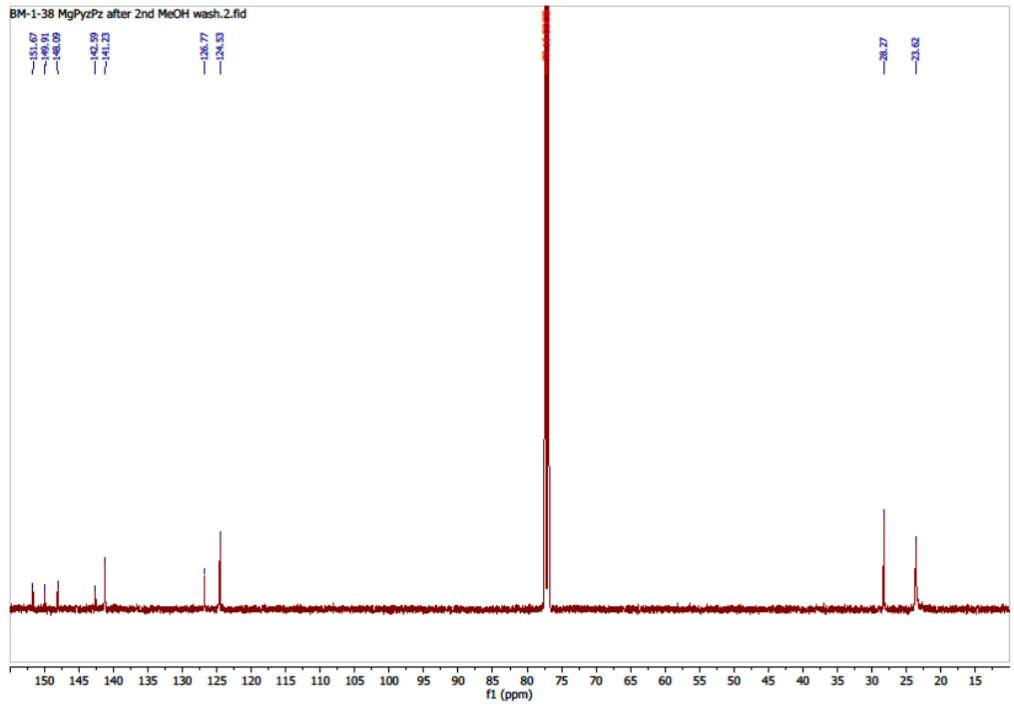

Figure 3.12. $^{13}C\{^{1}H\}$ NMR (125 MHz) of **5** in $CDCl_3$.

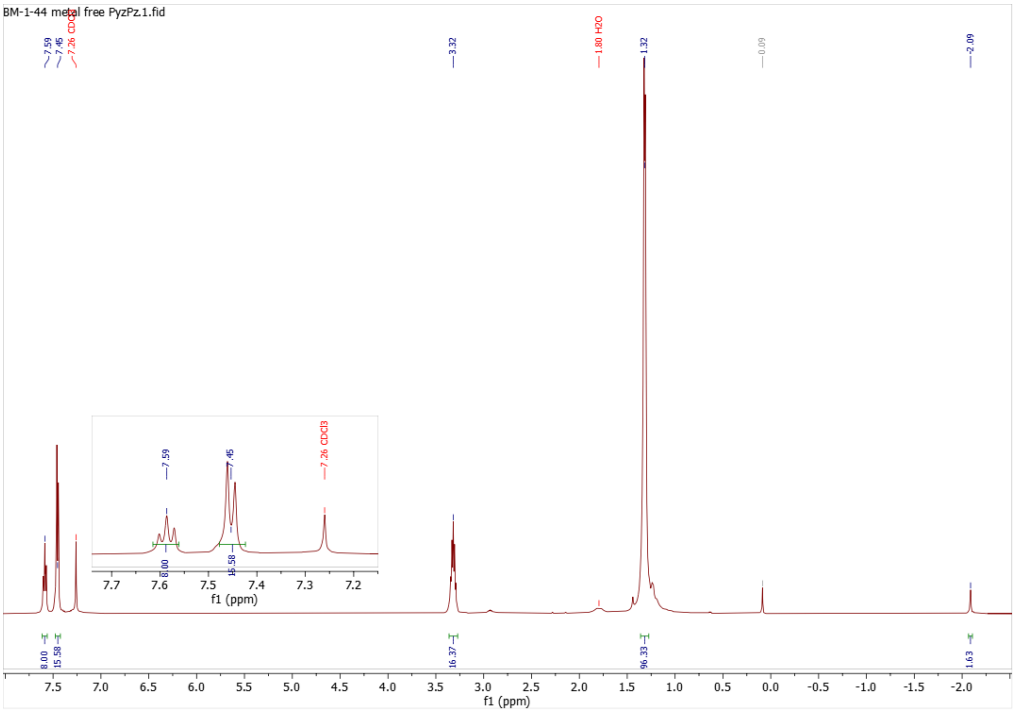

Figure 3.13. ^{1}H NMR (500 MHz) of **6** in $CDCl_3$.

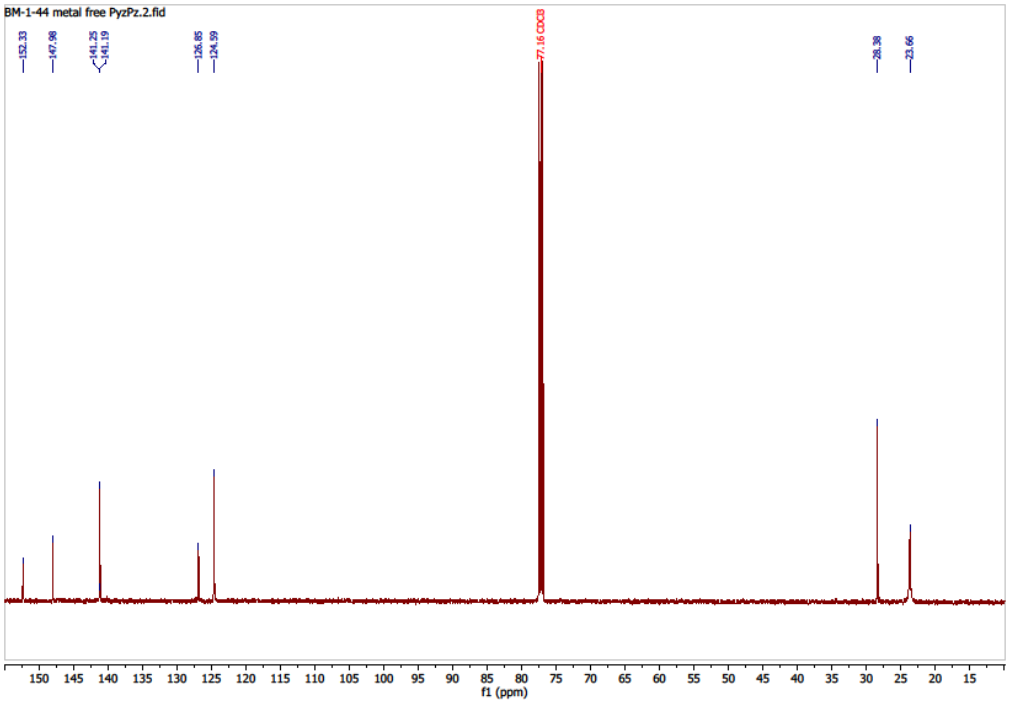

Figure 3.14. $^{13}C\{^{1}H\}$ NMR (125 MHz) of **6** in $CDCl_3$.

3.6). ^{1}H NMR spectra of the titanyl, magnesium, metal free compounds show the expected patterns for all protons although the methyl groups for the titanyl complex were found to be diastereotopic (Figures 3.7, 3.9, 3.11, 3.13). ^{13}C NMR spectra (Figures 3.8, 3.10, 3.12, 3.14) for all prepared compounds agree with their associated structures. NMR spectra were obtained using a Bruker AVANCE NEO 500 MHz spectrometer. The ^{1}H and ^{13}C NMR spectra of the red trimer were complicated by the asymmetric nature of this compound. The EPR spectrum of vanadyl complex **2** is shown in Figure 3.15. As expected, it has an axial symmetry and parameters that correlate well with the s = ½ $(d_{xy})^1$ electronic configuration of this complex (g_L = 1.98, g_I = 1.96). ATR-IR spectra of all macrocycles are given as well in Figures 3.16-3.19. It is interesting to point out that the number of intense transitions in the IR spectra are rather small, which is indicative of the high symmetry and conformational rigidity of these compounds. The V=O stretch in the reported spectrum of **2** is assigned based on the work of Binnemans and coworkers.[48]

Single-crystal X-ray crystallography

The X-ray crystal structures of the vanadyl complex and linear red trimer are shown in Figure 3.21. The unit cell of the vanadyl complex **2** is isostructural with the iron and cobalt analogs previously reported by McKeown and coworkers.[49, 50] It crystalizes from DCM and methanol in orthorhombic primitive cells with a length of 37.26760(6) Å. The nanopore structure of vanadyl complex **2** consists of tetrapyrazinoporphyrazine dimers whose metal-metal distance between dimers is 10.91941 Å. Each monomeric unit has the V=O fragment disordered over the tetrapyrazinoporphyrazine plane. These fragments form the nanoporous structure with walls constructed by four such dimers. The nanostructure's porous parameters are similar to the previously reported iron and cobalt analogs. Although McKeown and coauthors mention that the presence of the bidentate ligand (so-called wall ties) in the iron and cobalt structures is critical for the formation of the nanoporous walls and maintaining the stability, the lack of such bidentate ligand in our vanadyl complex indicates that the hydrophobic isopropyl group interactions can play at least as significant a role as the bidentate ligands. The large intermolecular distances of the cavity (about 3.7 nm) are critical for the application of the vanadyl and titanyl complexes in spintronics as it is expected that titanyl complex **4** will crystallize in a similar phase. The low quality of the crystal structure for the red trimer **3** precludes definitive elucidation of the terminal groups. However, the ^{13}C NMR spectrum of **3** has a clear signal at 167.91 ppm, while the crystallo-

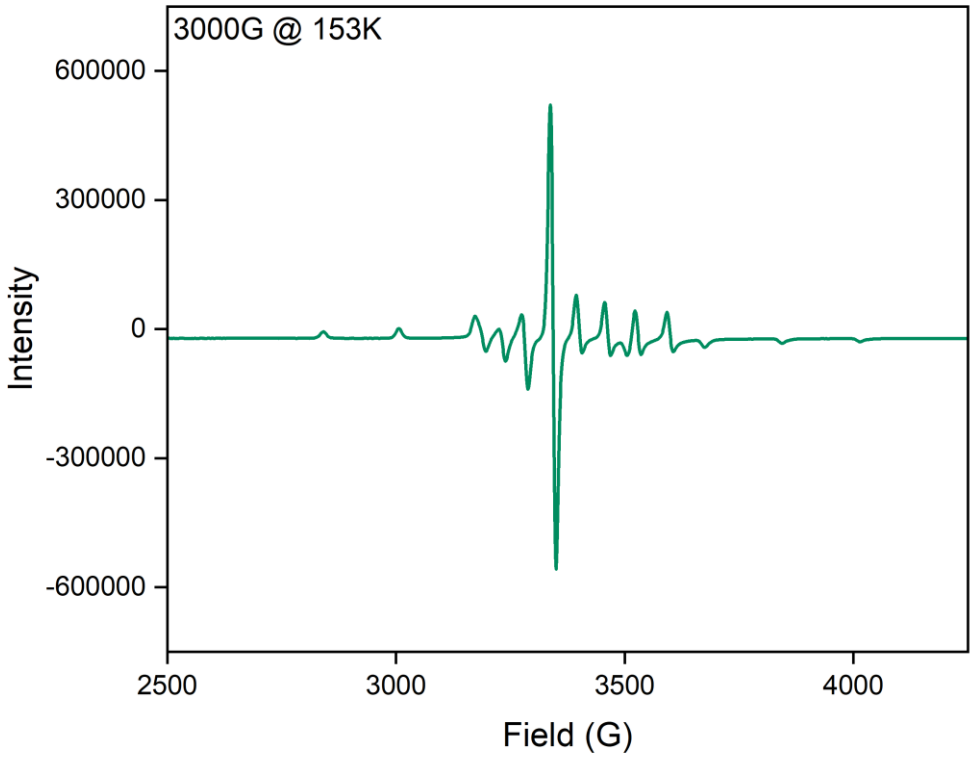

Figure 3.15. EPR spectrum of vanadyl complex **2** in frozen solution (DCM:THF 50/50 v/v) at 153 K.

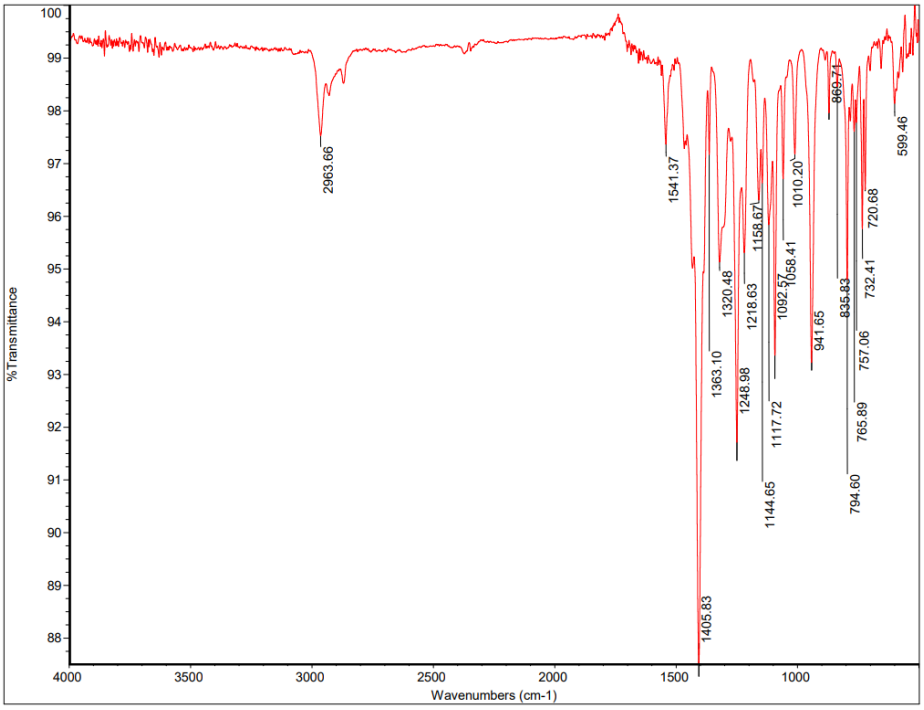

Figure 3.16. IR spectrum of vanadyl complex **2**.

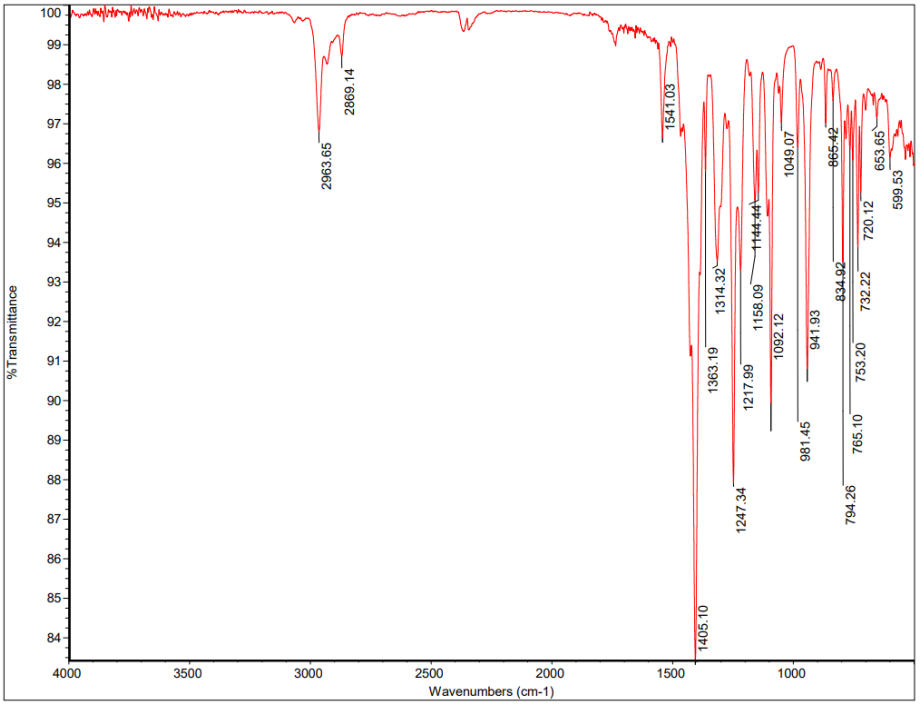

Figure 3.17. IR spectrum of titanyl complex **4.**

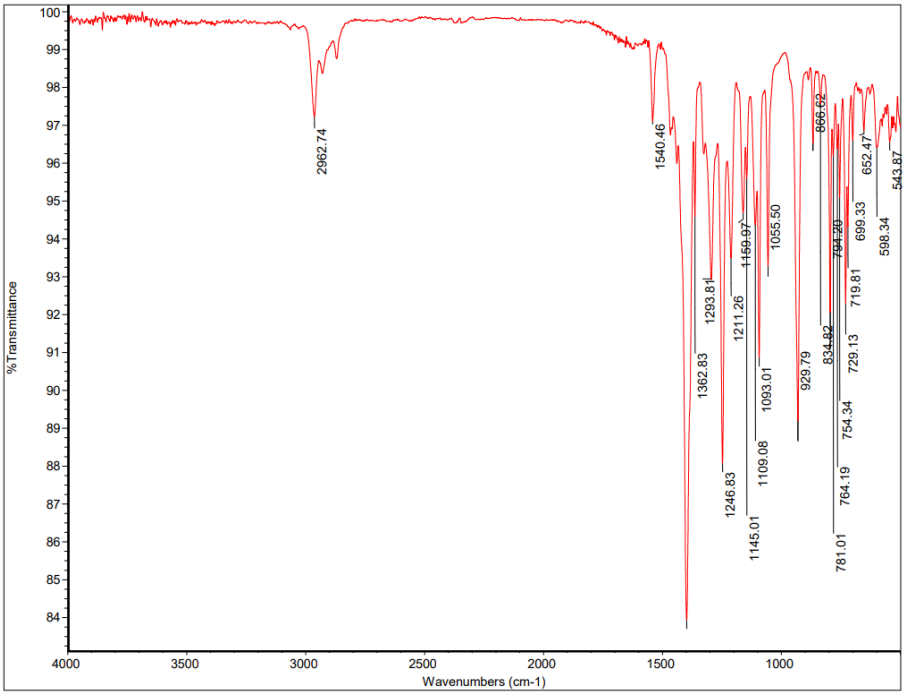

Figure 3.18. IR spectrum of magnesium complex **5**.

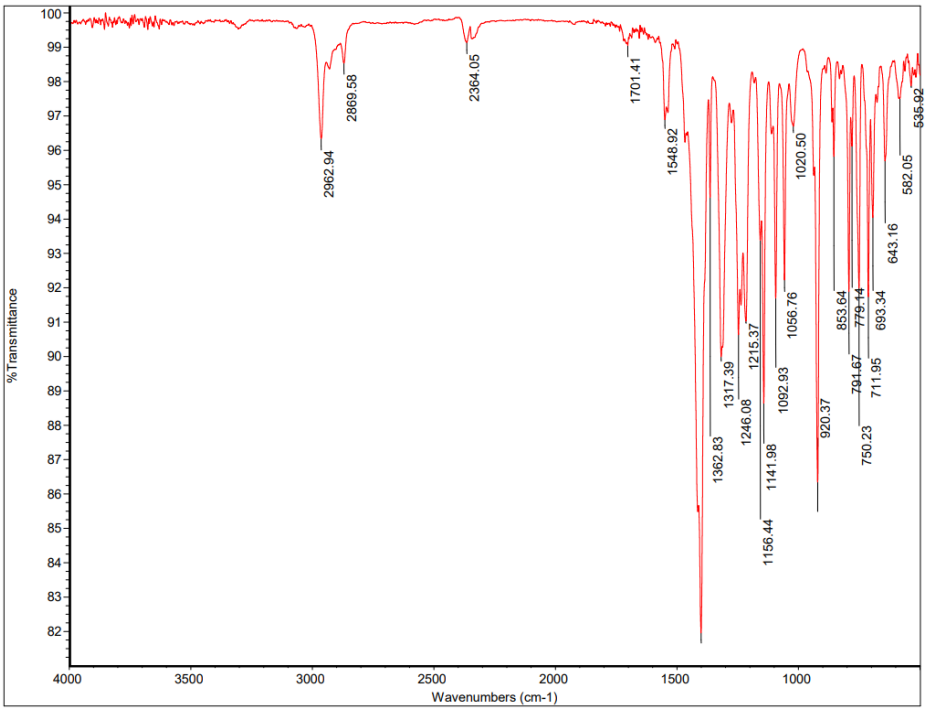

Figure 3.19. IR spectrum of metal free complex **6**.

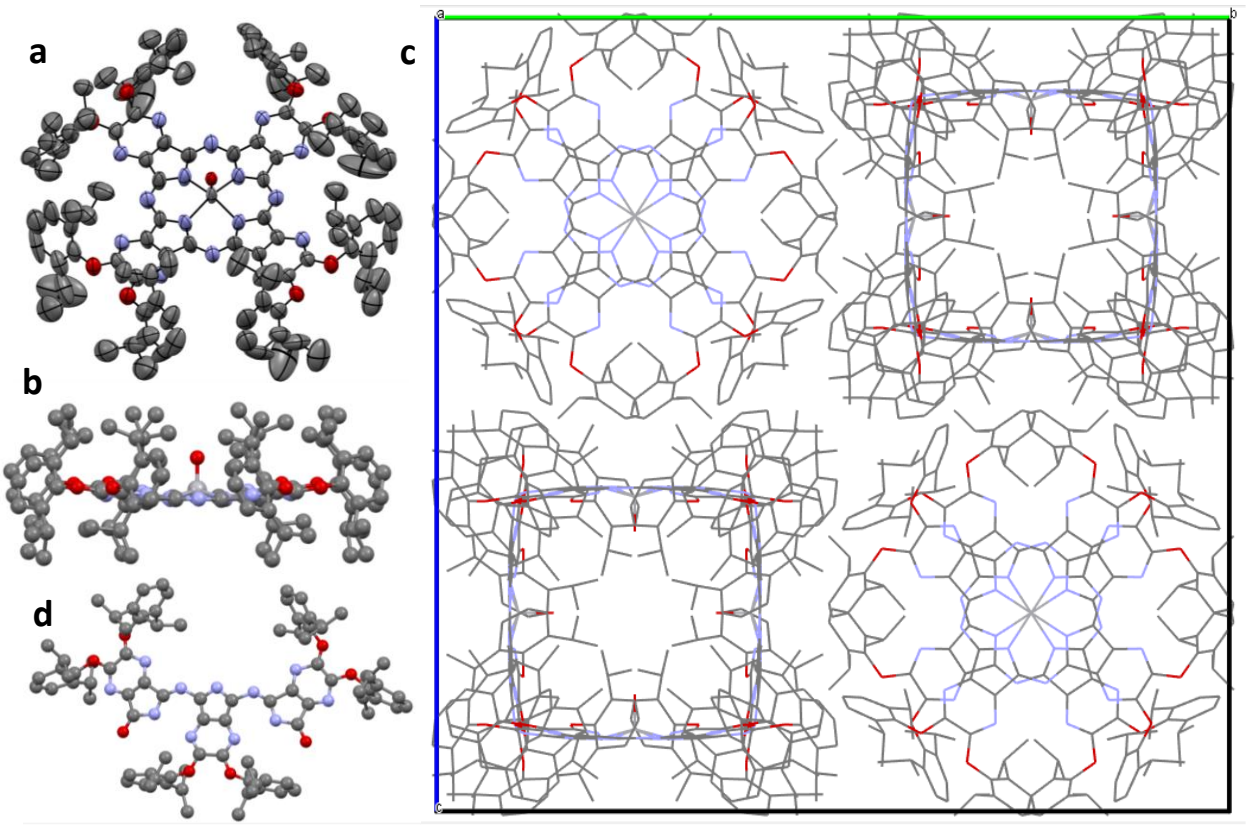

Figure 3.20. X-ray crystal structure of vanadyl complex **2** (a-c) and trimer **3** (d); (a): top view of **2**: (b): side view of **2**; (c): packing diagram for **2**.

Table 1. Legend for X-ray crystal structures in Figure 3.21.

Atom	*Color*
Carbon/Hydrogen	Dark gray
Metal center	Light gray
Nitrogen	Light blue
Oxygen	Red

graphically determined C=O bond distance is ~1.20 Å, which is characteristic for C=O double bonds rather than an imine group. From a molecular connectivity point of view (Figure 3.21d), it is clear that the driving force for the formation for the red trimer is the presence of strong hydrogen bonds between N-H fragments of the outer subunits and the pyrazine nitrogen atoms located in the central subunit.

Redox properties

The redox properties of all new macrocyclic compounds have been studied by cyclic voltammetry (CV) and differential pulse voltammetry (DPV) methods (Figure 3.22) with the numerical values shown in Table 2. In all cases one oxidation and two reduction processes have been observed. The reduction processes were found to be reversible. On the electrochemical scale, the oxidation of magnesium, metal free, and titanyl complexes are reversible, while the vanadyl complex seems to be partially irreversible. All of these redox events are of an organic nature and occur on the macrocycle as opposed to the metal center. In order to elucidate the spectroscopic signatures of the redox active species of all macrocyclic compounds of interest, spectroelectrochemical experiments were conducted along with chemical oxidations as presented in Figures 3.23-3.26. Chemical oxidation was accomplished using nitrosonium tetrafluoroborate ($NOBF_4$) and the reduction back to a neutral state by triethylamine (TEA). In the case of the lone oxidation process, the spectroelectrochemical experiments were indicative of the high reversibility. During the oxidation of all species, the intensity of the Q-band and charge transfer band in the 420-430 nm region decreases while a new band in the 660-670 nm region appear in the spectra, indicating oxidation occurs at the phenoxy substituents and pyrazinoporphyrazine core, respectively, of each molecule. This is correlated by TDDFT calculations (vide infra) that reveal the Q-band corresponds to π-π* transitions from the HOMO to LUMO and LUMO+1 energy levels and the charge transfer band corresponds to transitions from molecular orbitals localized on the phenoxy groups to the LUMO and LUMO+1 energy levels.

DFT and TDDFT calculations

The electronic structure and nature of the excited states in all macrocyclic complexes were probed by density functional theory (DFT) and time-dependent density functional theory (TDDFT) calculations using Gaussian 16.[51] The energy diagram of the compounds (**2-6**) and select images of their frontier orbitals are given in Figures 3.27-3.32 as well as in Table 3. First it should be

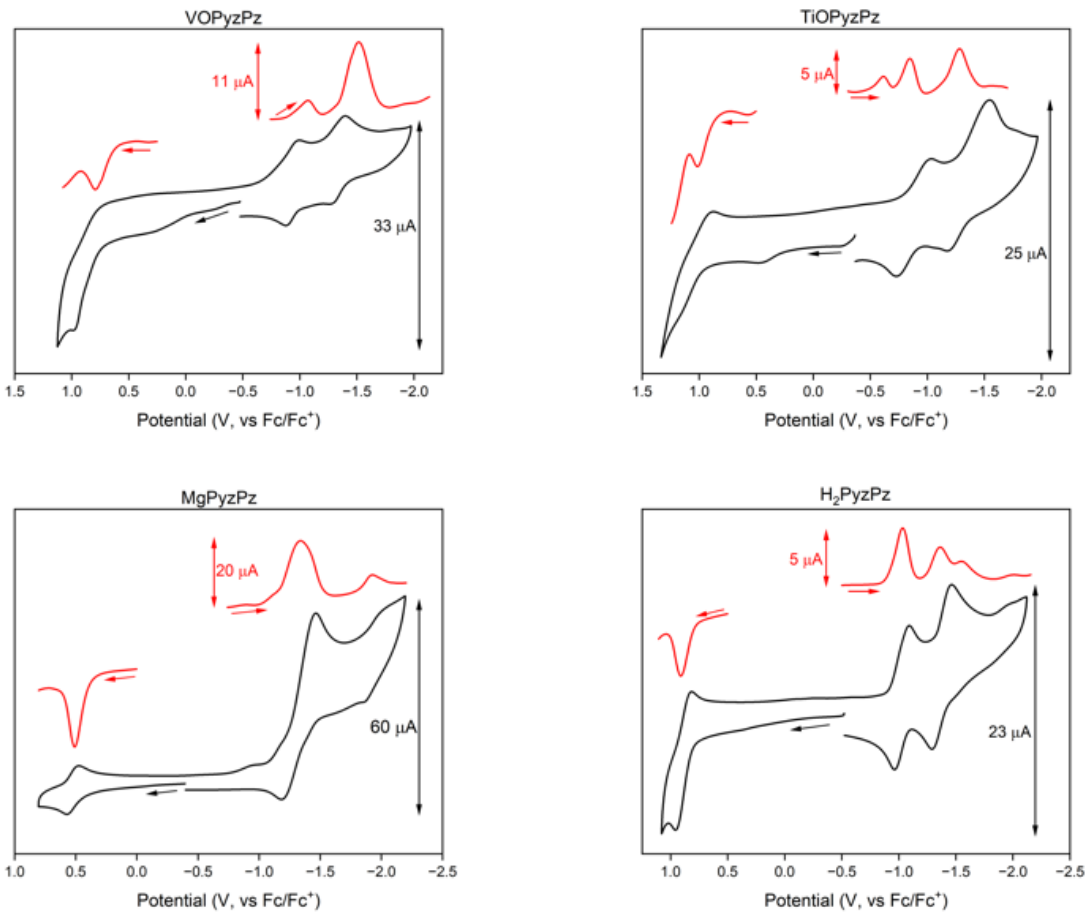

Figure 3.21. Plots of CV (black) and DPV (red) referenced to the ferrocene/ferrocenium couple for all macrocycles.

Table 2. Redox properties (DCM/0.1 M TBAP system) of the tetrapyrazinoporphyrazines.

Compound	*Redox Potential, V (Fc/Fc$^+$)*
VOPyzPz (2)	-0.97 (R_1); -1.33 (R_2); 0.87 (Ox_1)
TiOPyzPz (4)	-0.88 (R_1); -1.36 (R_2); 1.00 (Ox_3)
MgPyzPz (5)	-1.32 (R_1); -1.93 (R_2); 0.52 (Ox_1)
H_2PyzPz (6)	-1.03 (R_1); -1.38 (R_2); 0.89 (Ox_1)

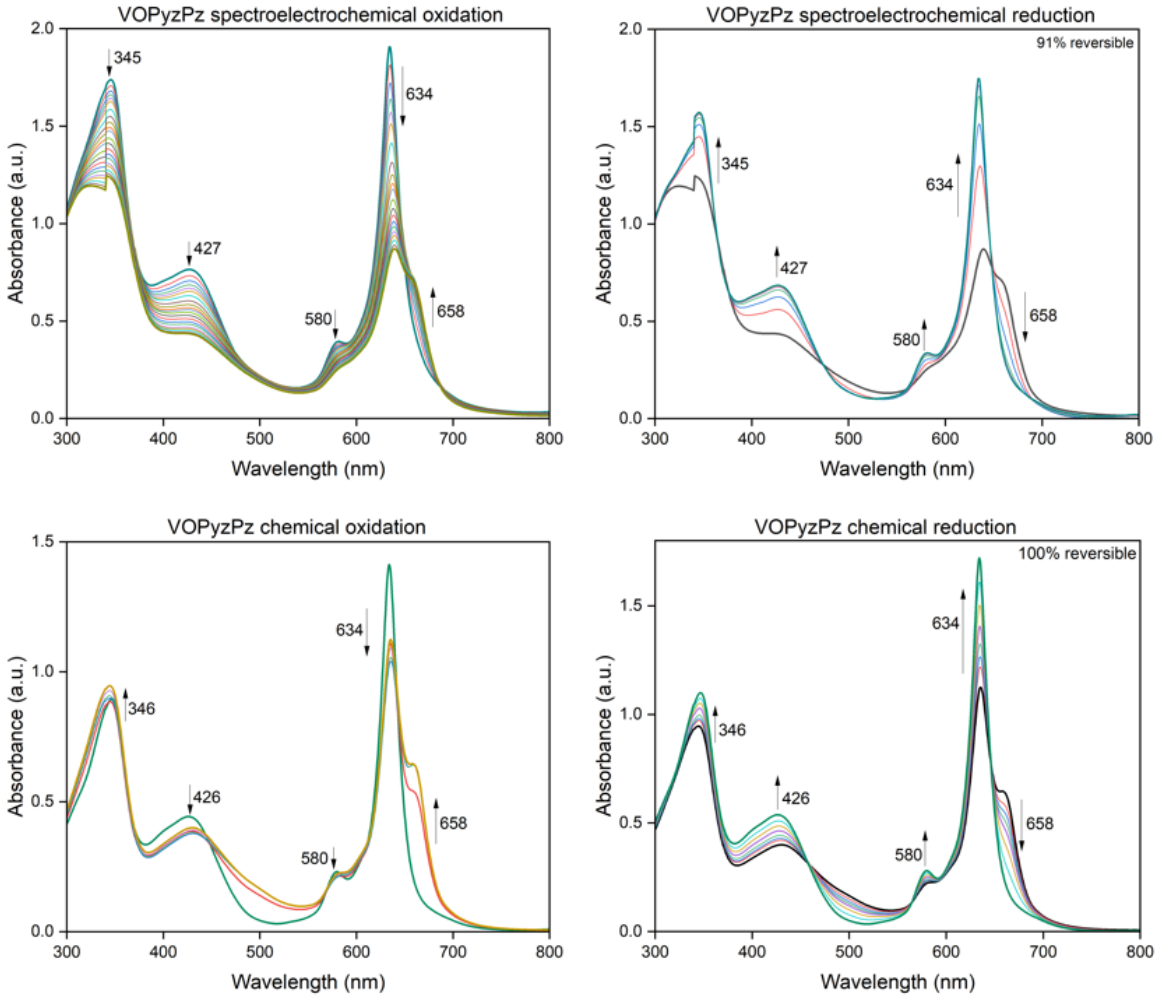

Figure 3.22. Chemical oxidation and SEC spectral transformations for vanadyl complex **2**.

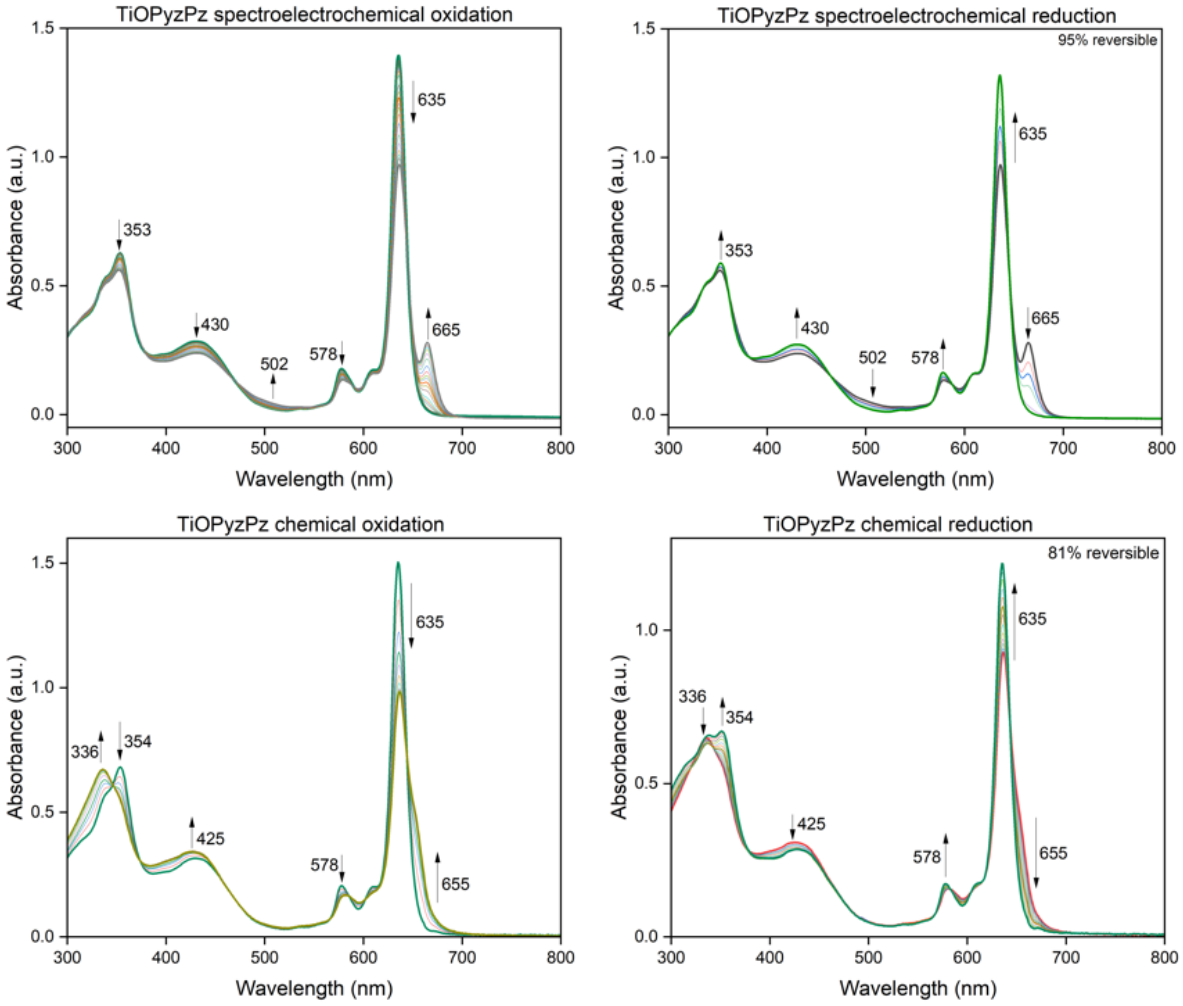

Figure 3.23. Chemical oxidation and SEC spectral transformations for titanyl complex **4**.

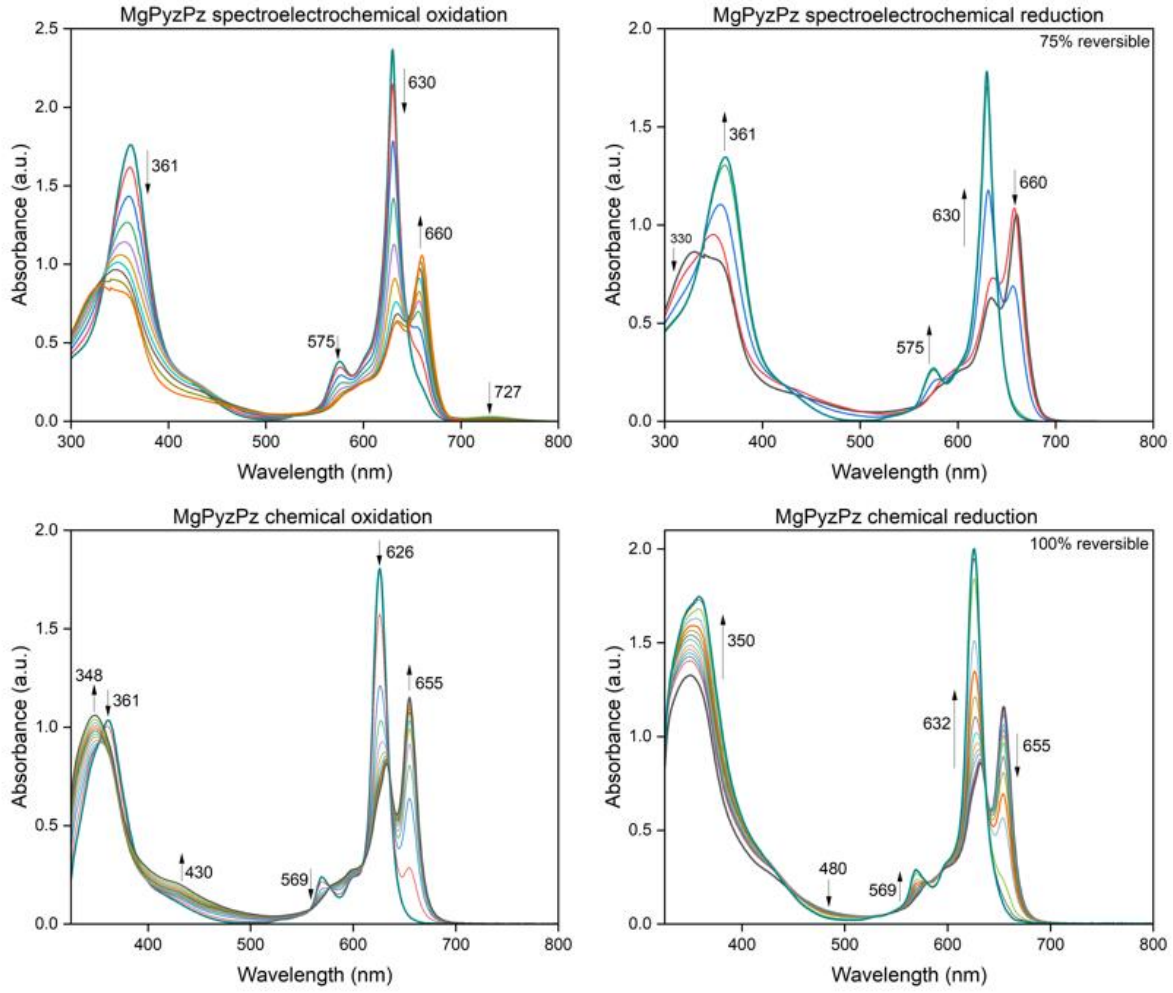

Figure 3.24. Chemical oxidation and SEC spectral transformations for magnesium complex **5**.

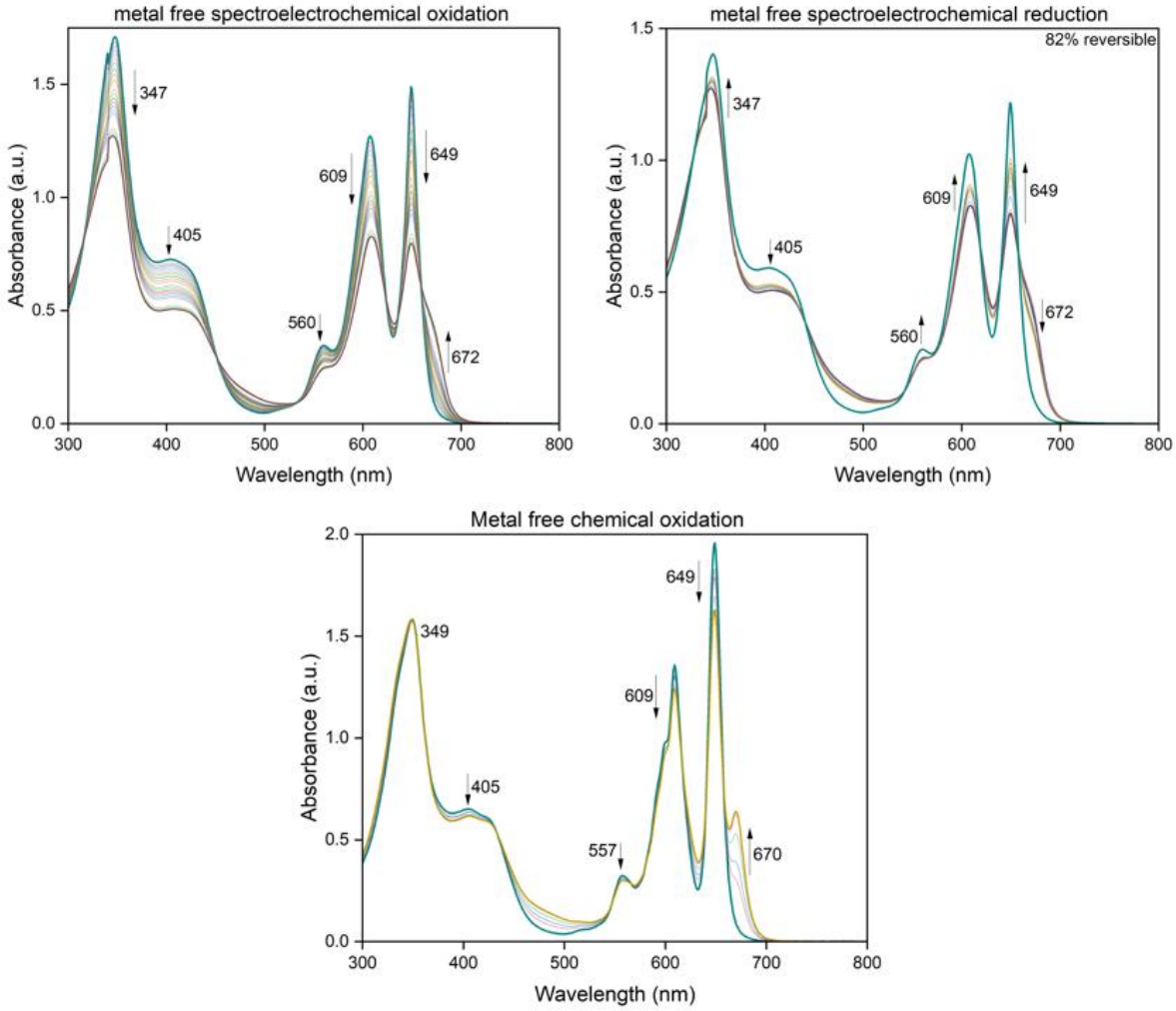

Figure 3.25. Chemical oxidation and SEC spectral transformations for metal free complex **6**.

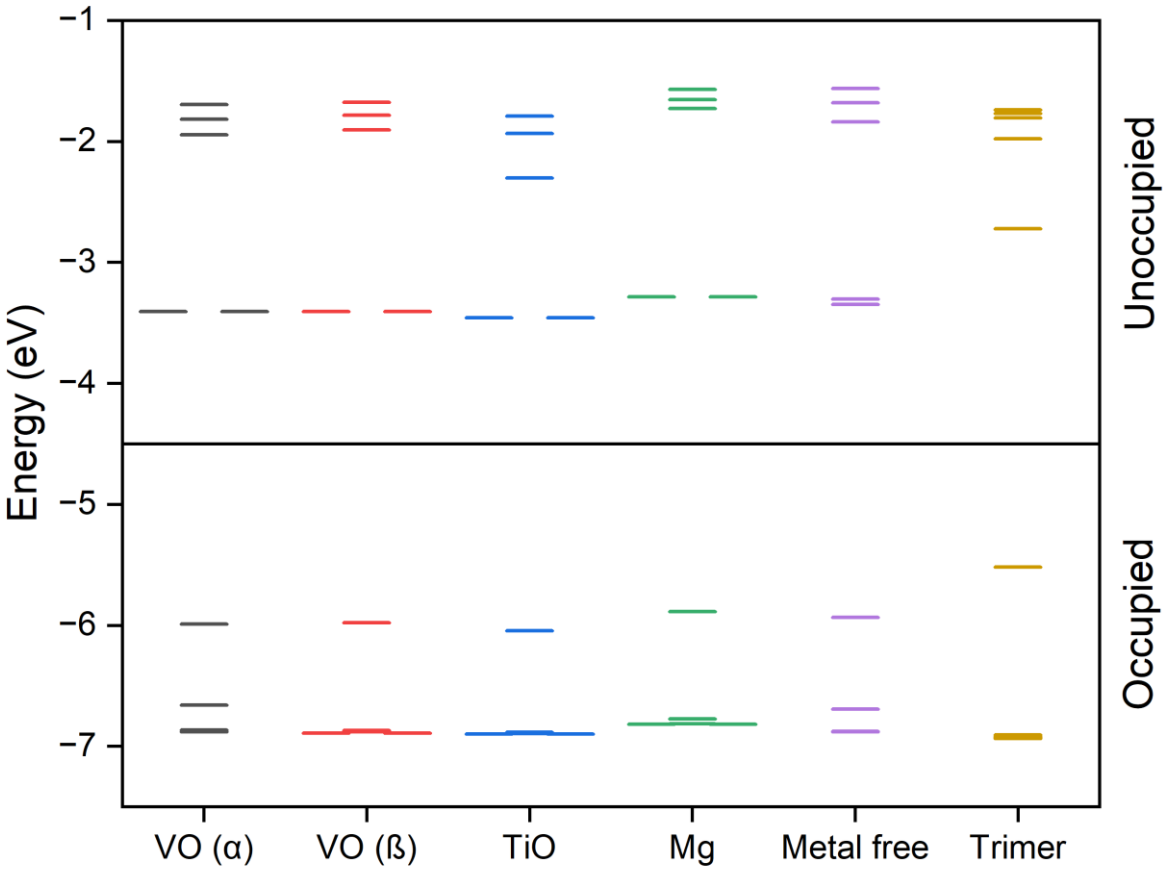

Figure 3.26. DFT-predicted (M06 functional) energy diagram for the target compounds.

a)

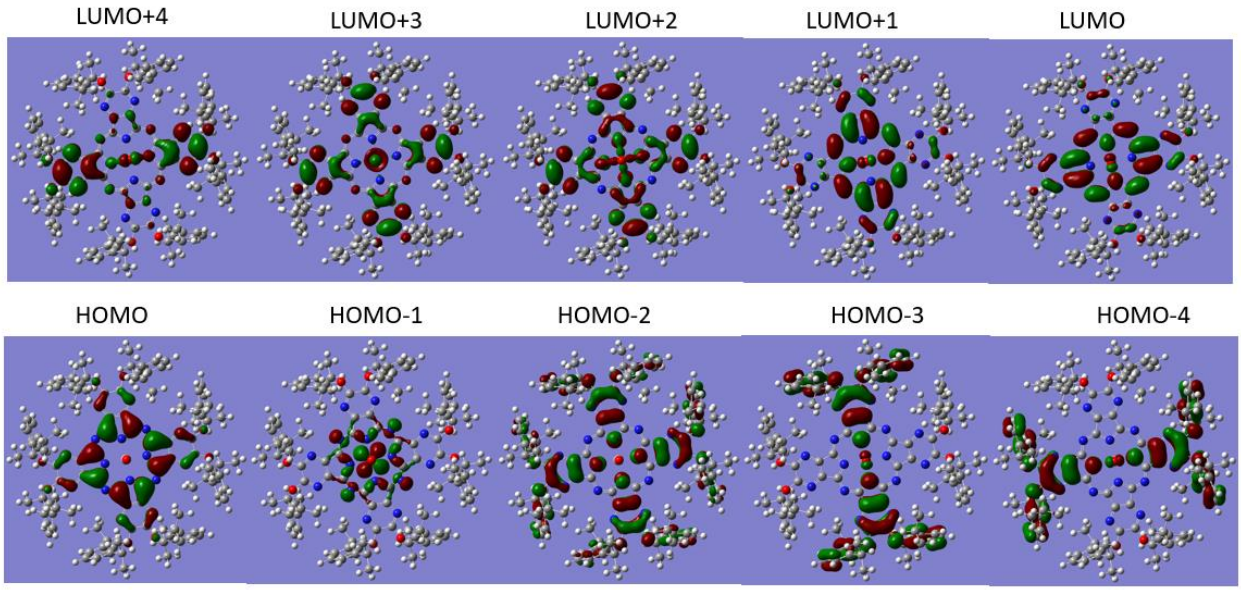

b)

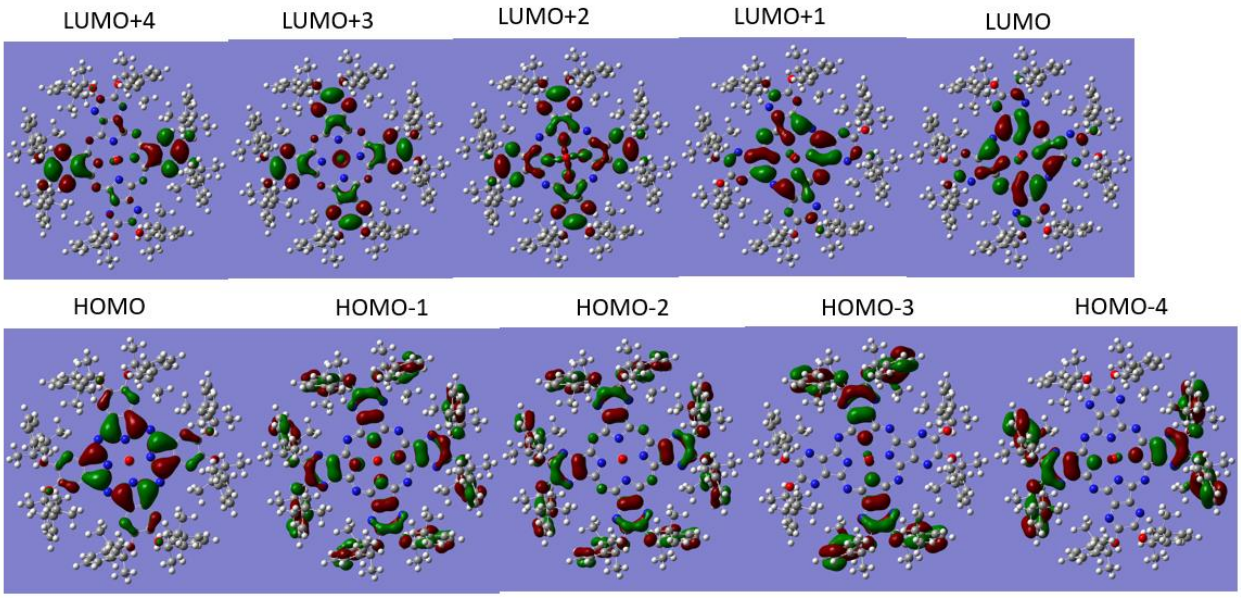

Figure 3.27. DFT-predicted (M06 functional) selected frontier MOs for vanadyl complex **2**. (a): α set; (b): β set.

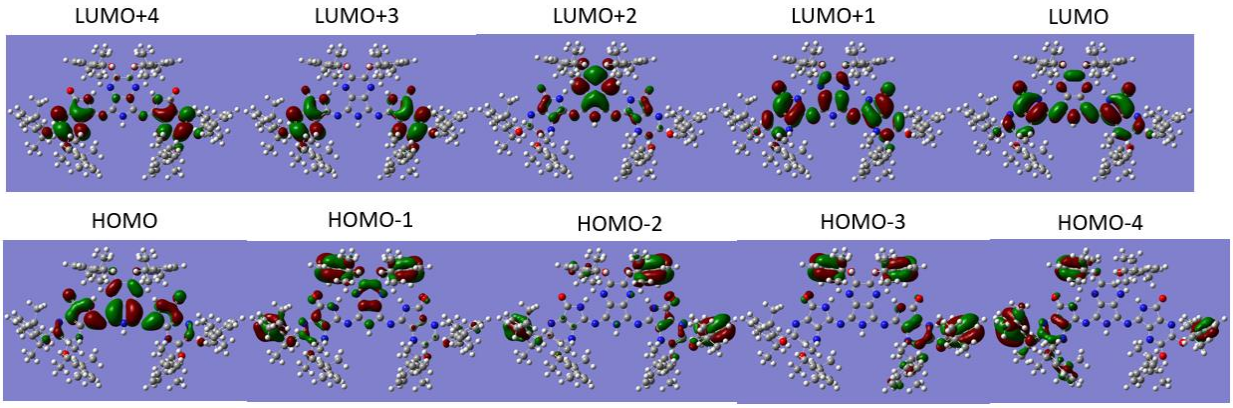

Figure 3.28. DFT predicted (M06 functional) selected frontier MOs for linear trimer **3**.

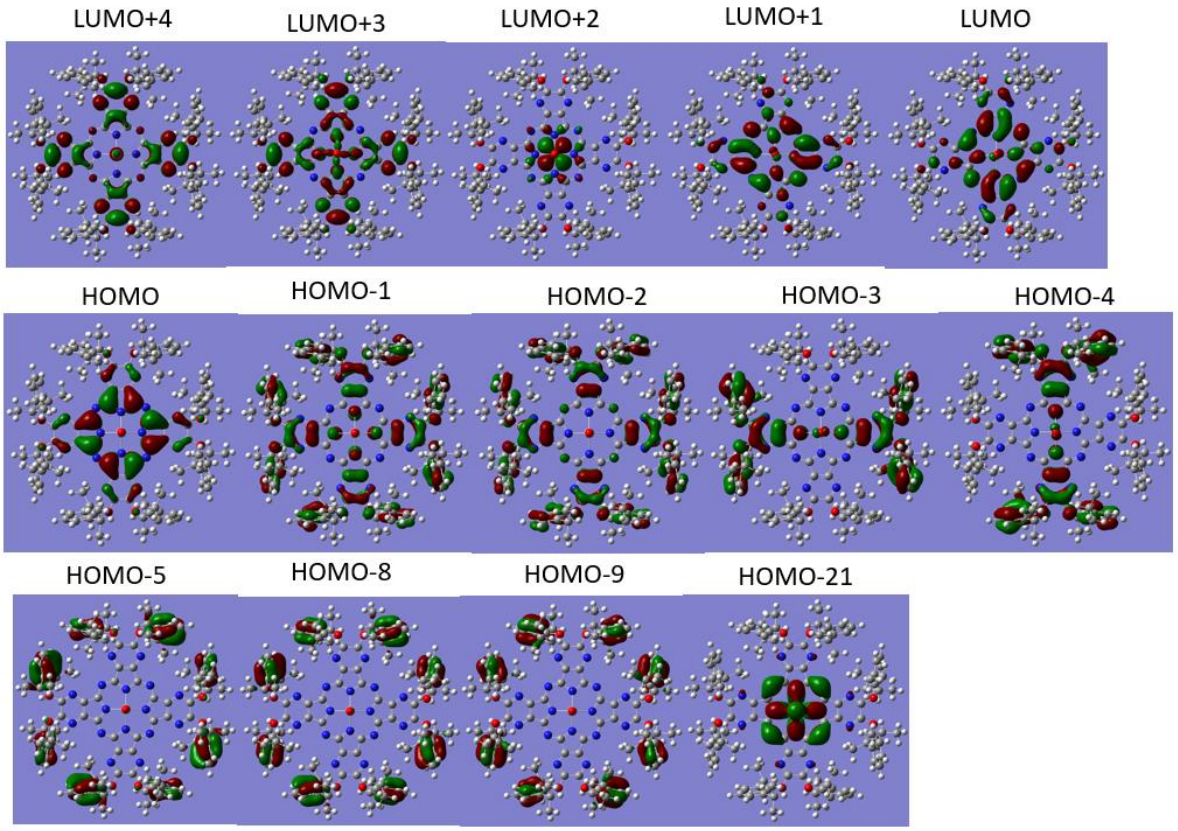

Figure 3.29. DFT-predicted (M06 functional) selected frontier MOs for titanyl complex **4**.

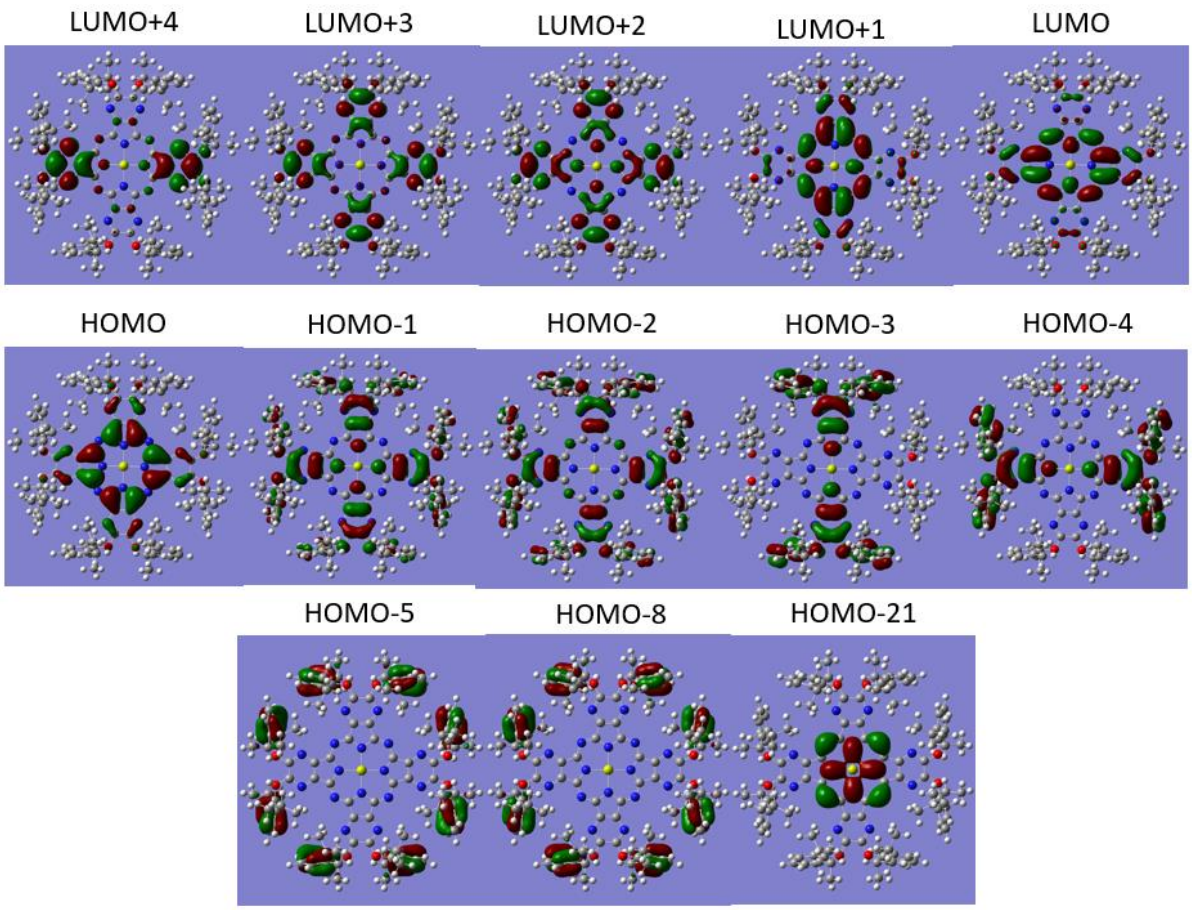

Figure 3.30. DFT-predicted (M06 functional) selected frontier MOs for magnesium complex **5**.

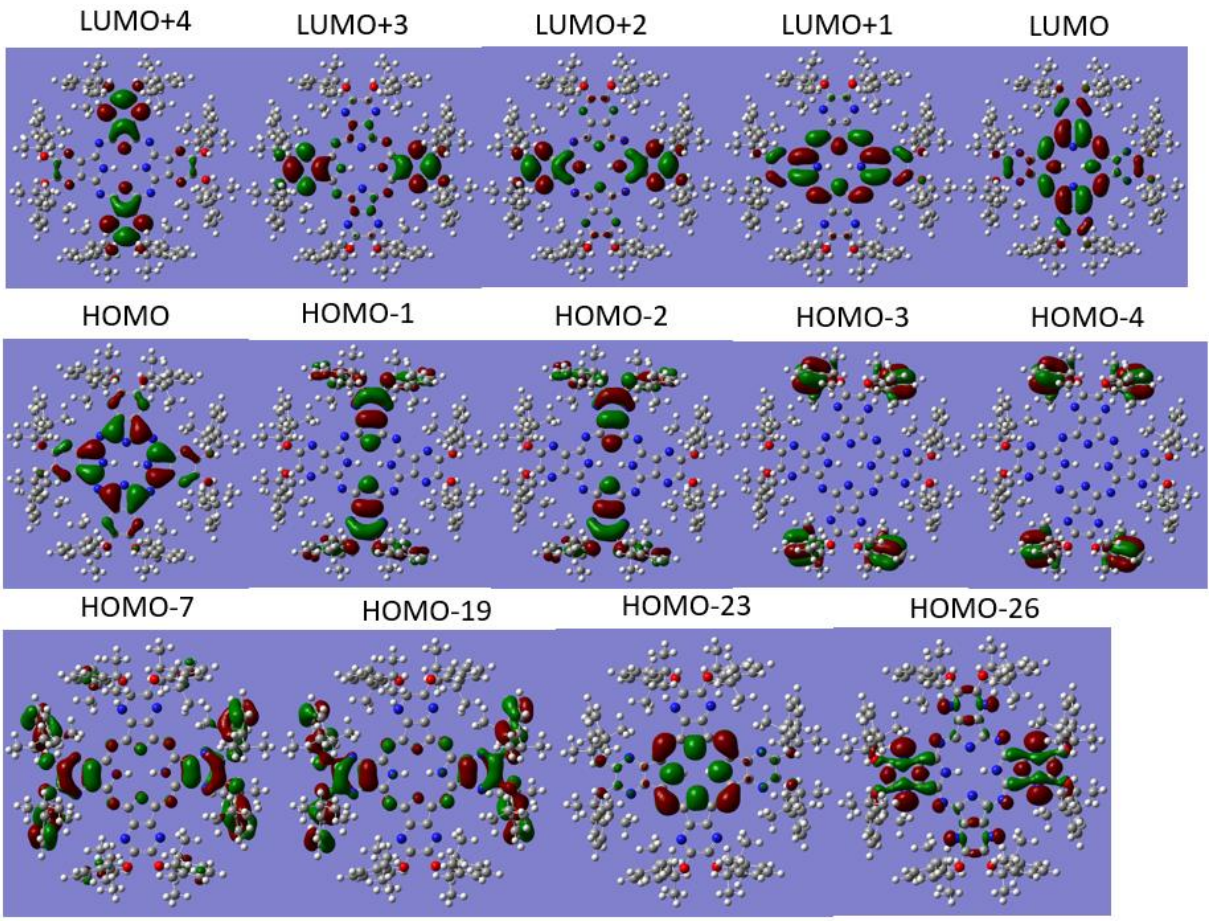

Figure 3.31. DFT-predicted (M06 functional) selected frontier MOs for metal free complex **6**.

Table 3. DFT-predicted (M06 functional) composition for the selected MOs in macrocyclic compounds **2**, **4-6**.

MO	*Energy/eV*	*% M (M=O)*	*% PyzPz Core*	*% Phenoxy*
V(O)PyzPz (α-set, 2)				
H-3	-6.882	1.24	33.98	64.78
H-2	-6.881	0.64	37.24	62.12
H-1	-6.661	62.16	36.67	1.18
HOMO	**-5.989**	**0**	**94.70**	**5.29**
LUMO	**-3.409**	**2.29**	**91.70**	**6.01**
L+1	-3.409	2.29	91.70	6.01
L+2	-1.946	3.10	66.91	29.99
L+3	-1.819	7.15	58.17	34.68
V(O)PyzPz (β-set, 2)				
H-4	-6.891	0.89	30.77	68.34
H-3	-6.891	0.89	30.77	68.34
H-2	-6.881	0.54	37.42	62.04
H-1	-6.871	0.08	36.85	63.06
HOMO	**-5.978**	**0.00**	**94.72**	**5.27**
LUMO	**-3.409**	**1.67**	**92.23**	**6.11**
L+1	-3.409	1.67	92.23	6.11
L+2	-1.905	1.10	66.79	32.11
L+3	-1.785	4.23	59.47	36.29
Ti(O)PyzPz (4)				
H-21	-7.896	11.22	86.29	2.50
H-4	-6.898	1.21	31.34	67.45
H-3	-6.898	1.21	31.34	67.45
H-2	-6.896	0.57	35.53	63.90
H-1	-6.883	0.08	35.94	63.98
HOMO	**-6.045**	**0**	**94.67**	**5.32**
LUMO	**-3.460**	**1.43**	**92.63**	**5.94**
L+1	-3.460	1.43	92.63	5.94
L+2	-2.304	57.07	42.49	0.44
L+3	-1.934	1.41	67.07	31.52
MgPyzPz (5)				
H-21	-7.666	1.74	96.44	1.82
H-4	-6.820	0	40.82	59.17
H-3	-6.820	0	40.82	59.17
H-2	-6.815	0.15	41.90	57.95
H-1	-6.776	0	48.69	51.31
HOMO	**-5.886**	**0**	**94.85**	**5.15**
LUMO	**-3.287**	**0**	**94.23**	**5.77**
L+1	-3.287	0	94.23	5.77
L+2	-1.731	0	65.67	34.33
L+3	-1.655	1.53	60.83	37.64
H_2PyzPz (6)				
H-26	-8.096		82.97	17.03
H-23	-7.786		93.03	6.97
H-19	-7.157		34.71	65.29
H-7	-6.900		34.36	65.64
H-4	-6.880		0.71	99.29

Table 3 continued.

MO	*Energy/eV*	*% M (M=O)*	*% PyzPz Core*	*% Phenoxy*
H-3	-6.877		1.23	98.77
H-2	-6.695		53.92	46.08
H-1	-6.694		54.01	45.99
HOMO	**-5.936**		**94.77**	**5.23**
LUMO	**-3.35**		**93.26**	**6.74**
L+1	-3.304		94.76	5.24
L+2	-1.839		64.68	35.32
L+3	-1.683		63.59	36.41

mentioned that all geometry optimizations, single point and TDDFT calculations, were conducted on the full structures of **2-6**. In these cases, the optimized geometry is indicative of the perpendicular orientation of 2,6-diisopropylphenoxy groups with respect to the macrocyclic plane which agrees well with all known X-ray crystal structures of this system.[49, 50, 52] In contrary, the usual truncation of the isopropyl groups from the initial structure of **2-6** leads to optimized geometries in which one of the phenoxy groups become fully conjugated with the macrocycle.

Such conjugation is expected for phthalocyanines and their analogs with sterically nonhindered aromatic substituents. Thus, optimization of the full structures (**2-6**) result in reasonable geometries. The DFT predicted HOMO for complexes **2-6** resembles the Gouterman a_{1u} (in a standard D_{4h} point group notation) orbital.[53, 54, 55] The LUMO and LUMO+1 in all compounds resemble Gouterman's pair of e_g orbitals. In case of the vanadyl complex **2**, the HOMO-1 (α-set) is a vanadyl-centered d_{xy} orbital, which agrees well with the observed EPR spectrum of this compound. The classic Gouterman's a_{2u} orbital in all macrocycles is well separated from the frontier orbitals energies and was predicted to be the HOMO-21 in the metal derivatives and HOMO-23 in the metal-free **6**. However, the HOMO-2 also has a_{2u} symmetry although it has no electron density on the inner nitrogen atoms and has a substantial contribution from the phenoxy groups (vide supra). In case of the linear trimer **3**, DFT-predicted HOMO, LUMO, and LUMO+1 are delocalized over the entire π-conjugated system (Figure 3.29).

Taking into consideration the large size of the systems and necessity to use a large basis set for the prediction of the excited state properties, the TDDFT calculations were conducted only for the diamagnetic compounds. TDDFT-predicted spectra of all macrocycles agree well with the experimental data (Figure 3.1). In case of the higher symmetry titanyl and magnesium complexes **4** and **5**, TDDFT calculations predict three degenerate pairs of transitions that are responsible for the observed Q-band, ~430 nm band, and Soret band in these compounds. The first pair of transitions (Table 3) originates from the HOMO → LUMO, LUMO+1 single-electron transitions and can be easily assigned as the traditional Q-band in the classic Gouterman's four-orbital model. According to TDDFT calculations, the ~420 nm band is dominated by the HOMO-2 → LUMO, LUMO+1 single-electron transitions. The HOMO-2 in these compounds has a_{2u} symmetry but very different electron density distribution from the classic Gouterman's a_{2u} orbital. More important, this orbital has predominant (~67%) contribution from the peripheral phenoxy groups,

Table 4. Major TDDFT-predicted excited state contributions for all compounds using the M06 exchange correlation functional in the gas phase.

Excited State	*λ (nm)*	*E (cm^{-1})*	*Osc. Str., f*	*% Contributions*	*Assignment*
Open-chain trimer 3					
1	526	18996	1.124	H→L (93%)	
2	448	22331	0.3503	H→L+2 (91%)	
Ti(O)PyzPz (4)					
1, 2	593	16876	0.3375	H→L/L+1 (81%)	Q-band
9, 10	429	23336	0.4553	H-2→L/L+1 (79%)	CT
58, 59	332	30143	0.5918	H-21→L/L+1 (56%)	Soret band
MgPyzPz (5)					
1, 2	584	17131	0.3941	H→L/L+1 (90%)	Q-band
8, 9	419	23869	0.4481	H-2→L/L+1 (81%)	CT
56, 57	327	30625	1.257	H-21→L/L+1 (72%)	Soret band
H_2PyzPz (6)					
1	584	17097	0.3603	H→L+1 (87%)	Qx-band
2	579	17263	0.4161	H→L (90%)	Qy-band
7	412	24284	0.2966	H-7→L+1 (72%)	CT
9	409	24418	0.5954	H-7→L(74%)	CT
37	375	26671	0.2277	H-19→L (90%)	?
56	323	30945	1.34	H-23→L+1 (58%)	Soret band
57	322	31059	0.7202	H-23→L (58%), H-26→L+1 (23%)	Soret band
58	321	31103	0.2385	H-26→L+1 (68%), H-23→L (19%)	?

while the LUMO and LUMO+1 are almost entirely localized at the macrocycle. Thus, this pair of transitions has a significant charge-transfer (OPh → Pc) charge-transfer character. Finally, the third pair of intense transitions predicted by TDDFT calculations in the 300-350 nm spectral envelope belongs to the Soret band and dominated by the Gouterman's a_{2u} (HOMO-21) → e_g (LUMO, LUMO+1) single-electron transitions. Reduction of the effective symmetry from four-fold in the metal containing complexes **2**, **4**, and **5** to two-fold in metal-free **6** results in a larger number of allowed transitions (Table 4). Nevertheless, the Q- and Soret-bands still can be easily identified in the TDDFT calculations although the TDDFT-predicted splitting of the Q_x and Q_y bands is rather small. Finally, TDDFT predicts two intense transitions in the 400-600 nm spectral envelope for the open-chain trimer **3** (Figure 3.1). The lowest energy band is almost pure HOMO → LUMO single-electron excitation that involve all three subunits of the trimer. The second intense band is dominated by the HOMO → LUMO+2 single-electron excitation (Table 4). Since the HOMO is delocalized over all three subunits of the trimer, while the LUMO+2 has a significant localization at the central subunit, this transition has a substantial charge-transfer character.

CHAPTER FOUR
CONCLUSIONS

In this thesis, synthetic strategies for the preparation of titanyl and vanadyl tetrapyrazinoporphyrazines with eight 2,6-diisopropylphenoxy groups located at the peripheral positions of the macrocycle were introduced. Formation of a red-colored open-chain trimer was also observed at specific reaction conditions. Characterization of this compound is incomplete and will continue to be investigated using the methods typical of phthalocyanines and their derivatives. The (magneto)optical spectroscopy of the new compounds reveal the expected trends although DFT and TDDFT calculations predict substantial charge-transfer (OPh → PyzPz) character for the bands observed between 400 and 500 nm. The X-ray crystal structure of the vanadyl complex **2** is very close to those published for cobalt and iron analogues and confirms the crucial role intermolecular hydrophobic interactions play in stabilizing that system. Redox properties of the new compounds show the expected trends with observable oxidation and reduction waves. The EPR spectrum of complex **2** confirms its axial symmetry and the presence of the EPR-active d_{xy} orbital. Samples of the final target compounds **2** and **4** have been sent to the Hadt group for further EPR studies performed in either a frozen solvent glass or as a solid state dilution. It is believed the architecture designed by McKeown these compounds are modeled after will serve to overcome the challenges experienced during previous research into molecular qubits attemping to boost spin coherence times in these systems. Future work could entail changing the paramagnetic and diamagnetic metal centers, potentially further enhancing coherence effects, but as discussed and referenced in the introduction vanadyl phthalocyanines (the vanadyl ion in general) have performed quite well to date.

REFERENCES

1. Tcherniac, J.; Braun, A. On the products of the action of acetic anhydride on phthalamide. *Ber. Deut. Chem. Ges.* **1907**, *40* (2), 2709–2714.
2. Lobbert, G. Phthalocyanines. Ullmann's Encyclopedia of Industrial Chemistry. **2000**.
3. Gregory, P. Industrial Applications of Phthalocyanines. *J. Porphyrins and Phthalocyanines.* **2000**, *4* (4), 432–437.
4. Gu, D.; Chen, Q.; Tang, X.; Gan, F.; Shen, S.; Liu, K.; Xu, H. Application of Phthalocyanine Thin Films in Optical Recording. *Opt. Commun.* **1995**, *121*, 12–129.
5. TheExpressWire. Worldwide Demand For Phthalocyanine Pigments Market Is Growing At A CAGR of 4.8% By 2027 | 185 Report Pages https://www.digitaljournal.com/pr/worldwide-demand-for-phthalocyanine-pigments-market-is-growing-at-a-cagr-of-4-8-by-2027-185-report-pages (accessed 2022 -10 -21).
6. Linstead, R. P. Phthalocyanines. Part I. A New Type of Synthetic Colouring Matters. *J. Chem. Soc.* **1934**, 1016–1017.
7. Linstead, R. P.; Dent, C. E. Phthalocyanines. Part IV. Copper Phthalocyanines. *J. Chem. Soc.* **1934**, 1027–1031.
8. Edmondson, S. J.; Hill, J. S.; Issacs, N. S.; Mitchell, P. C. H. High-Pressure Conditions for Improved Synthesis of Phthalocyanines. *J. Chem Soc, Dalt. Trans.* **1990**, 1115–1118.
9. Tomoda, H.; Saito, S.; Ogawa, S.; Shiraishi, S. Synthesis of Phthalocyanines from Phthalonitrile with Organic Strong Bases. *Chem. Lett.* **1980**, 1277–1280.
10. Tomoda, H.; Saito, S.; Shiraishi, S. Synthesis of Metallophthalocyanines from Phthalonitrile with Strong Organic Bases. *Chem. Lett.* **1983**, 313–316.
11. *Handbook of Porphyrin Science*. Kadish, K., Smith, K., Guilard, R., Eds.; World Scientific: Singapore, **2019**; Vol. 45, pp. 4–6.
12. Lo, P.-C.; Rodriguez-Morgade, M. S.; Pandey, R.; Ng, D.; Torres, T.; Dumoulin, F. The Unique Features and Promises of Phthalocyanines as Advanced Photosensitizers for Photodynamic Therapy of Cancer. *Chem. Soc. Rev.* **2020**, *49* (4), 1035–1324.
13. Halaskova, M.; Rahali, A.; Almeida-Marrero, V.; Machacek, M.; Kucera, R.; Jamoussi, B.; Torres, T.; Novakova, V.; de la Escosura, A.; Zimcik, P. Peripherally Crowded Cationic

Phthalocyanines as Efficient Photosensitizers for Photodynamic Therapy. *ACS Med. Chem. Lett*. **2021**, *12*, 502–207.

14. Kim, M.; Darafsheh, A. Light Sources and Dosimetry Techniques for Photodynamic Therapy. *Photochem. and Photobiol.* **2020**, *96*, 280–294.
15. Chodos, A. December 1958: Invention of the Laser https://www.aps.org/publications/apsnews/200312/history.cfm.
16. Ladd, T. D.; Jelezko, F.; Laflamme, R.; Nakamura, Y.; Monroe, C.; O'Brien, J. L. Quantum Computers. *Nature Reviews*. **2010**, *464*, 45–53.
17. DiVincenzo, D. P. The Physical Implementation of Quantum Computation. *Fortschr. Phys.* **2000**, *48*, 771–783.
18. Fataftah, M. S.; Krzyaniak, M. D.; Vlaisavljevich, B.; Wasielewski, M. R.; Zadrozny, J. M.; Freedman, D. E. Metal–Ligand Covalency Enables Room Temperature Molecular Qubit Candidates. *Chem. Sci*. **2019**, *10* (27), 6707–6714.
19. Bader, K.; Winkler, M.; van Slageren, J. Tuning of Molecular Qubits: Very Long Coherence and Spin–Lattice Relaxation Times. *Chem. Commun*. **2016**, *52* (18), 3623–3626.
20. Atzori, M.; Tesi, L.; Morra, E.; Chiesa, M.; Sorace, L.; Sessoli, R. Room-Temperature Quantum Coherence and Rabi Oscillations in Vanadyl Phthalocyanine: Toward Multifunctional Molecular Spin Qubits. *J. Amer. Chem. Soc.* **2016**, *138* (7), 2154–2157.
21. Cimatti, I.; Bondì, L.; Serrano, G.; Malavolti, L.; Cortigiani, B.; Velez-Fort, E.; Betto, D.; Ouerghi, A.; Brookes, N. B.; Loth, S.; Mannini, M.; Totti, F.; Sessoli, R. Vanadyl Phthalocyanines on Graphene/SiC: Toward a Hybrid Architecture for Molecular Spin Qubits. *Nanoscale Horiz*. **2019**, *4* (5), 1202–1210.
22. Bonizzoni, C.; Ghirri, A.; Atzori, M.; Sorace, L.; Sessoli, R.; Affronte, M. Coherent Coupling between Vanadyl Phthalocyanine Spin Ensemble and Microwave Photons: Towards Integration of Molecular Spin Qubits into Quantum Circuits. *Sci. Rep*. **2017**, *7* (1).
23. Follmer, A. H.; Ribson, R. D.; Oyala, P. H.; Chen, G. Y.; Hadt, R. G. Understanding Covalent versus Spin–Orbit Coupling Contributions to Temperature-Dependent Electron

Spin Relaxation in Cupric and Vanadyl Phthalocyanines. *J. Phys. Chem. A.* **2020**, *124* (44), 9252–9260.

24. Kazmierczak, N. P.; Mirzoyan, R.; Hadt, R. G. The Impact of Ligand Field Symmetry on Molecular Qubit Coherence. *J. Amer. Chem. Soc.* **2021**, 143 (42), 17305–17315.
25. Novakova, V.; Donzello, M.; Ercolani, C.; Zimcik, P.; Stuzhin, P. Tetrapyrazinoporphyrazines and Their Metal Derivatives. Part II: Electronic Structure, Electrochemical, Spectral, Photophysical and Other Application Related Properties. *Coord. Chem. Rev.* **2018**, *361*, 1–73.
26. Zimcik, P.; Novakova, V.; Kopecky, K.; Miletin, M.; Uslu Kobak, R. Z.; Svandrlikova, E.; Váchová, L.; Lang, K. Magnesium Azaphthalocyanines: An Emerging Family of Excellent Red-Emitting Fluorophores. *Inorg. Chem.* **2012**, *51* (7), 4215–4223.
27. McKeown, N.; Maksheed, S.; Msayib, K.; Ooi, L.-L.; Helliwell, M.; Warren, J. A Phthalocyanine Clathrate of Cubic Symmetry Containing Interconnected Solvent-Filled Voids of Nanometer Dimensions. *Angew. Chem. Int. Ed.* **2005**, *44* (46), 7546–7549.
28. Maksheed, S.; Ibrahim, F.; Samuel, J.; Helliwell, M.; Warren, J.; Bezzu, C. G.; McKeown, N. Clathrate Formation from Octaazaphthalocyanines Possessing Bulky Phenoxyl Substituents: A New Cubic Crystal Containing Solvent-Filled, Nanoscale Voids. *Chem. Eur. J.* **2008**, *14*, 4810–4815.
29. Mack, J.; Stillman, M. J.; Kobayashi, N. Application of MCD Spectroscopy to Porphyrinoids. *Coord. Chem. Rev.* **2007**, *251* (3-4), 429–453.
30. Nevonen, D. E. Spectroscopic and TDDFT-Based Electronic Structure Analysis of Porphyrin and Phthalocyanine Derivatives, and Their Transition Metal Complexes. Ph.D. Thesis, University of Manitoba, Winnipeg, Canada, 2022.
31. Elgrishi, N.; Rountree, K. J.; McCarthy, B. D.; Rountree, E. S.; Eisenhart, T. T.; Dempsey, J. L. A Practical Beginner's Guide to Cyclic Voltammetry. *J. Chem. Ed.* **2017**, *95* (2), 197–206.
32. Lawson-Wood, K.; Upstone, S.; Evans, K. Determination of Relative Fluorescence Quantum Yields Using the FL6500 Fluorescence Spectrometer; Perkin-Elmer, Inc., 2018.
33. Kubin, R. F.; Fletcher, A. N. Fluorescence Quantum Yields of Some Rhodamine Dyes. *J. Lumin.* **1982**, *27*, 455–462.

34. Staroverov, V. N.; Scuseria, G. N.; Tao, J.; Perdew, J. P.; Comparative assessment of a new nonempirical density functional: Molecules and hydrogen-bonded complexes. *J. Chem. Phys.* **2003**, *119*, 12129-12137.
35. Tao, J. M.; Perdew, J. P.; Staroverov, V. N.; Scuseria, G. E. Climbing the Density Functional Ladder: Nonempirical Meta–Generalized Gradient Approximation Designed for Molecules and Solids. *Phys. Rev. Lett.* **2003**; *91*, 146401.
36. Wachters, A. J. H. Gaussian Basis Set for Molecular Wavefunctions Containing Third-Row Atoms. *J. Chem. Phys.* **1970**, *52*, 1033-1036.
37. McLean, A. D.; Chandler, G. S. Contracted Gaussian basis sets for molecular calculations. I. Second row atoms, *Z*=11–18. *J. Chem. Phys.* **1980**, *72*, 5639-5648.
38. Zhao, Y.; Truhlar, D. G. The M06 suite of density functionals for main group thermochemistry, thermochemical kinetics, noncovalent interactions, excited states, and transition elements: two new functionals and systematic testing of four M06-class functionals and 12 other functionals. *Theor. Chem. Acc.* **2008**, *120*, 215-241.
39. Tenderholt, A. L. QMForge, version 2.1; Stanford University: Stanford, CA, 2011.
40. Palatinus, L, Chapuis, G. SUPERFLIP – a computer program for the solution of crystal structures by charge flipping in arbitrary dimensions. *J. Appl. Cryst*. **2007**, *40*, 786–790.
41. Sheldrick, G. M. *Acta Cryst*. **2008**, A64, 112-122.
42. Betteridge, P. W.; Carruthers, J. R.; Copper, R. I.; Prout, K.; Watkin, D. J. CRYSTALS version 12: software for guided crystal structure analysis. *J. Appl. Cryst*. **2003**, 36, 1487.
43. A. L. Spek. A Multipurpose Crystallographic Tool. 2005, Utrecht University. Utrecht, The Netherlands.
44. Novakova, V.; Zimcik, P.; Miletin, M.; Vůjtěch, P.; Franzová, Š. The Synthesis, Photochemical and Photophysical Properties of Zinc Aryloxy- and Alkyloxy Azaphthalocyanines. *Dyes Pigm*. 2010, *87* (2), 173–179.
45. Kolarova, M.; Mulaku, A.; Miletin, M.; Novakova, V.; Zimcik, P. Magnesium Phthalocyanines and Tetrapyrazinoporphyrazines: The Influence of a Solvent and a Delivery System on a Dissociation of Central Metal in Acidic Media. *Pharmaceuticals*. **2022**, *15*, 409-422.

46. Belosludov, R. V.; Nevonen, D.; Rhoda, H. M.; Sabin, J. R.; Nemykin, V. N. Simultaneous Prediction of the Energies of Qx and Qy Bands and Intramolecular Charge-Transfer Transitions in Benzoannulated and Non-Peripherally Substituted Metal-Free Phthalocyanines and Their Analogues: No Standard TDDFT Silver Bullet Yet. *J. Phys. Chem. A*. **2018**, *123* (1), 132–152.
47. Kobayashi, N.; Ogata, H.; Nonaka, N.; Luk'yanets, E. A. Effect of Peripheral Substitution on the Electronic Absorption and Fluorescence Spectra of Metal-Free and Zinc Phthalocyanines. *Chem. Eur. J.* **2003**, *9* (20), 5123–5134.
48. Sleven, J.; Cardinaels, T.; Binnemans, K.; Guillon, D.; Donnio, B. Thermal and Optical Behaviour of Octa-Alkoxy Substituted Phthalocyaninatovanadyl Complexes. *Liq. Cryst*. **2002**, *29* (11), 1425–1433.
49. Bezzu, C. G.; Helliwell, M.; Warren, J.; Allan, D.; McKeown, N. Heme-like Coordination Chemistry within Nanoporous Molecular Crystals. *Science*. **2010**, *327* (5793), 1627–1630.
50. Bezzu, C. G.; Kariuki, B.; Helliwell, M.; Tuna, F.; Warren, J.; Allan, D.; McKeown, N. In-Situ Coordination Chemistry within Cobalt-Containing Phthalocyanine Nanoporous Crystals. *CrystEngComm*. **2013**, *15*, 1545–1550.
51. *Gaussian 16, Revision B.01*, Frisch MJ, Trucks GW, Schlegel HB,Scuseria GE, Robb MA, Cheeseman JR, Scalmani G, Barone V, Petersson GA,Nakatsuji H, Li X, Caricato M, Marenich AV, Bloino J, Janesko BG, Gomperts R,Mennucci B, Hratchian HP, Ortiz JV, Izmaylov AF, Sonnenberg JL, Williams-YoungD, Ding F, Lipparini F, Egidi F, Goings J, Peng B, Petrone A, Henderson T,Ranasinghe D, Zakrzewski VG, Gao J, Rega N, Zheng G, Liang W, Hada M, Ehara M,Toyota K, Fukuda R, Hasegawa J, Ishida M, Nakajima T, Honda Y, Kitao O, Nakai H,Vreven T, Throssell K, Montgomery JA Jr, Peralta JE, Ogliaro F, Bearpark MJ,Heyd JJ, Brothers EN, Kudin KN, Staroverov VN, Keith TA, Kobayashi R, Normand J,Raghavachari K, Rendell AP, Burant JC, Iyengar SS, Tomasi J, Cossi M, Millam JM,Klene M, Adamo C, Cammi R, Ochterski JW, Martin RL, Morokuma K, Farkas O,Foresman JB, Fox DJ. *Gaussian, Inc.*,Wallingford CT, 2016.
52. McKeown, N. B. Nanoporous Molecular Crystals. *J. Mat Chem*. **2010**, *20* (47), 10588.
53. Gouterman, M. Spectra of Porphyrins. *J. Mol. Spectr*. **1961**, *6*, 138–163.

54. Gouterman, M.; Wagnière, G. H.; Snyder, L. C. Spectra of Porphyrins: Part II. Four Orbital Model. *J. Mol. Spectr*. **1963**, *11* (1-6), 108–127.
55. Weiss, C.; Kobayashi, H.; Gouterman, M. Spectra of Porphyrins: Part III. Self-Consistent Molecular Orbital Calculations of Porphyrin and Related Ring Systems. *J. Mol. Spectr.* **1965**, *16* (2), 415–450.

APPENDIX

Table A1. Optimized coordinates for linear trimer 3.

N	3.93963	1.49956	-0.34441
N	-3.93988	1.50375	-0.31372
C	-1.15611	0.43283	0.11426
C	0.71235	1.77966	0.02459
C	1.15538	0.43115	0.09831
C	3.50319	0.20385	-0.07566
C	4.7108	-0.62707	-0.10122
C	5.79923	0.17888	-0.3821
C	5.32602	1.57595	-0.57365
C	-5.32707	1.58166	-0.53694
C	-5.79955	0.18327	-0.35294
C	-4.71627	-0.61735	-0.03885
C	-3.50581	0.20994	-0.03177
C	-0.71214	1.7807	0.03432
N	-0.00053	-0.30941	0.16971
N	-2.31799	-0.26246	0.15109
N	2.31599	-0.26674	0.11545
C	-7.17848	-1.57131	-0.22804
C	-6.04888	-2.4077	0.09324
C	-0.72648	4.04237	-0.00897
C	0.72944	4.04129	-0.01965
C	6.03705	-2.42459	-0.00767
C	7.17098	-1.58408	-0.30192
N	7.05505	-0.28945	-0.48748
N	4.81384	-1.95668	0.0886
N	-7.05546	-0.28468	-0.45929
N	-4.82507	-1.94084	0.18708
N	-1.42687	2.94245	0.00941
N	1.42836	2.94032	-0.01109
O	-8.37747	-2.18903	-0.27001
O	-6.32142	-3.71461	0.28534
O	8.36314	-2.21014	-0.38958
O	6.30663	-3.73405	0.17097
O	1.29785	5.26221	-0.03007
O	-1.29304	5.26418	-0.01046
C	-5.27229	-4.57749	0.68271
C	-5.17291	-4.88024	2.04555
C	-4.46119	-5.15185	-0.30188
C	-4.19332	-5.8063	2.4213
C	-3.49964	-6.07328	0.12799
C	-3.36216	-6.39699	1.47444

Table A1 continued.

H	-4.08113	-6.0654	3.46998
H	-2.84814	-6.5405	-0.60481
C	-9.5039	-1.46256	-0.72564
C	-9.91861	-1.69834	-2.0418
C	-10.19141	-0.63499	0.1687
C	-11.08383	-1.05085	-2.46766
C	-11.35146	-0.01428	-0.30802
C	-11.79399	-0.21452	-1.61205
H	-11.43627	-1.20374	-3.48348
H	-11.91265	0.63911	0.35355
H	-12.69589	0.27935	-1.96058
C	-2.68983	5.37852	0.20117
C	-3.1552	5.45993	1.51691
C	-3.50672	5.51091	-0.92947
C	-4.52883	5.67721	1.68672
C	-4.86817	5.72608	-0.70105
C	-5.37605	5.80605	0.59316
H	-4.93521	5.74239	2.69195
H	-5.54611	5.80516	-1.54256
H	-6.43972	5.95753	0.74529
C	2.69739	5.3743	0.16395
C	3.50068	5.50283	-0.97681
C	3.17899	5.45714	1.47374
C	4.86528	5.71549	-0.7654
C	4.55508	5.67157	1.6264
C	5.38917	5.79657	0.52235
H	5.53306	5.79161	-1.61527
H	4.97394	5.7374	2.62645
H	6.45499	5.9455	0.66119
C	9.53688	-1.42923	-0.5197
C	10.30577	-1.24805	0.63621
C	9.91557	-0.96708	-1.78473
C	11.51211	-0.55287	0.49583
C	11.13226	-0.28069	-1.86892
C	11.92263	-0.07065	-0.7431
H	12.13525	-0.38683	1.36969
H	11.46108	0.09795	-2.83226
H	12.86194	0.46647	-0.83245
C	5.22863	-4.62938	0.36969
C	4.7796	-5.34907	-0.74361
C	4.73855	-4.81826	1.66631
C	3.77645	-6.29968	-0.52364

Table A1 continued.

C	3.73832	-5.78309	1.83093
C	3.2578	-6.51536	0.74953
H	3.3976	-6.87651	-1.3622
H	3.32919	-5.95905	2.82155
C	5.24983	-4.02074	2.85579
C	5.88706	-4.93723	3.91505
C	4.12895	-3.15865	3.4639
H	6.03276	-3.34628	2.49875
H	6.70445	-5.5255	3.48939
H	6.28827	-4.34206	4.74164
H	5.1539	-5.63408	4.3332
H	3.67899	-2.51371	2.70592
H	3.33757	-3.78327	3.89083
H	4.52502	-2.52896	4.26727
C	5.33344	-5.10142	-2.1386
C	4.28284	-4.40473	-3.0237
C	5.84045	-6.39598	-2.79586
H	6.19165	-4.4316	-2.04013
H	3.92941	-3.47874	-2.56294
H	4.70529	-4.16399	-4.00471
H	3.41358	-5.05132	-3.18225
H	6.59579	-6.885	-2.17512
H	5.02807	-7.10997	-2.96378
H	6.29038	-6.17457	-3.76871
C	9.85091	-1.76234	1.99394
C	9.44878	-0.59352	2.91286
C	10.91727	-2.64749	2.66059
H	8.96763	-2.38545	1.83233
H	8.67666	0.02679	2.45023
H	9.06389	-0.96938	3.86665
H	10.30769	0.05038	3.12794
H	11.19514	-3.48515	2.0155
H	11.82631	-2.08279	2.89012
H	10.5359	-3.05468	3.60233
C	9.06576	-1.18805	-3.02617
C	9.80761	-2.04877	-4.06432
C	8.61188	0.15195	-3.63244
H	8.16981	-1.73995	-2.72945
H	10.10028	-3.01416	-3.64247
H	9.16709	-2.2346	-4.9325
H	10.71399	-1.54963	-4.42112
H	8.08927	0.75946	-2.8907

Table A1 continued.

H	9.46628	0.72793	-4.00234
H	7.93873	-0.02212	-4.47837
C	2.88916	5.43952	-2.36935
C	3.88973	5.00662	-3.44943
C	2.24153	6.78956	-2.73538
H	2.09159	4.68781	-2.34346
H	4.41734	4.0918	-3.16756
H	3.36298	4.82545	-4.39097
H	4.63736	5.78257	-3.6425
H	1.48269	7.07594	-2.00404
H	2.99808	7.57981	-2.77092
H	1.76439	6.73237	-3.71931
C	2.27314	5.33838	2.68959
C	2.30697	6.62244	3.53739
C	2.63143	4.10538	3.53819
H	1.24634	5.21472	2.33485
H	2.02258	7.49478	2.94332
H	1.61298	6.54166	4.38023
H	3.30591	6.80458	3.94549
H	2.5885	3.18959	2.94326
H	3.64141	4.18945	3.95139
H	1.93576	4.00233	4.37734
C	-2.91232	5.44914	-2.32948
C	-2.26474	6.79802	-2.69991
C	-3.92726	5.02233	-3.3985
H	-2.11694	4.69478	-2.31512
H	-1.49615	7.08007	-1.97714
H	-1.79981	6.74176	-3.68971
H	-3.01911	7.59076	-2.72432
H	-4.45459	4.10857	-3.11274
H	-4.67454	5.80126	-3.58062
H	-3.41248	4.84184	-4.34675
C	-2.23483	5.33729	2.72143
C	-2.58699	4.10532	3.57403
C	-2.25357	6.62122	3.56989
H	-1.21296	5.20991	2.35404
H	-2.55478	3.18963	2.97829
H	-1.88124	3.99944	4.40436
H	-3.59138	4.19285	3.99996
H	-1.97313	7.49266	2.97264
H	-3.24685	6.80695	3.99003
H	-1.54978	6.53762	4.40429

Table A1 continued.

C	-4.59596	-4.80321	-1.77589
C	-4.9606	-6.04019	-2.61539
C	-3.31596	-4.12866	-2.30134
H	-5.41651	-4.08826	-1.8804
H	-5.88695	-6.50008	-2.26079
H	-5.0972	-5.76106	-3.66508
H	-4.17188	-6.79793	-2.5735
H	-3.06322	-3.25248	-1.70013
H	-2.4658	-4.81794	-2.2714
H	-3.45041	-3.81157	-3.34064
C	-9.13642	-2.60226	-2.98303
C	-8.46314	-1.77913	-4.09701
C	-10.01825	-3.71528	-3.57391
H	-8.35069	-3.08779	-2.39868
H	-7.82093	-0.99897	-3.68009
H	-7.85143	-2.42502	-4.73554
H	-9.21007	-1.2911	-4.73137
H	-10.48479	-4.31057	-2.7846
H	-10.81486	-3.3081	-4.2044
H	-9.416	-4.38558	-4.19534
C	-6.06961	-4.22297	3.08371
C	-5.26225	-3.24692	3.95985
C	-6.80759	-5.26082	3.94601
H	-6.82988	-3.64813	2.54859
H	-4.7468	-2.50162	3.34877
H	-5.92167	-2.72409	4.66032
H	-4.50559	-3.77923	4.54539
H	-7.39359	-5.94474	3.32644
H	-6.11198	-5.8588	4.54313
H	-7.49023	-4.75956	4.63931
C	-9.72345	-0.40491	1.59709
C	-10.75769	-0.92111	2.61334
C	-9.39375	1.07889	1.83951
H	-8.80577	-0.97926	1.74963
H	-10.96555	-1.98387	2.46206
H	-10.38784	-0.78676	3.63498
H	-11.70447	-0.37849	2.52867
H	-8.66425	1.44085	1.11206
H	-10.29087	1.7013	1.75934
H	-8.98294	1.21778	2.84498
H	-3.32255	2.31745	-0.29125
H	3.32193	2.31302	-0.32472

Table A1 continued.

H	-0.00051	-1.31913	0.21748
O	-5.94803	2.5842	-0.81977
O	5.94311	2.57317	-0.88293
H	2.48113	-7.259	0.90034
H	-2.60906	-7.11453	1.7857

Table A2. Optimized coordinates for titanyl complex **4**.

N	0.2221	1.97256	0.40558
N	-1.97256	0.2221	0.40558
N	-0.2221	-1.97256	0.40558
C	2.63651	-1.43137	0.32962
C	4.21392	0.22466	0.18207
C	2.88769	0.80769	0.30585
C	1.43137	2.63651	0.32962
C	1.15953	4.06045	0.22272
C	-0.22466	4.21392	0.18207
C	-0.80769	2.88769	0.30585
C	-2.63651	1.43137	0.32962
C	-4.06045	1.15953	0.22272
C	-4.21392	-0.22466	0.18207
C	-2.88769	-0.80769	0.30585
C	-1.43137	-2.63651	0.32962
C	-1.15953	-4.06045	0.22272
C	0.22466	-4.21392	0.18207
C	0.80769	-2.88769	0.30585
C	4.06045	-1.15953	0.22272
N	1.97256	-0.2221	0.40558
N	2.10973	-2.64586	0.29617
N	2.64586	2.10973	0.29617
N	-2.10973	2.64586	0.29617
N	-2.64586	-2.10973	0.29617
C	-1.438	-6.26706	0.03479
C	0.	-6.42567	-0.02257
C	6.26706	-1.438	0.03479
C	6.42567	0.	-0.02257
C	1.438	6.26706	0.03479
C	0.	6.42567	-0.02257
C	-6.26706	1.438	0.03479
C	-6.42567	0.	-0.02257
N	-0.82875	5.4127	0.04319
N	2.01859	5.09791	0.14834
N	-5.09791	2.01859	0.14834
N	-5.4127	-0.82875	0.04319
N	-2.01859	-5.09791	0.14834
N	0.82875	-5.4127	0.04319
N	5.09791	-2.01859	0.14834
N	5.4127	0.82875	0.04319
O	-2.1442	-7.41016	-0.05283
O	0.4285	-7.69696	-0.13725

Table A2 continued.

O	-7.69696	-0.4285	-0.13725
O	-7.41016	2.1442	-0.05283
O	-0.4285	7.69696	-0.13725
O	2.1442	7.41016	-0.05283
O	7.69696	0.4285	-0.13725
O	7.41016	-2.1442	-0.05283
C	1.79403	-7.96582	-0.39209
C	2.7016	-7.98359	0.6722
C	2.12595	-8.31927	-1.70617
C	4.01201	-8.37532	0.37609
C	3.45014	-8.70217	-1.94617
C	4.38548	-8.73121	-0.91612
H	4.74954	-8.3975	1.17243
H	3.74886	-8.9843	-2.95142
H	5.40665	-9.03967	-1.11969
C	-3.54228	-7.38786	0.16719
C	-4.39526	-7.04507	-0.88692
C	-3.98775	-7.82512	1.42053
C	-5.76943	-7.14959	-0.64526
C	-5.37179	-7.91	1.60836
C	-6.25564	-7.5759	0.58685
H	-6.46663	-6.88546	-1.43423
H	-5.75901	-8.24368	2.56659
H	-7.32652	-7.65375	0.74961
C	7.38786	-3.54228	0.16719
C	7.04507	-4.39526	-0.88692
C	7.82512	-3.98775	1.42053
C	7.14959	-5.76943	-0.64526
C	7.91	-5.37179	1.60836
C	7.5759	-6.25564	0.58685
H	6.88546	-6.46663	-1.43423
H	8.24368	-5.75901	2.56659
H	7.65375	-7.32652	0.74961
C	7.96582	1.79403	-0.39209
C	7.98359	2.7016	0.6722
C	8.31927	2.12595	-1.70617
C	8.37532	4.01201	0.37609
C	8.70217	3.45014	-1.94617
C	8.73121	4.38548	-0.91612
H	8.3975	4.74954	1.17243
H	8.9843	3.74886	-2.95142
H	9.03967	5.40665	-1.11969

Table A2 continued.

C	-1.79403	7.96582	-0.39209
C	-2.7016	7.98359	0.6722
C	-2.12595	8.31927	-1.70617
C	-4.01201	8.37532	0.37609
C	-3.45014	8.70217	-1.94617
C	-4.38548	8.73121	-0.91612
H	-4.74954	8.3975	1.17243
H	-3.74886	8.9843	-2.95142
H	-5.40665	9.03967	-1.11969
C	3.54228	7.38786	0.16719
C	4.39526	7.04507	-0.88692
C	3.98775	7.82512	1.42053
C	5.76943	7.14959	-0.64526
C	5.37179	7.91	1.60836
C	6.25564	7.5759	0.58685
H	6.46663	6.88546	-1.43423
H	5.75901	8.24368	2.56659
H	7.32652	7.65375	0.74961
C	-7.96582	-1.79403	-0.39209
C	-7.98359	-2.7016	0.6722
C	-8.31927	-2.12595	-1.70617
C	-8.37532	-4.01201	0.37609
C	-8.70217	-3.45014	-1.94617
C	-8.73121	-4.38548	-0.91612
H	-8.3975	-4.74954	1.17243
H	-8.9843	-3.74886	-2.95142
H	-9.03967	-5.40665	-1.11969
C	-7.38786	3.54228	0.16719
C	-7.04507	4.39526	-0.88692
C	-7.82512	3.98775	1.42053
C	-7.14959	5.76943	-0.64526
C	-7.91	5.37179	1.60836
C	-7.5759	6.25564	0.58685
H	-6.88546	6.46663	-1.43423
H	-8.24368	5.75901	2.56659
H	-7.65375	7.32652	0.74961
C	3.02193	8.18187	2.54073
C	3.27409	9.59734	3.08698
C	3.08271	7.13442	3.66823
H	2.01189	8.17215	2.1235
H	3.21807	10.34416	2.29061
H	2.52449	9.84933	3.84364

Table A2 continued.

H	4.25852	9.67997	3.55823
H	2.88297	6.12934	3.28768
H	4.07085	7.12134	4.13945
H	2.34418	7.36191	4.44379
C	3.88155	6.58533	-2.24215
C	4.34654	5.15167	-2.55456
C	4.29613	7.56352	-3.35597
H	2.78883	6.58061	-2.20665
H	4.04609	4.46178	-1.7635
H	3.91151	4.81081	-3.50015
H	5.4355	5.09902	-2.65062
H	3.93784	8.57585	-3.14936
H	5.38462	7.60785	-3.46229
H	3.8815	7.24318	-4.31726
C	-2.30953	7.61405	2.09407
C	-3.10613	6.3944	2.59084
C	-2.47136	8.81386	3.04478
H	-1.25081	7.34185	2.09455
H	-2.98345	5.54577	1.9152
H	-2.76287	6.09916	3.58777
H	-4.17518	6.61924	2.65982
H	-1.87962	9.66989	2.7087
H	-3.51647	9.13273	3.10945
H	-2.143	8.54572	4.05405
C	-1.10389	8.278	-2.83267
C	-1.04555	9.60338	-3.61023
C	-1.38434	7.09459	-3.77807
H	-0.12052	8.12498	-2.38117
H	-0.83986	10.44454	-2.94305
H	-0.25205	9.56412	-4.36304
H	-1.98466	9.80927	-4.13333
H	-1.4056	6.1474	-3.2326
H	-2.35172	7.21227	-4.27716
H	-0.61247	7.02959	-4.55202
C	-8.18187	3.02193	2.54073
C	-9.59734	3.27409	3.08698
C	-7.13442	3.08271	3.66823
H	-8.17215	2.01189	2.1235
H	-10.34416	3.21807	2.29061
H	-9.84933	2.52449	3.84364
H	-9.67997	4.25852	3.55823
H	-6.12934	2.88297	3.28768

Table A2 continued.

H	-7.12134	4.07085	4.13945
H	-7.36191	2.34418	4.44379
C	-6.58533	3.88155	-2.24215
C	-5.15167	4.34654	-2.55456
C	-7.56352	4.29613	-3.35597
H	-6.58061	2.78883	-2.20665
H	-4.46178	4.04609	-1.7635
H	-4.81081	3.91151	-3.50015
H	-5.09902	5.4355	-2.65062
H	-8.57585	3.93784	-3.14936
H	-7.60785	5.38462	-3.46229
H	-7.24318	3.8815	-4.31726
C	-7.61405	-2.30953	2.09407
C	-6.3944	-3.10613	2.59084
C	-8.81386	-2.47136	3.04478
H	-7.34185	-1.25081	2.09455
H	-5.54577	-2.98345	1.9152
H	-6.09916	-2.76287	3.58777
H	-6.61924	-4.17518	2.65982
H	-9.66989	-1.87962	2.7087
H	-9.13273	-3.51647	3.10945
H	-8.54572	-2.143	4.05405
C	-8.278	-1.10389	-2.83267
C	-9.60338	-1.04555	-3.61023
C	-7.09459	-1.38434	-3.77807
H	-8.12498	-0.12052	-2.38117
H	-10.44454	-0.83986	-2.94305
H	-9.56412	-0.25205	-4.36304
H	-9.80927	-1.98466	-4.13333
H	-6.1474	-1.4056	-3.2326
H	-7.21227	-2.35172	-4.27716
H	-7.02959	-0.61247	-4.55202
C	7.61405	2.30953	2.09407
C	6.3944	3.10613	2.59084
C	8.81386	2.47136	3.04478
H	7.34185	1.25081	2.09455
H	5.54577	2.98345	1.9152
H	6.09916	2.76287	3.58777
H	6.61924	4.17518	2.65982
H	9.66989	1.87962	2.7087
H	9.13273	3.51647	3.10945
H	8.54572	2.143	4.05405

Table A2 continued.

C	8.278	1.10389	-2.83267
C	9.60338	1.04555	-3.61023
C	7.09459	1.38434	-3.77807
H	8.12498	0.12052	-2.38117
H	10.44454	0.83986	-2.94305
H	9.56412	0.25205	-4.36304
H	9.80927	1.98466	-4.13333
H	6.1474	1.4056	-3.2326
H	7.21227	2.35172	-4.27716
H	7.02959	0.61247	-4.55202
C	8.18187	-3.02193	2.54073
C	9.59734	-3.27409	3.08698
C	7.13442	-3.08271	3.66823
H	8.17215	-2.01189	2.1235
H	10.34416	-3.21807	2.29061
H	9.84933	-2.52449	3.84364
H	9.67997	-4.25852	3.55823
H	6.12934	-2.88297	3.28768
H	7.12134	-4.07085	4.13945
H	7.36191	-2.34418	4.44379
C	6.58533	-3.88155	-2.24215
C	5.15167	-4.34654	-2.55456
C	7.56352	-4.29613	-3.35597
H	6.58061	-2.78883	-2.20665
H	4.46178	-4.04609	-1.7635
H	4.81081	-3.91151	-3.50015
H	5.09902	-5.4355	-2.65062
H	8.57585	-3.93784	-3.14936
H	7.60785	-5.38462	-3.46229
H	7.24318	-3.8815	-4.31726
C	1.10389	-8.278	-2.83267
C	1.04555	-9.60338	-3.61023
C	1.38434	-7.09459	-3.77807
H	0.12052	-8.12498	-2.38117
H	0.83986	-10.44454	-2.94305
H	0.25205	-9.56412	-4.36304
H	1.98466	-9.80927	-4.13333
H	1.4056	-6.1474	-3.2326
H	2.35172	-7.21227	-4.27716
H	0.61247	-7.02959	-4.55202
C	-3.88155	-6.58533	-2.24215
C	-4.34654	-5.15167	-2.55456

Table A2 continued.

C	-4.29613	-7.56352	-3.35597
H	-2.78883	-6.58061	-2.20665
H	-4.04609	-4.46178	-1.7635
H	-3.91151	-4.81081	-3.50015
H	-5.4355	-5.09902	-2.65062
H	-3.93784	-8.57585	-3.14936
H	-5.38462	-7.60785	-3.46229
H	-3.8815	-7.24318	-4.31726
C	2.30953	-7.61405	2.09407
C	3.10613	-6.3944	2.59084
C	2.47136	-8.81386	3.04478
H	1.25081	-7.34185	2.09455
H	2.98345	-5.54577	1.9152
H	2.76287	-6.09916	3.58777
H	4.17518	-6.61924	2.65982
H	1.87962	-9.66989	2.7087
H	3.51647	-9.13273	3.10945
H	2.143	-8.54572	4.05405
C	-3.02193	-8.18187	2.54073
C	-3.27409	-9.59734	3.08698
C	-3.08271	-7.13442	3.66823
H	-2.01189	-8.17215	2.1235
H	-3.21807	-10.34416	2.29061
H	-2.52449	-9.84933	3.84364
H	-4.25852	-9.67997	3.55823
H	-2.88297	-6.12934	3.28768
H	-4.07085	-7.12134	4.13945
H	-2.34418	-7.36191	4.44379
O	0.	0.	2.68388
Ti	0.	0.	1.04994

Table A3. Optimized coordinates for magnesium complex **5**.

N	0.	2.00873	0.
N	2.00873	0.	0.
N	0.	-2.00873	0.
C	-2.79581	-1.12827	-0.01039
C	-4.18947	0.69834	0.01821
C	-2.79581	1.12827	0.01039
C	-1.12827	2.79581	-0.01039
C	-0.69834	4.18947	-0.01821
C	0.69834	4.18947	0.01821
C	1.12827	2.79581	0.01039
C	2.79581	1.12827	-0.01039
C	4.18947	0.69834	-0.01821
C	4.18947	-0.69834	0.01821
C	2.79581	-1.12827	0.01039
C	1.12827	-2.79581	-0.01039
C	0.69834	-4.18947	-0.01821
C	-0.69834	-4.18947	0.01821
C	-1.12827	-2.79581	0.01039
C	-4.18947	-0.69834	-0.01821
N	-2.00873	0.	0.
N	-2.39811	-2.39811	0.
N	-2.39811	2.39811	0.
N	2.39811	2.39811	0.
N	2.39811	-2.39811	0.
C	0.72192	-6.42467	-0.02549
C	-0.72192	-6.42467	0.02549
C	-6.42467	-0.72192	-0.02549
C	-6.42467	0.72192	0.02549
C	-0.72192	6.42467	-0.02549
C	0.72192	6.42467	0.02549
C	6.42467	0.72192	-0.02549
C	6.42467	-0.72192	0.02549
Mg	0.	0.	0.
N	1.43029	5.32213	0.04716
N	-1.43029	5.32213	-0.04716
N	5.32213	1.43029	-0.04716
N	5.32213	-1.43029	0.04716
N	1.43029	-5.32213	-0.04716
N	-1.43029	-5.32213	0.04716
N	-5.32213	-1.43029	-0.04716
N	-5.32213	1.43029	0.04716
O	1.29724	-7.64464	-0.03539

Table A3 continued.

O	-1.29724	-7.64464	0.03539
O	7.64464	-1.29724	0.03539
O	7.64464	1.29724	-0.03539
O	1.29724	7.64464	0.03539
O	-1.29724	7.64464	-0.03539
O	-7.64464	1.29724	0.03539
O	-7.64464	-1.29724	-0.03539
C	-2.68681	-7.76333	0.26868
C	-3.57795	-7.59905	-0.79716
C	-3.07646	-8.15644	1.55511
C	-4.93001	-7.84423	-0.53339
C	-4.44053	-8.3879	1.76417
C	-5.36015	-8.23412	0.73122
H	-5.65538	-7.72141	-1.33178
H	-4.78358	-8.69431	2.74808
H	-6.41414	-8.42459	0.91063
C	2.68681	-7.76333	-0.26868
C	3.57795	-7.59905	0.79716
C	3.07646	-8.15644	-1.55511
C	4.93001	-7.84423	0.53339
C	4.44053	-8.3879	-1.76417
C	5.36015	-8.23412	-0.73122
H	5.65538	-7.72141	1.33178
H	4.78358	-8.69431	-2.74808
H	6.41414	-8.42459	-0.91063
C	-7.76333	-2.68681	-0.26868
C	-7.59905	-3.57795	0.79716
C	-8.15644	-3.07646	-1.55511
C	-7.84423	-4.93001	0.53339
C	-8.3879	-4.44053	-1.76417
C	-8.23412	-5.36015	-0.73122
H	-7.72141	-5.65538	1.33178
H	-8.69431	-4.78358	-2.74808
H	-8.42459	-6.41414	-0.91063
C	-7.76333	2.68681	0.26868
C	-7.59905	3.57795	-0.79716
C	-8.15644	3.07646	1.55511
C	-7.84423	4.93001	-0.53339
C	-8.3879	4.44053	1.76417
C	-8.23412	5.36015	0.73122
H	-7.72141	5.65538	-1.33178
H	-8.69431	4.78358	2.74808

Table A3 continued.

H	-8.42459	6.41414	0.91063
C	2.68681	7.76333	0.26868
C	3.57795	7.59905	-0.79716
C	3.07646	8.15644	1.55511
C	4.93001	7.84423	-0.53339
C	4.44053	8.3879	1.76417
C	5.36015	8.23412	0.73122
H	5.65538	7.72141	-1.33178
H	4.78358	8.69431	2.74808
H	6.41414	8.42459	0.91063
C	-2.68681	7.76333	-0.26868
C	-3.57795	7.59905	0.79716
C	-3.07646	8.15644	-1.55511
C	-4.93001	7.84423	0.53339
C	-4.44053	8.3879	-1.76417
C	-5.36015	8.23412	-0.73122
H	-5.65538	7.72141	1.33178
H	-4.78358	8.69431	-2.74808
H	-6.41414	8.42459	-0.91063
C	7.76333	-2.68681	0.26868
C	7.59905	-3.57795	-0.79716
C	8.15644	-3.07646	1.55511
C	7.84423	-4.93001	-0.53339
C	8.3879	-4.44053	1.76417
C	8.23412	-5.36015	0.73122
H	7.72141	-5.65538	-1.33178
H	8.69431	-4.78358	2.74808
H	8.42459	-6.41414	0.91063
C	7.76333	2.68681	-0.26868
C	7.59905	3.57795	0.79716
C	8.15644	3.07646	-1.55511
C	7.84423	4.93001	0.53339
C	8.3879	4.44053	-1.76417
C	8.23412	5.36015	-0.73122
H	7.72141	5.65538	1.33178
H	8.69431	4.78358	-2.74808
H	8.42459	6.41414	-0.91063
C	-2.07274	8.31584	-2.68742
C	-2.15578	9.70716	-3.33752
C	-2.25309	7.20303	-3.73682
H	-1.07206	8.21847	-2.25924
H	-2.01339	10.49831	-2.59671

Table A3 continued.

H	-1.38061	9.81381	-4.1029
H	-3.12311	9.87007	-3.82313
H	-2.17583	6.21238	-3.28097
H	-3.23399	7.272	-4.21833
H	-1.48964	7.28403	-4.51758
C	-3.12521	7.18347	2.18787
C	-3.75744	5.84177	2.5993
C	-3.42329	8.28352	3.22245
H	-2.04084	7.04695	2.16418
H	-3.54112	5.06546	1.86276
H	-3.36604	5.52163	3.57084
H	-4.84493	5.92638	2.6903
H	-2.94646	9.22813	2.94638
H	-4.49906	8.46433	3.31287
H	-3.05214	7.98839	4.20925
C	3.12521	7.18347	-2.18787
C	3.75744	5.84177	-2.5993
C	3.42329	8.28352	-3.22245
H	2.04084	7.04695	-2.16418
H	3.54112	5.06546	-1.86276
H	3.36604	5.52163	-3.57084
H	4.84493	5.92638	-2.6903
H	2.94646	9.22813	-2.94638
H	4.49906	8.46433	-3.31287
H	3.05214	7.98839	-4.20925
C	2.07274	8.31584	2.68742
C	2.15578	9.70716	3.33752
C	2.25309	7.20303	3.73682
H	1.07206	8.21847	2.25924
H	2.01339	10.49831	2.59671
H	1.38061	9.81381	4.1029
H	3.12311	9.87007	3.82313
H	2.17583	6.21238	3.28097
H	3.23399	7.272	4.21833
H	1.48964	7.28403	4.51758
C	8.31584	2.07274	-2.68742
C	9.70716	2.15578	-3.33752
C	7.20303	2.25309	-3.73682
H	8.21847	1.07206	-2.25924
H	10.49831	2.01339	-2.59671
H	9.81381	1.38061	-4.1029
H	9.87007	3.12311	-3.82313

Table A3 continued.

H	6.21238	2.17583	-3.28097
H	7.272	3.23399	-4.21833
H	7.28403	1.48964	-4.51758
C	7.18347	3.12521	2.18787
C	5.84177	3.75744	2.5993
C	8.28352	3.42329	3.22245
H	7.04695	2.04084	2.16418
H	5.06546	3.54112	1.86276
H	5.52163	3.36604	3.57084
H	5.92638	4.84493	2.6903
H	9.22813	2.94646	2.94638
H	8.46433	4.49906	3.31287
H	7.98839	3.05214	4.20925
C	7.18347	-3.12521	-2.18787
C	5.84177	-3.75744	-2.5993
C	8.28352	-3.42329	-3.22245
H	7.04695	-2.04084	-2.16418
H	5.06546	-3.54112	-1.86276
H	5.52163	-3.36604	-3.57084
H	5.92638	-4.84493	-2.6903
H	9.22813	-2.94646	-2.94638
H	8.46433	-4.49906	-3.31287
H	7.98839	-3.05214	-4.20925
C	8.31584	-2.07274	2.68742
C	9.70716	-2.15578	3.33752
C	7.20303	-2.25309	3.73682
H	8.21847	-1.07206	2.25924
H	10.49831	-2.01339	2.59671
H	9.81381	-1.38061	4.1029
H	9.87007	-3.12311	3.82313
H	6.21238	-2.17583	3.28097
H	7.272	-3.23399	4.21833
H	7.28403	-1.48964	4.51758
C	-7.18347	3.12521	-2.18787
C	-5.84177	3.75744	-2.5993
C	-8.28352	3.42329	-3.22245
H	-7.04695	2.04084	-2.16418
H	-5.06546	3.54112	-1.86276
H	-5.52163	3.36604	-3.57084
H	-5.92638	4.84493	-2.6903
H	-9.22813	2.94646	-2.94638
H	-8.46433	4.49906	-3.31287

Table A3 continued.

H	-7.98839	3.05214	-4.20925
C	-8.31584	2.07274	2.68742
C	-9.70716	2.15578	3.33752
C	-7.20303	2.25309	3.73682
H	-8.21847	1.07206	2.25924
H	-10.49831	2.01339	2.59671
H	-9.81381	1.38061	4.1029
H	-9.87007	3.12311	3.82313
H	-6.21238	2.17583	3.28097
H	-7.272	3.23399	4.21833
H	-7.28403	1.48964	4.51758
C	-8.31584	-2.07274	-2.68742
C	-9.70716	-2.15578	-3.33752
C	-7.20303	-2.25309	-3.73682
H	-8.21847	-1.07206	-2.25924
H	-10.49831	-2.01339	-2.59671
H	-9.81381	-1.38061	-4.1029
H	-9.87007	-3.12311	-3.82313
H	-6.21238	-2.17583	-3.28097
H	-7.272	-3.23399	-4.21833
H	-7.28403	-1.48964	-4.51758
C	-7.18347	-3.12521	2.18787
C	-5.84177	-3.75744	2.5993
C	-8.28352	-3.42329	3.22245
H	-7.04695	-2.04084	2.16418
H	-5.06546	-3.54112	1.86276
H	-5.52163	-3.36604	3.57084
H	-5.92638	-4.84493	2.6903
H	-9.22813	-2.94646	2.94638
H	-8.46433	-4.49906	3.31287
H	-7.98839	-3.05214	4.20925
C	-2.07274	-8.31584	2.68742
C	-2.15578	-9.70716	3.33752
C	-2.25309	-7.20303	3.73682
H	-1.07206	-8.21847	2.25924
H	-2.01339	-10.49831	2.59671
H	-1.38061	-9.81381	4.1029
H	-3.12311	-9.87007	3.82313
H	-2.17583	-6.21238	3.28097
H	-3.23399	-7.272	4.21833
H	-1.48964	-7.28403	4.51758
C	3.12521	-7.18347	2.18787

Table A3 continued.

C	3.75744	-5.84177	2.5993
C	3.42329	-8.28352	3.22245
H	2.04084	-7.04695	2.16418
H	3.54112	-5.06546	1.86276
H	3.36604	-5.52163	3.57084
H	4.84493	-5.92638	2.6903
H	2.94646	-9.22813	2.94638
H	4.49906	-8.46433	3.31287
H	3.05214	-7.98839	4.20925
C	-3.12521	-7.18347	-2.18787
C	-3.75744	-5.84177	-2.5993
C	-3.42329	-8.28352	-3.22245
H	-2.04084	-7.04695	-2.16418
H	-3.54112	-5.06546	-1.86276
H	-3.36604	-5.52163	-3.57084
H	-4.84493	-5.92638	-2.6903
H	-2.94646	-9.22813	-2.94638
H	-4.49906	-8.46433	-3.31287
H	-3.05214	-7.98839	-4.20925
C	2.07274	-8.31584	-2.68742
C	2.15578	-9.70716	-3.33752
C	2.25309	-7.20303	-3.73682
H	1.07206	-8.21847	-2.25924
H	2.01339	-10.49831	-2.59671
H	1.38061	-9.81381	-4.1029
H	3.12311	-9.87007	-3.82313
H	2.17583	-6.21238	-3.28097
H	3.23399	-7.272	-4.21833
H	1.48964	-7.28403	-4.51758

Table A4. Optimized coordinates for metal-free complex **6**.

N	0.	0.	2.02406
N	0.	-1.94959	0.
N	0.	0.	-2.02406
C	-0.01054	2.76119	-1.10094
C	0.0191	4.16723	0.69368
C	0.01054	2.76119	1.10094
C	-0.01243	1.14996	2.78833
C	-0.01942	0.69864	4.16587
C	0.01942	-0.69864	4.16587
C	0.01243	-1.14996	2.78833
C	-0.01054	-2.76119	1.10094
C	-0.0191	-4.16723	0.69368
C	0.0191	-4.16723	-0.69368
C	0.01054	-2.76119	-1.10094
C	-0.01243	-1.14996	-2.78833
C	-0.01942	-0.69864	-4.16587
C	0.01942	0.69864	-4.16587
C	0.01243	1.14996	-2.78833
C	-0.0191	4.16723	-0.69368
N	0.	1.94959	0.
N	0.00176	2.40162	-2.38403
N	-0.00176	2.40162	2.38403
N	0.00176	-2.40162	2.38403
N	-0.00176	-2.40162	-2.38403
C	-0.02646	-0.72424	-6.39973
C	0.02646	0.72424	-6.39973
C	-0.02508	6.39884	-0.72055
C	0.02508	6.39884	0.72055
C	-0.02646	0.72424	6.39973
C	0.02646	-0.72424	6.39973
C	-0.02508	-6.39884	0.72055
C	0.02508	-6.39884	-0.72055
N	0.04928	-1.43213	5.2991
N	-0.04928	1.43213	5.2991
N	-0.04782	-5.29486	1.43071
N	0.04782	-5.29486	-1.43071
N	-0.04928	-1.43213	-5.2991
N	0.04928	1.43213	-5.2991
N	-0.04782	5.29486	-1.43071
N	0.04782	5.29486	1.43071
O	-0.0378	-1.29458	-7.6187
O	0.0378	1.29458	-7.6187

Table A4 continued.

O	0.0326	-7.6197	-1.29792
O	-0.0326	-7.6197	1.29792
O	0.0378	-1.29458	7.6187
O	-0.0378	1.29458	7.6187
O	0.0326	7.6197	1.29792
O	-0.0326	7.6197	-1.29792
C	0.26202	2.6869	-7.743
C	1.54481	3.0813	-8.14243
C	-0.80898	3.57123	-7.5775
C	1.74489	4.44582	-8.37898
C	-0.55346	4.92395	-7.82794
C	0.70715	5.35979	-8.22407
H	2.72561	4.79365	-8.68989
H	-1.35522	5.64527	-7.70397
H	0.87986	6.4142	-8.41799
C	-0.26202	-2.6869	-7.743
C	-1.54481	-3.0813	-8.14243
C	0.80898	-3.57123	-7.5775
C	-1.74489	-4.44582	-8.37898
C	0.55346	-4.92395	-7.82794
C	-0.70715	-5.35979	-8.22407
H	-2.72561	-4.79365	-8.68989
H	1.35522	-5.64527	-7.70397
H	-0.87986	-6.4142	-8.41799
C	-0.26652	7.73821	-2.68617
C	-1.55359	8.12931	-3.07646
C	0.79973	7.5778	-3.57769
C	-1.76241	8.3636	-4.44005
C	0.53658	7.82585	-4.92935
C	-0.72843	8.21456	-5.35941
H	-2.74667	8.669	-4.783
H	1.33594	7.70679	-5.65436
H	-0.90739	8.40826	-6.41295
C	0.26652	7.73821	2.68617
C	1.55359	8.12931	3.07646
C	-0.79973	7.5778	3.57769
C	1.76241	8.3636	4.44005
C	-0.53658	7.82585	4.92935
C	0.72843	8.21456	5.35941
H	2.74667	8.669	4.783
H	-1.33594	7.70679	5.65436
H	0.90739	8.40826	6.41295

Table A4 continued.

C	0.26202	-2.6869	7.743
C	1.54481	-3.0813	8.14243
C	-0.80898	-3.57123	7.5775
C	1.74489	-4.44582	8.37898
C	-0.55346	-4.92395	7.82794
C	0.70715	-5.35979	8.22407
H	2.72561	-4.79365	8.68989
H	-1.35522	-5.64527	7.70397
H	0.87986	-6.4142	8.41799
C	-0.26202	2.6869	7.743
C	-1.54481	3.0813	8.14243
C	0.80898	3.57123	7.5775
C	-1.74489	4.44582	8.37898
C	0.55346	4.92395	7.82794
C	-0.70715	5.35979	8.22407
H	-2.72561	4.79365	8.68989
H	1.35522	5.64527	7.70397
H	-0.87986	6.4142	8.41799
C	0.26652	-7.73821	-2.68617
C	1.55359	-8.12931	-3.07646
C	-0.79973	-7.5778	-3.57769
C	1.76241	-8.3636	-4.44005
C	-0.53658	-7.82585	-4.92935
C	0.72843	-8.21456	-5.35941
H	2.74667	-8.669	-4.783
H	-1.33594	-7.70679	-5.65436
H	0.90739	-8.40826	-6.41295
C	-0.26652	-7.73821	2.68617
C	-1.55359	-8.12931	3.07646
C	0.79973	-7.5778	3.57769
C	-1.76241	-8.3636	4.44005
C	0.53658	-7.82585	4.92935
C	-0.72843	-8.21456	5.35941
H	-2.74667	-8.669	4.783
H	1.33594	-7.70679	5.65436
H	-0.90739	-8.40826	6.41295
C	2.19603	3.11277	7.15579
C	3.23546	3.40197	8.25368
C	2.60652	3.74777	5.81505
H	2.16729	2.02886	7.01582
H	2.9601	2.92339	9.19761
H	4.21939	3.02702	7.95399

Table A4 continued.

H	3.33173	4.47664	8.43765
H	1.86682	3.53897	5.0397
H	2.70344	4.83435	5.90348
H	3.57493	3.35256	5.49051
C	-2.68263	2.08372	8.30146
C	-3.72978	2.26978	7.18738
C	-3.33373	2.17059	9.69205
H	-2.26015	1.08047	8.2049
H	-3.27364	2.19024	6.19707
H	-4.51487	1.51077	7.26758
H	-4.20569	3.25338	7.25587
H	-2.59453	2.02547	10.48421
H	-3.8155	3.13996	9.8538
H	-4.10257	1.39884	9.79815
C	2.68263	-2.08372	8.30146
C	3.72978	-2.26978	7.18738
C	3.33373	-2.17059	9.69205
H	2.26015	-1.08047	8.2049
H	3.27364	-2.19024	6.19707
H	4.51487	-1.51077	7.26758
H	4.20569	-3.25338	7.25587
H	2.59453	-2.02547	10.48421
H	3.8155	-3.13996	9.8538
H	4.10257	-1.39884	9.79815
C	-2.19603	-3.11277	7.15579
C	-3.23546	-3.40197	8.25368
C	-2.60652	-3.74777	5.81505
H	-2.16729	-2.02886	7.01582
H	-2.9601	-2.92339	9.19761
H	-4.21939	-3.02702	7.95399
H	-3.33173	-4.47664	8.43765
H	-1.86682	-3.53897	5.0397
H	-2.70344	-4.83435	5.90348
H	-3.57493	-3.35256	5.49051
C	2.19032	-7.16226	3.12464
C	3.22599	-8.26081	3.42417
C	2.60033	-5.81925	3.75504
H	2.16624	-7.02711	2.04017
H	2.95065	-9.20637	2.94882
H	4.2124	-7.96534	3.0522
H	3.31712	-8.44003	4.50019
H	1.86362	-5.04398	3.53566

Table A4 continued.

H	2.68954	-5.90208	4.8429
H	3.57223	-5.4992	3.36452
C	-2.68653	-8.28153	2.07241
C	-3.72112	-7.15353	2.24435
C	-3.3554	-9.66334	2.16271
H	-2.25529	-8.19581	1.07198
H	-3.25171	-6.16978	2.16135
H	-4.50215	-7.22865	1.48055
H	-4.20428	-7.21009	3.22531
H	-2.62477	-10.46537	2.02872
H	-3.84744	-9.81327	3.12891
H	-4.11902	-9.76506	1.38514
C	2.68653	-8.28153	-2.07241
C	3.72112	-7.15353	-2.24435
C	3.3554	-9.66334	-2.16271
H	2.25529	-8.19581	-1.07198
H	3.25171	-6.16978	-2.16135
H	4.50215	-7.22865	-1.48055
H	4.20428	-7.21009	-3.22531
H	2.62477	-10.46537	-2.02872
H	3.84744	-9.81327	-3.12891
H	4.11902	-9.76506	-1.38514
C	-2.19032	-7.16226	-3.12464
C	-3.22599	-8.26081	-3.42417
C	-2.60033	-5.81925	-3.75504
H	-2.16624	-7.02711	-2.04017
H	-2.95065	-9.20637	-2.94882
H	-4.2124	-7.96534	-3.0522
H	-3.31712	-8.44003	-4.50019
H	-1.86362	-5.04398	-3.53566
H	-2.68954	-5.90208	-4.8429
H	-3.57223	-5.4992	-3.36452
C	2.68653	8.28153	2.07241
C	3.72112	7.15353	2.24435
C	3.3554	9.66334	2.16271
H	2.25529	8.19581	1.07198
H	3.25171	6.16978	2.16135
H	4.50215	7.22865	1.48055
H	4.20428	7.21009	3.22531
H	2.62477	10.46537	2.02872
H	3.84744	9.81327	3.12891
H	4.11902	9.76506	1.38514

Table A4 continued.

C	-2.19032	7.16226	3.12464
C	-3.22599	8.26081	3.42417
C	-2.60033	5.81925	3.75504
H	-2.16624	7.02711	2.04017
H	-2.95065	9.20637	2.94882
H	-4.2124	7.96534	3.0522
H	-3.31712	8.44003	4.50019
H	-1.86362	5.04398	3.53566
H	-2.68954	5.90208	4.8429
H	-3.57223	5.4992	3.36452
C	2.19032	7.16226	-3.12464
C	3.22599	8.26081	-3.42417
C	2.60033	5.81925	-3.75504
H	2.16624	7.02711	-2.04017
H	2.95065	9.20637	-2.94882
H	4.2124	7.96534	-3.0522
H	3.31712	8.44003	-4.50019
H	1.86362	5.04398	-3.53566
H	2.68954	5.90208	-4.8429
H	3.57223	5.4992	-3.36452
C	-2.68653	8.28153	-2.07241
C	-3.72112	7.15353	-2.24435
C	-3.3554	9.66334	-2.16271
H	-2.25529	8.19581	-1.07198
H	-3.25171	6.16978	-2.16135
H	-4.50215	7.22865	-1.48055
H	-4.20428	7.21009	-3.22531
H	-2.62477	10.46537	-2.02872
H	-3.84744	9.81327	-3.12891
H	-4.11902	9.76506	-1.38514
C	-2.19603	3.11277	-7.15579
C	-3.23546	3.40197	-8.25368
C	-2.60652	3.74777	-5.81505
H	-2.16729	2.02886	-7.01582
H	-2.9601	2.92339	-9.19761
H	-4.21939	3.02702	-7.95399
H	-3.33173	4.47664	-8.43765
H	-1.86682	3.53897	-5.0397
H	-2.70344	4.83435	-5.90348
H	-3.57493	3.35256	-5.49051
C	-2.68263	-2.08372	-8.30146
C	-3.72978	-2.26978	-7.18738

Table A4 continued.

C	-3.33373	-2.17059	-9.69205
H	-2.26015	-1.08047	-8.2049
H	-3.27364	-2.19024	-6.19707
H	-4.51487	-1.51077	-7.26758
H	-4.20569	-3.25338	-7.25587
H	-2.59453	-2.02547	-10.48421
H	-3.8155	-3.13996	-9.8538
H	-4.10257	-1.39884	-9.79815
C	2.68263	2.08372	-8.30146
C	3.72978	2.26978	-7.18738
C	3.33373	2.17059	-9.69205
H	2.26015	1.08047	-8.2049
H	3.27364	2.19024	-6.19707
H	4.51487	1.51077	-7.26758
H	4.20569	3.25338	-7.25587
H	2.59453	2.02547	-10.48421
H	3.8155	3.13996	-9.8538
H	4.10257	1.39884	-9.79815
C	2.19603	-3.11277	-7.15579
C	3.23546	-3.40197	-8.25368
C	2.60652	-3.74777	-5.81505
H	2.16729	-2.02886	-7.01582
H	2.9601	-2.92339	-9.19761
H	4.21939	-3.02702	-7.95399
H	3.33173	-4.47664	-8.43765
H	1.86682	-3.53897	-5.0397
H	2.70344	-4.83435	-5.90348
H	3.57493	-3.35256	-5.49051
H	0.	0.	-1.01029
H	0.	0.	1.01029

VITA

Originally from Georgia, Benjamin Marx grew up in Peachtree City, Georgia. After being homeschooled during his grade school career, he attended Berry College and received a Bachelor of Science degree in Biochemistry. He began college intending to apply for medical school, but after thoroughly enjoying undergraduate research with his organic chemistry professor, he changed paths and applied for graduate school. He chose to attend the University of Tennessee, Knoxville to pursue a Master of Science degree in Chemistry with a concentration in Organic Chemistry. His research interest includes synthesis of functional dyes for advancements in molecular technologies. After graduation, he plans to stay in Knoxville to continue his career in the sciences. He is very grateful for the constant support from family back in Georgia and friends while in school as he moves on to the next phase of his life.